UNIVERSITÄT PADERBORN
Die Universität der Informationsgesellschaft

FAKULTÄT FÜR
ELEKTROTECHNIK,
INFORMATIK UND
MATHEMATIK

Investigation on High Spectral Efficiency Coherent Optical OFDM Transmission Systems

Von der Fakultät für Elektrotechnik, Informatik und Mathematik
der Universität Paderborn

zur Erlangung des akademischen Grades

Doktor der Ingenieurwissenschaften (Dr.-Ing.)

genehmigte Dissertation

von

M.Sc. Saleh Ibrahim Saied Saleh Hussin

Erster Gutachter: Prof. Dr.-Ing. Reinhold Noé
Zweiter Gutachter: Prof. Dr.-Ing. Ulrich Hilleringmann

Tag der mündlichen Prüfung: 07.07.2015

Paderborn 2015

Diss. EIM-E/318

Declaration

I hereby declare that I am the sole author of this dissertation and I have not presented it to any other university for a degree award or anywhere else for academic purpose.

I understand that my dissertation may be made electronically available to the public.

Saleh Hussin

UNIVERSITÄT PADERBORN
Die Universität der Informationsgesellschaft

FAKULTÄT FÜR
ELEKTROTECHNIK,
INFORMATIK UND
MATHEMATIK

Dissertation abstract:

Investigation on High Spectral
Efficiency Coherent Optical OFDM Transmission Systems

Orthogonal frequency division multiplexing (OFDM) belongs to multicarrier technology which is used in many broadband wired and wireless communication systems. It is used to combat multipath fading. Although, OFDM systems are complex compared to single carrier systems due to design of their transmitter and receiver and also the associated signal processing, significant benefits are achieved.

Optical OFDM systems can be classified into three approaches according to the detection scheme. The approaches are direct detection optical OFDM (DDO-OFDM), coherent optical OFDM (CO-OFDM) and self coherent optical OFDM (SCO-OFDM). The most important drawbacks of CO-OFDM are the high peak-to-average power ratio (PAPR), high sensitivity to frequency offset and phase noise. The present dissertation introduces the performance of different pulse shaping techniques. Furthermore, it presents new algorithms to reduce the phase noise effects and compares the system performance with different existing algorithms. Moreover, the performance of a new system design is investigated. The provided dissertation includes four original contributions.

Initially, the theoretical principles of OFDM are presented with detailing on the advantages and disadvantages of OFDM compared to the single carrier modulation technology. The theoretical fundamentals of optical OFDM and the differences between the three systems are followed. Furthermore, performance of the three existing optical OFDM systems are elaborated and compared. A square root raised-cosine pulse shaping of OFDM symbols is suggested to enhance the efficiency of CO-OFDM systems. Next, the different kinds of the phase noise effects on the OFDM signals are defined and the impact of the laser and nonlinear phase noise is reported. Different existing phase noise compensation algorithms are presented. Moreover, the modified and new phase noise compensation schemes are provided and compared with the existing algorithms. Finally, a discrete Fourier transform spread OFDM (DFT-S-OFDM) is shown. It is used to minimize the PAPR causing further enhancement in nonlinear tolerance. A novel self coherent DFT-S-OFDM (SDFT-S-OFDM) optical system which combines the benefits from both SCO-OFDM and DFT-S-OFDM systems is investigated. A detailed comparison among SDFT-S-OFDM, optical DFT-S-OFDM, SCO-OFDM and CO-OFDM systems is simulated.

UNIVERSITÄT PADERBORN
Die Universität der Informationsgesellschaft

FAKULTÄT FÜR
ELEKTROTECHNIK,
INFORMATIK UND
MATHEMATIK

Zusammenfassung der Dissertation:

Investigation on High Spectral
Efficiency Coherent Optical OFDM Transmission Systems

Orthogonales Frequenzmultiplex (Orthogonal frequency division multiplexing, OFDM) gehört zur Mehrträgertechnologie, welche in vielen breitbandigen, drahtgebundenen und drahtlosen Kommunikationssystemen verwendet wird. Dadurch lassen sich die Nachteile aufgrund der Mehrwegeausbreitung eindämmen. Obwohl OFDM Systeme sowohl beim Sender als auch beim Empfänger und der zugehörigen Signalverarbeitung im Vergleich zu Systemen mit einzelnem Träger komplex sind, lassen sich doch erhebliche Vorteile erzielen.

Die optischen OFDM Systeme können entsprechend ihres Empfängerentwurfs in drei Gruppen klassifiziert werden. Diese sind optischer Direktempfang (DDO-OFDM), kohärent optisches OFDM (CO-OFDM) und selbstkohärentes optisches OFDM (SCO-OFDM). Die wichtigsten Nachteile des CO-OFDM sind das hohe Verhältnis zwischen der Spitzen- und Durchschnittsleistung (PAPR) und die hohe Empfindlichkeit gegenüber Frequenzoffset und Phasenrauschen. Die vorliegende Arbeit stellt die Effizienz der verschiedenen Pulsformungstechniken vor. Außerdem stellt sie neue Algorithmen vor, um Phasenrauscheffekte zu reduzieren und vergleicht die Effizienz des Systems mit verschiedenen existierenden Algorithmen. Darüber hinaus wird der Nutzen eines neuen Systemdesign untersucht. Die vorliegende Dissertation enthält vier Beiträge.

Zunächst werden die theoretischen Grundlagen von OFDM vorgestellt und die Vor- und Nachteile gegenüber der Modulation auf einen einzigen Träger vorgestellt. Die theoretischen Grundlagen von optischem OFDM und die Unterschiede zwischen den drei Systemen werden als nächstes dargestellt. Darüber hinaus wird auch die Leistungsfähigkeit der drei bestehenden optischen OFDM Systeme untersucht und miteinander verglichen. Ein Root-Raised-Cosine-Impulsformungsfilter für OFDM Symbole wird vorgeschlagen, um die Effizienz von CO-OFDM Systemen zu verbessern. Als nächstes werden die verschiedenen Arten von Phasenrauschen und deren Auswirkung auf die OFDM Signale analysiert. Die Auswirkung von Laser- und nichtlinearem Phasenrauschen wird untersucht. Verschiedene Kompensationsalgorithmen für das Phasenrauschen werden vorgestellt. Darüber hinaus werden die modifizierten und die neuen Kompensationsverfahren mit bereits existierenden Algorithmen verglichen. Schließlich wird ein Verfahren mit verbreiterter diskreter Fourier-Transformation, OFDM (DFT-S-OFDM) gezeigt. Es wird verwendet, um die PAPR zu minimieren, was eine weitere Verbesserung betreffend der nichtlinearen Toleranz bedeutet. Ein neuartiges optisches selbstkohärentes System, DFT-S-OFDM (SDFT-S-OFDM), welches die Vorteile von sowohl SCO-OFDM als auch von DFT-S-OFDM Systemen kombiniert, wird hierbei untersucht. In Simulationen werden SDFT-S-OFDM, optisches DFT-S-OFDM, SCO-OFDM und CO-OFDM Systeme detailliert verglichen.

Acknowledgements

In the name of God, Most Gracious, Most Merciful

Finishing the doctoral study is like taking a long, long journey for me, before I can finally reach the end. I have been often frustrated and exhausted when I still could not see one corner of the peak after working night and day. I have also experienced many happiness and excitement after reaching every small target. Along the way, I have got a lot of guidance, support, encouragement and companionship from many people, to whom I am full of gratitude.

I would like to express my sincere gratitude to my supervisor Prof. Dr.-Ing. Reinhold Noé, for his academic advices, generous help, supervision and guidance during my doctorate study. I am lucky to work with Kidsanapong Puntsri. He was very friendly and co-operative during the whole time. We had very good technical discussion. I would like to thank Assoc. Prof. Mohammed Awadallah for advices and proofreading tips. Special thanks go to Dr.-Ing. David Sandel and to all of my colleagues and technical staff at the optical communications and high frequency engineering group at the University of Paderborn for the enormous help. Thanks also to our technical staff Bernhard Stute for his help. I am heartily thankful to all my friends whose sincere support kept me going through difficult times.

Finally, I would like to take the opportunity to express my love and gratitude to my family. I would express a deep sense of gratitude to my mother, for her continuous, unlimited moral support and prayers throughout my life. She has been a constant source of love, encouragement and inspiration in my entire life including this dissertation work. I am also deeply grateful to my sweetheart wife Mona for her great support, patience, continuous encouragement, unlimited sacrifice and taking care of our children Abd El Rahman and Yassien. My sons brought so much joy to my life which has been and continue to be a great source of encouragement. No words of appreciation could ever reward them for all they have done for me. I am, and will ever be, indebted to them for all achievements in my life. Thanks Allah who made all of that is possible for me.

My sincere gratitude to you all,

Saleh Hussin

Dedication

To my beloved mother who always dreamed of this day, my lovely wife who has always been there through the hard times, my children whom I wish to give the best out of this experience.

Table of Contents

List of Figures

List of Tables

Acronyms

Acronym	*Description*
3GPP	Third Generation Partnership Project
4G	Fourth Generation
ADC	Analog to Digital Converter
ADSL	Asymmetric Digital Subscriber Line
AM	Amplitude Modulation
ASE	Amplified Spontaneous Emission
ASK	Amplitude Shift Keying
AWGN	Additive White Gaussian Noise
BBC	British Broadcasting Corporation
BER	Bit Error Ratio
CD	Chromatic Dispersion
CO-OFDM	Coherent Optical OFDM
CP	Cyclic Prefix
CPE	Common Phase Error
DAB	Digital Audio Broadcasting
DAC	Digital-to-Analog Converter
DC	Direct Current
DCF	Dispersion Compensating Fiber
DDFT-S-OFDM	Distributed sub-band mapping DFT-S-OFDM
DDO-OFDM	Direct Detection Optical OFDM
DFT	Discrete Fourier Transforms
DFT-S-OFDM	Discrete Fourier Transform Spread OFDM
DGD	Differential Group Delay
DSB	Double Side Bands
DSP	Digital Signal Processing
DVB	Digital Video Broadcasting
EDFA	Erbium-Doped Fiber Amplifiers
E-RFP	Enhancement-RFP
FDM	Frequency Division Multiplexing
FEC	Forward Error Correction
FFT	fast Fourier transformation
FIR	Finite Impulse Response
FM	Frequency Modulation
FSK	Frequency Shift Keying
FWM	Four-Wave Mixing
I/Q	In-phase/Quadrature
ICI	Inter-Carrier Interference
IDFT	Inverse Discrete Fourier Transforms
IDFT-S-OFDM	Interleaved sub-band mapping DFT-S-OFDM
IEEE	Institute of Electrical and Electronics Engineers

IF	Intermediate Frequency
IFFT	Inverse Fast Fourier Transformation
ISI	Inter-Symbol Interference
J-SPM	Joint-SPM
Laser	Light Amplification by Stimulated Emission of Radiation
LDFT-S-OFDM	Localized sub-band mapping DFT-S-OFDM
LO	Local Oscillator
LPF	Low-Pass Filter
LPN	Laser Phase Noise
LTE	Long-Term Evolution
MAE	Mean Absolute Error
MBWA	Mobile Broadband Wireless Access
MIMO	Multiple Input Multiple Output
ML	Maximum Likelihood
MMSE	Minimum Mean Squared Error
MSCO-OFDM	Modified SCO-OFDM
MZM	Mach Zehnder Modulator
NLSE	Nonlinear Schrodinger equation
OA	Optical Amplifier
OBPF	Optical Band-Pass Filter
OBSF	Optical Band-Stop Filter
OFDM	Orthogonal Frequency Division Multiplexing
OSNR	Optical Signal to Noise Ratio
OTR	Optical-To-RF
P/S	Parallel to Serial
PAPR	Peak-to-Average Power Ratio
PBC	Polarization Beam Combiner
PBS	Polarization Beam Splitter
PCM	Pulse Code Modulation
PD	Photo Diode
PDL	Polarization Dependent Loss
PDM	Polarization Division Multiplexing
PM	Phase Modulation
PMD	Polarization Mode Dispersion
PPF	Partial Pilot Filling
PRBS	Pseudo Random Binary Sequence
PSK	Phase Shift Keying
PSR	Pilot-to-Signal Ratio
QAM	Quadrature Amplitude Modulation
QPSK	Quadrature Phase Shift Keying
RC	Raised Cosine
RFP	Radio-Frequency Pilot
RMSE	Root Mean-Squared Error
ROP	Received Optical Power
RTO	RF-To-Optical

Rx	Receiver
S/P	Serial to Parallel
SBS	Stimulated Brillouin Scattering
SC-FDM	Single Carrier Frequency Division Multiplexing
SCO-OFDM	Self Coherent Optical OFDM
SDFT-S-OFDM	Self DFT-S-OFDM
SNR	Signal to Noise Ratio
SPM	Self Phase Modulation
SR-RC	Square Root Raised-Cosine
SRS	Stimulated Raman Scattering
SSMF	Standard Single Mode Fiber
TS	Training Symbol
TV	Television
Tx	Transmitter
U.S.	United States
Washington D.C.	Washington District of Columbia
WDM	Wavelength-Division Multiplexing
WiMAX	Worldwide Interoperability for Microwave Access
WLAN	Wireless Local Areas Network
XPM	Cross-Phase Modulation
ZF	Zero Forcing
ZP	Zero Padding

List of Symbols

Variable	*Unit*	*Description*
$\boldsymbol{R}$	bit/sec	Bit rate
$\boldsymbol{N_{sc}}$		Number of OFDM subcarriers
$\Delta \boldsymbol{f}$	Hz	Frequency spacing
$\boldsymbol{T_s}$	sec	Symbol duration
$\boldsymbol{\omega_k}$	rad/sec	Angular frequency at k^{th} subcarrier
$\emptyset_{\boldsymbol{k}}$	rad	Phase at k^{th} subcarrier
$\boldsymbol{T_g}$	sec	Guard time
$\boldsymbol{N_g, N_{cp}}$		Guard sample
$\boldsymbol{t_d}$	sec	Delay time
$\boldsymbol{f_s}$	Hz	Sampling frequency
$\varepsilon_{\boldsymbol{cp}}$		Cyclic prefix overhead
$\boldsymbol{T_0}$	sec	OFDM observation period
$\varepsilon_{\boldsymbol{ts}}$		Training overhead
$\boldsymbol{N_{ts}}$		Number of training symbols
$\boldsymbol{N_{sy}}$		Number of OFDM symbols
i		OFDM symbol index
k		OFDM subcarrier index
$\boldsymbol{Y, R}$		Received OFDM data symbols
$\boldsymbol{H}$		Channel transfer function
$\boldsymbol{X}$, T		Transmitted OFDM data symbols
$\boldsymbol{M}$		QAM modulation level
$\boldsymbol{DGD}$	sec	Differential group delay
$\boldsymbol{D}$	sec/m^2	Chromatic dispersion parameter
$\boldsymbol{c}$	m/sec	Light speed
$\boldsymbol{f_c}$	Hz	Optical carrier frequency
$\Delta\nu$	Hz	Laser linewidth
$\hat{\boldsymbol{f}}_{\boldsymbol{off}}$	Hz	Estimated frequency offset
$\emptyset_{\boldsymbol{D}}$	rad	Chromatic dispersion phase dispersion
$\boldsymbol{\alpha}$		Roll off factor
$\boldsymbol{N_{zp}}$		No. of zero padding in one OFDM symbol
$\boldsymbol{N_{FFT}}$		IFFT/FFT size
$\boldsymbol{N_P}$		No. of pilots in one OFDM symbol
$\emptyset_{\boldsymbol{ld}}$	rad	Phase noise of laser

$\boldsymbol{\lambda}$	m	Wavelength
$\boldsymbol{M(d)}$		Timing metric function
$\boldsymbol{R_{cor}(d)}$		Correlation function of the received signal
$\boldsymbol{C_{IQ}(i)}$		I and Q components of known TS
$\boldsymbol{n}$		Refractive index
$\boldsymbol{n_0}$		Refractive index for the linear effec
$\boldsymbol{n_2}$	m^2/W	Kerr factor (second-order refractive index)
$\boldsymbol{A_{eff}}$	m^2	Effective core area of the fiber
$\boldsymbol{P}$	W	Launched power
$\boldsymbol{\beta}$		Propagation constant
$\boldsymbol{\beta_0}$		Propagation constant for the linear effect
$\boldsymbol{\gamma}$	$W^{-1}\ m^{-1}$	Nonlinear coefficient
$\boldsymbol{P_0}$	W	Initial launch power
$\boldsymbol{L_{eff}}$	m	Effective length
$\boldsymbol{L_{Nl}}$	m	Nonlinear length

Chapter 1: Introduction

1.1 Overview

Communication can be defined as exchange of data between two or a group of people. The communication history dates back to the old ages; the communication methods have gradually been improved, from smoke signals, semaphore to telegraph. In 1837, Morse developed telegraph and transmitted the word "What hath God wrought" between Washington District of Columbia (Washington D.C.) and Baltimore. In 1875, Alexander Graham Bell invented the telephone and made the first analog communication experimental by transmitting the real time speech. The electrical Phone invention is the cumulative work of many people between 1854 -1879. Many conflicts and lawsuits were occurred to determine the inventor. A German scientist Johann Philipp Reis invented the first prototype telephone in 1861 which is called Reis telephone. The Reis telephone is used to transmit sound but it failed to receive the spoken word successfully. A patent caveat was submitted at the United States (U.S.) Patent Office for a device which is called Sound Telegraph by Antonio Meucci in 1871. Antonio did not have enough money to submit a patent. Finally, Alexander Graham Bell made the first analog communication experimental by transmitting the real time speech in 1875 using his prototype. In 1876, Bell granted the U.S. patent for the telephone. Thomas Edison said: "The first inventor of a telephone was Phillip Reis of Germany only musical not articulating. The first person to publicly exhibit a telephone for transmission of articulate speech was A. G. Bell. The first practical commercial telephone for transmission of articulate speech was invented by myself. Telephones used throughout the world are mine and Bell's. Mine is used for transmitting. Bell's is used for receiving." [1, 2].

Heinrich Hertz proved experimentally the existence of electromagnetic waves in 1887 which is known as Hertzian waves. Based on Hertizan waves, Marconi invented the first wireless telegraphy system and won the Nobel Prize in Physics in 1909 for his patent. A revolution in wireless communications was quickly followed by super-heterodyne radio in 1918 and pulse code modulation (PCM) in 1937. In 1939, the first commercial television (TV) broadcasting was transmitted by the British broadcasting corporation (BBC). The first

coaxial cables are developed in the 1940s. The required for long distance communications were increased [1, 2].

Optical communications came into real in 1960s. Between 1959 and 1960, light amplification by stimulated emission of radiation (Laser) had been invented. In 1966, Kao and Hockham proposed the first optical fiber communication with high attenuation about 1000 dB/km which was not comparable with coaxial cables (5 dB/km). The optical fiber was successfully fabricated in 1970 and the losses were greatly reduced about 20 dB/km. In the 1970s the optical fiber losses were decreased to below 5 dB/km. The first commercial optical communication system was proposed in 1975 [3].

Optical communication systems sometimes called light wave systems, it use high optical carrier frequencies over 100 THz. It deployed worldwide for telecommunications applications since 1980. Optical communication systems can be classified into two categories: guided and unguided systems. In the case of guided optical system, it uses optical fibers to guide the optical signal. Therefore, it is called fiber optical communications. While in unguided optical system, the optical signal is emitted in the space which is called free-space optical communications. An accurate pointing between the transmitter and receiver is required.

The fiber optical communications can be classified according to transmission distance into two categories: short haul and long haul transmission systems compared with intercity distances (~ 80 km). Short haul transmission systems operate at low bit rates over distances of less than 10 km which is not very cost-effective. Long haul transmission systems operate at high bit rates over distance more 80 km. Moreover, there are commercial products using distance of 25, 40, 60 km. Using optical amplifiers, transmission distances of thousands of kilometers can be realized [4].

The first generation of fiber optical communications operated at a bit rate of 45 Mb/s with repeater spacing up to 10 km. Single-mode fiber is used in the second generation instead of multi-mode fiber to reduce the fiber dispersion. Hence, the system bit rate was increased to 1.7 Gb/s over 50 km. In 1990, the third generation is launched with bit rate of 2.5 Gb/s. After 1985, erbium-doped fiber amplifiers (EDFA) are developed. Therefore, the fourth generation used optical amplifiers and wavelength-division multiplexing (WDM) technique

to increase the repeater spacing up to 60-80 km and the system bit rate up to 10 Tb/s in 2001[4].

Optical communication systems can also be categorized according to modulation techniques into single-carrier and multicarrier modulations. In the case of single-carrier modulation the data are carried in a single carrier frequency, or equivalently wavelength. Such technique is the conventional format in the optical communication for many years. The WDM and orthogonal frequency division multiplexing (OFDM) are forms of multicarrier modulation techniques. In multi-carrier systems, the transmitted high-bit-rate serial data are divided into low-bit-rate parallel streams to be transmitted over multiple carriers. The WDM multiplexes several optical carrier signals at different wavelengths on a single optical fiber [5]. The technology of OFDM was proposed for the first time in 1966 by Chang of Bell Labs [6] without cyclic prefix (CP) extension. The importance of insert CP was presented in 1980 which is vital for OFDM implementations [7]. The application of OFDM in the wireless mobile communication was pioneered in 1985 [8]. The application of OFDM is widely used for digital audio broadcasting (DAB) and digital video broadcasting (DVB) in Europe and for asymmetric digital subscriber line (ADSL) high data rate wired communications. It has been used in major communication standard, for example standardized in wireless local areas network (WLAN) which known as institute of electrical and electronics engineers (IEEE) 802.11 a/b, fourth generation (4G) mobile network and long-term evolution (LTE) network. Also, it uses in worldwide interoperability for microwave access (WiMAX) which known as IEEE 802.16 and Mobile Broadband Wireless Access (MBWA) IEEE 802.20.

In 1996, the research on OFDM in optical communication is started. The application of OFDM in optical communication system for long haul transmission has been investigated since 2001 by few groups [9]. The optical OFDM systems can be classified into three approaches according to the detection scheme. The approaches are:

1. In 2006, direct detection optical OFDM (DDO-OFDM) was first investigated by Lowery [10] which is looking into a simple implementation based on low cost optical components.
2. In 2006, Shieh [11] investigated coherent optical OFDM (CO-OFDM), which can mitigate chromatic dispersion (CD). In 2007, Shieh [12] proved that CO-OFDM can mitigate polarization mode dispersion (PMD).

3. Self coherent optical OFDM (SCO-OFDM) was investigated in 2008 by Xu [13].

The interest in OFDM in the optical communication is evidenced by an increase in the number of conference papers, journal publications and many experimental implementations of optical OFDM systems.

1.2 Motivation of the Dissertation

In this section, the motivation of the work accomplished in this dissertation is explained. The theoretical fundamentals for OFDM were presented. The different architectures of optical OFDM were explained. The performance analyses among those systems are provided. As well as CO-OFDM systems combine the advantages of coherent detection and OFDM modulation, it exhibits advantages over conventional single-carrier systems. However, it has a number of disadvantages. The drawbacks of CO-OFDM are the high peak-to-average power ratio (PAPR) and the high sensitivity to frequency offset and phase noise. Phase noise in CO-OFDM transmission system is generated not only by transmitter laser and receiver local oscillator (LO), but also by nonlinear optical fiber transmission which produces a nonlinear phase noise. Moreover, it is prone to in-phase/quadrature (I/Q) imbalance. Hence, it is essential to study CO-OFDM transmission in presence of phase noise. Furthermore, it is important to develop algorithms to compensate (i) laser phase noise (LPN), (ii) nonlinear phase noise and (iii) enhance the performance of optical OFDM transmission systems. Consequently, the ultimate objective of the dissertation is to focus on topics in relation to enhance CO-OFDM system performance. Toward achieving such objective, the dissertation will focus on:

- Improving the efficiency of CO-OFDM systems by using different pulse shaping.
- Developing laser phase noise compensation methods in CO-OFDM transmission.
- Developing fiber nonlinearity mitigation techniques in CO-OFDM transmission.
- Enhancing optical OFDM systems by combing the advantages of SCO-OFDM and discrete Fourier transform spread OFDM (DFT-S-OFDM).

1.3 Contribution of the Dissertation

To achieve the objectives listed in the previous section; the dissertation provides a set of techniques which mainly improve the performance of the CO-OFDM systems. The contributions of the dissertation are listed as follows:

In Chapter 3, non-rectangular window functions like square root raised-cosine or raised-cosine windows smoothen the spectra ends and suppress side-lobes more strongly. Therefore, a square root raised-cosine window of OFDM symbols is proposed to enhance out-of-band power suppression of the OFDM spectral. Hence, the efficiency of CO-OFDM systems is improved. Numerical simulation results of CO-OFDM systems over 2400 km are investigated using VPItransmissionMakerTM.

In Chapter 4, performance analysis of radio frequency pilot (RFP) phase noise compensation for CO-OFDM transmission systems via common phase error (CPE) equalizer is presented. Such technique uses the RFP technique to mitigate the effect of the laser phase noise in combination with the CPE method. Also, it is significant for fiber nonlinearities mitigation. A numerical simulation is carried out to investigate the partial pilot filling (PPF) phase noise compensation algorithm for LPN in CO-OFDM systems. Moreover, it compared to conventional CPE algorithm and RFP based phase noise compensation scheme. The PPF compensation for nonlinear phase noise mitigation has been analyzed for a 1200-km CO-OFDM transmission system with inline dispersion compensation. The simulation results show that PPF scheme effectively compensates self phase modulation (SPM) induced by fiber nonlinearity. Furthermore, frequency domain dual compensators scheme for laser and nonlinear phase noise mitigation is proposed for CO-OFDM long haul transmission systems. The first compensator is similar to the CPE compensator. The second compensator estimates the phase noise of the remaining intermediate samples by linear interpolation using every two consecutive pilots.

Chapter 5 provides a new DFT-S-OFDM architecture by extracting the optical carrier from the optical OFDM signal at the receiver. The effects of phase noise for various laser linewidths and of received optical power on system performance are evaluated. In addition, the tolerance of the investigated system for mitigation of fiber nonlinearities in long-haul systems is shown. The system performance is investigated and compared to conventional DFT-S-OFDM. The analysis has been simulated with VPItransmissionMaker™ V9.0.

1.4 Outline of the Dissertation

The dissertation is organized in six chapters and a list of references. Chapter 1 presents an overview on dissertation, research motivation and the contributions of the dissertation.

Following the introduction, OFDM principles in the wireless communication systems are presented in Chapter 2. The chapter illustrates theoretical principles of OFDM with detailing on the advantages and disadvantages of OFDM compared to the single carrier modulation technology. Challenges in OFDM transmission systems are presented

Optical OFDM systems are represented in details in Chapter 3. The chapter provides the theoretical fundamentals for Optical OFDM systems and the different classifications which proposed for Optical OFDM systems. Performance of the three existing approaches are elaborated and compared. The principles of an OFDM signal processing algorithms related to frame synchronization, frequency offset compensation and channel estimation are presented. Moreover, polarization division multiplexing (PDM) optical OFDM systems are explained. Finally, the principle of a square root raised-cosine pulse shaping of OFDM symbols to enhance the efficiency of CO-OFDM systems is discussed.

Chapter 4 presents laser and nonlinear phase noise components in CO-OFDM transmission systems. The effect of laser and nonlinear phase noise on the performance of CO-OFDM transmission systems is provided. The chapter presents the cause and solution of laser and nonlinear phase noise effect on CO-OFDM systems performance. Different existing algorithms of laser and nonlinear phase noise compensation will be discussed in detail. Three new approaches are presented and compared numerically.

Chapter 5 represents DFT-S-OFDM in optical systems. A new self coherent optical DFT-S-OFDM (SDFT-S-OFDM) system architecture which combines the benefits from both SCO-OFDM and DFT-S-OFDM systems will be investigated. Principle of the new system is presented with numerical simulations.

Finally, Chapter 6 summarizes and concludes the outcomes of the dissertation. The dissertation ends with a comprehensive bibliography of all references cited throughout it.

1.5 Publications

The content of the dissertation is the result of collaborative research on phase noise compensation aspects and enhance the system performance of CO-OFDM systems, which have been published in various reputed forums. Here is a list of relevant publications with the author's participation.

1. **S. Hussin** and R. Noé, "Fiber nonlinearity Mitigation in CO-OFDM Systems using Dual Compensators," in *27th IEEE PHOTONICS CONFERENCE (IPC)*, 12-16 Oct. 2014, San Diego, California, USA.
2. **S. Hussin** and R. Noé, M.F. Panhwar, "Fiber Nonlinearity Tolerance of Partial Pilot Filling in CO-OFDM in Transmission Systems," in *IEEE 19th Opto-Electronics and Communications Conference (OECC)*, 6-10 July 2014, Melbourne, Australia.
3. **S. Hussin** and R. Noé, M.F. Panhwar, "Improvement of RF-Pilot Phase Noise Compensation for CO-OFDM Transmission Systems via Common Phase Error Equalizer," *in IEEE 19th Opto-Electronics and Communications Conference (OECC)*, 6-10 July 2014, Melbourne, Australia.
4. **S. Hussin**, K. Puntsri, M.F. Panhwar and R, Noé, "Partial Pilot Filling for Phase Noise Compensation in Coherent Optical OFDM Systems", *in IEEE 18th Opto-Electronics and Communications Conference (OECC)*, 30 Jun-4 July 2013, Kyoto, Japan.
5. K. Puntsri, O. Jan, A. Al-Bermani, D. Sandel, C. Wördehoff, **S. Hussin**, M. F. Panhwar, U. Rückert and R. Noé, "Pilot-aided CD and PN Compensation Simultaneously in CO-OFDM Systems", *in IEEE 18th Opto-Electronics and Communications Conference (OECC)*, 30 Jun-4 July 2013, Kyoto, Japan.
6. **S. Hussin**, K. Puntsri, M.F. Panhwar, D. Sandel and R, Noé, "Efficiency Enhancement of CO-OFDM Systems Using Different Pulse Shapes", *in IEEE 18th Opto-Electronics and Communications Conference (OECC),* 30 Jun-4 July 2013, Kyoto, Japan.
7. **S. Hussin**, K. Puntsri and R. Noé, "Analysis of partial pilot filling phase noise compensation for CO-OFDM systems," *IEEE Photonics Technology Letters*, vol. 25, no. 12, pp. 1099–1102, 2013.
8. K. Puntsri,O. Jan, Omar, A. Al-Bermani, C. Wördehoff, D. Sandel, David, M. F. Panhwar, **S. Hussin**, U. Rückert and R. Noé ," ISI Tolerance of Cyclic Prefix Free Coherent Optical OFDM Communication systems", *in 14th ITG- symposium* "*Photonische Netze",* 6-7 May 2013, Leipzig, Germany.
9. K. Puntsri, O. Jan, A. Al-Bermani, C. Wördehoff, D. Sandel, **S. Hussin**, M. F. Panhwar, R. Noé and U. Rückert, "An Ultralow Complexity Algorithm for Frame Synchronization and IQ Alignment in CO-OFDM Systems," *in Optical Fiber Communication and*

National Fiber Optic Engineers Conference (OFC/NFOEC), JTh2A.4.3, 19-21 March. 2013, Anaheim, California, USA.

10. K. Puntsri, D. Sandel, **S. Hussin**, O. Jan, A. Al-Bermani, M. F. Panhwar and R. Noé ," A Low Complexity and High Accuracy Frame Synchronization for Optical OFDM and PolMux-Optical OFDM, " *in 25th IEEE Photonics Conference (IPC)*, 23-27 Sept. 2012, San Francisco, California , USA.
11. **S. Hussin**, K. Puntsri and R. Noé, "Efficiency Enhancement of RF-Pilot-Based Phase Noise Compensation for Coherent Optical OFDM,*" in IEEE 17th International OFDM Workshop (InOWo'12)*, 29-30 Aug. 2012, Essen, Germany.
12. K. Puntsri, V. Mirvoda, **S. Hussin**, Omar H.A. Jan, A. Al-Bermani, M. F. Panhwar and R. Noé, " A Low Complexity and High Accuracy Frame Synchronization for PolMux-Optical OFDM," *in ITG-Workshop section 5.3.1 Modeling of photonic components and systems*, 5-6 July 2012, Nurnberg, Germany.
13. K. Puntsri, D. Sandel, **S. Hussin**, O. Jan, A. Al-Bermani and R. Noé, " A Novel Method for IQ Imbalance Compensation in CO- OFDM systems," *in IEEE 17th Opto-Electronics and Communications Conference (OECC)*, 2-6 July 2012, Busan, Korea.
14. **S. Hussin**, K. Puntsri and R. Noé, "Performance Analysis of RF-Pilot Phase Noise Compensation Techniques in Coherent Optical OFDM Systems," *in IEEE 17th European Conference on Network and Optical Communications (NOC)*, 20-22 June 2012, Barcelona, Spain.
15. **S. Hussin**,K. Puntsri and R. Noé, "Performance Analysis of Optical OFDM systems,*" in IEEE 3rd International Congress on Ultra Modern Telecommunications and Control Systems (ICUMT)*, 5-7 Oct. 2011, Budapest, Hungary.
16. K. Puntsri, S. Hoffmann, **S. Hussin**, A. Al-Bermani and R. Noé, "A Low Complexity and High Accuracy Frame Synchronization for Optical OFDM Systems," *in IEEE 16th Opto-Electronics and Communications Conference (OECC)*, 4-8 July 2011, Kaohsiung, Taiwan.

Chapter 2: OFDM Principles

2.1 Introduction

The chapter provides an introduction to the OFDM principles in wireless communication systems. Section 2.2 explains the single carrier systems and multicarrier systems describing its differences. An initial overview of OFDM compared to the conventional multicarrier techniques and the importance of orthogonality will be presented in Section 2.3. The system design and mathematical description of basic OFDM, fast Fourier transformation (FFT) and CP is explained in Section 2.4. Furthermore, advantages and disadvantages between OFDM and single carrier systems are reported. Finally, the theoretical results of systems performance will be discussed in Section 2.5.

2.2 Single Carrier vs. Multi Carrier

All wireless communication systems modulate the information signal to be effectively transmitted over the communication channel. Different methods of modulation techniques have been developed according to whether the information signal is an analogue or a digital signal.

Single carrier modulation system transmitted the information signal serially over the channel by modulating only a sinusoidal signal (carrier signal). It modifies only one of three parameters of the carrier signal which are amplitude, frequency, or phase according to the information signal. The techniques are called amplitude modulation (AM), frequency modulation (FM) and phase modulation (PM), respectively, according to the parameter of the carrier signal which is modified for the analogue communication. In the case of the digital communications, the modulation techniques are called amplitude shift keying (ASK), frequency shift keying (FSK) and phase shift keying (PSK) [14].

In the wireless communication systems, radio channels are often modeled as linear time-variant model. The channels are strongly affected by multipath propagation (frequency selective fading channel) caused by reflection, diffraction and scattering as shown in Fig. 2.1. Therefore, the received signal will contain not only a direct light of sight wave but also a large number of reflected and diffracted waves with various time delays. Such signals overlap each other which results in inter-symbol interference (ISI). As the data rate increases,

the time duration of each bit will be smaller causing the system to become more prone to noise. As the single carrier system uses a wideband channel, therefore the signal will interfere highly with neighboring signals. Such type of interference is known as crosstalk. A very complex signal processing using a complex equalizer is required to compensate for the interferences [15]. These problems have been studied and proposed many solutions.

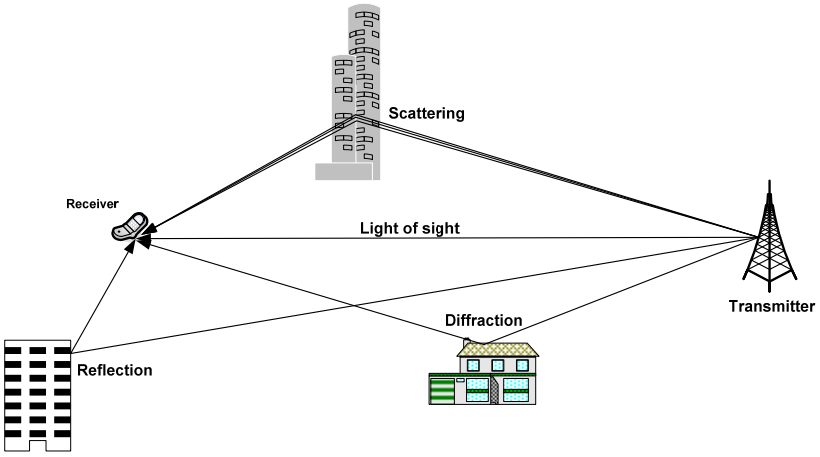

Fig. 2.1: Multipath propagation with various effects.

Parallel data transmission known as multicarrier technique can be used to combat ISI which is caused by frequency selective fading channels. Multicarrier system has been invented in 1957 [16]. It is used in the military applications due to the system complexity and restriction of using the frequency bands. The first proposal was published in 1967 [17]. Whereas, the available bandwidth is divided into N non-overlapping sub-bands (sub-channels or subcarriers). Then, the subcarriers are frequency multiplexed. Instead of transmitting serial data symbols, the high data stream R is divided into N blocks of data symbols with reduced data rate of R/N. It are summed together and transmitted in parallel by modulating the N separated narrow band subcarriers. Therefore, it gives the same data rate of an equivalent single carrier system. The guard bands between adjacent subcarriers are used to prevent the possible interference among adjacent subcarriers which known as inter-carrier interference (ICI). The guard bands produce a waste of spectrum. At the receiver, the wideband signal is separated into the original narrowband subcarriers for demodulation using a group of filter banks [18, 19]. Using error-correcting codes, data can be recovered correctly the received signal. Figure 2.1 illustrates the spectrum of the conventional signal carrier system and non-overlapping multicarrier technique.

The main advantage of multicarrier techniques such as frequency division multiplexing (FDM) is less prone to channel distortions. It introduces ISI less than single carrier system at same data rates. The equalization complexity in the receiver is reduced dramatically. While, the main drawbacks are large number of filter banks required in the transmitter and receiver. It reduces the spectrum efficiency due to use guard bands between adjacent subcarriers [15].

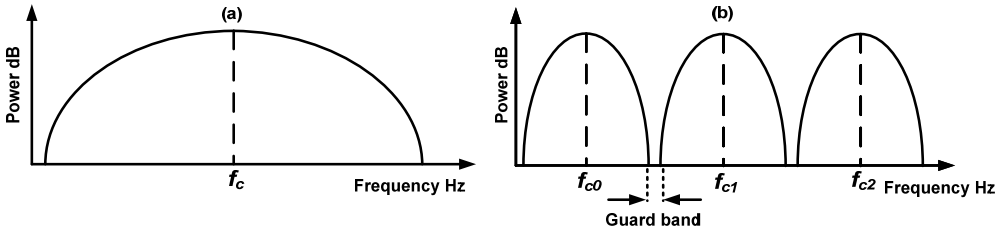

Fig. 2.2: Concept of (a) single carrier technique; (b) non-overlapping multicarrier technique.

2.3 OFDM Fundamentals

To overcome the inefficient use of the available spectrum, the OFDM is proposed in 1966 by Chang [6] as an overlapping multicarrier technique. The OFDM is a special case of FDM where the guard bands between adjacent subcarriers can be removed. Figure 2.3 shows the spectra difference between the non-overlapping technique and overlapping. OFDM can save bandwidth compared to non-overlapping technique [15]. The subcarriers are orthogonal to each other to recognize the overlapping and reduce the ICI between subcarriers.

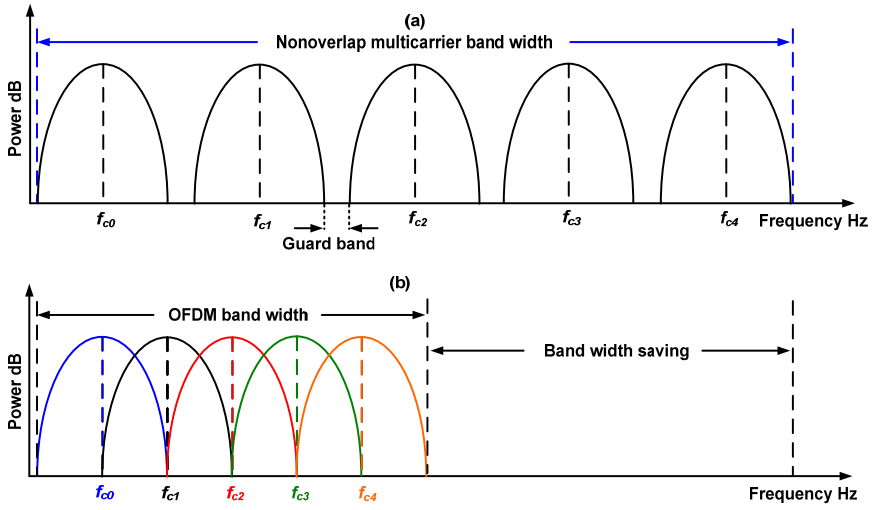

Fig. 2.3: Concept of multicarrier techniques (a) Non-overlapping; (b) Overlapping (OFDM).

Frequency offset in the OFDM systems loses the orthogonality among the OFDM subcarriers, which leads to ICI and hence degrades the system performance.

In the early OFDM scheme, Chang used an analog implementation of Fourier transforms. Figure 2.4 shows Change system with N transmitting filters [6]. $A(f)$ and $\alpha(f)$ are the amplitude and phase characteristic of the transmitting filters, respectively. While, the amplitude and phase characteristic of the transmission medium are $H(f)$ and $\eta(f)$, respectively. Change system used an extremely complex structure of analog oscillators and filters to generate orthogonal subcarriers.

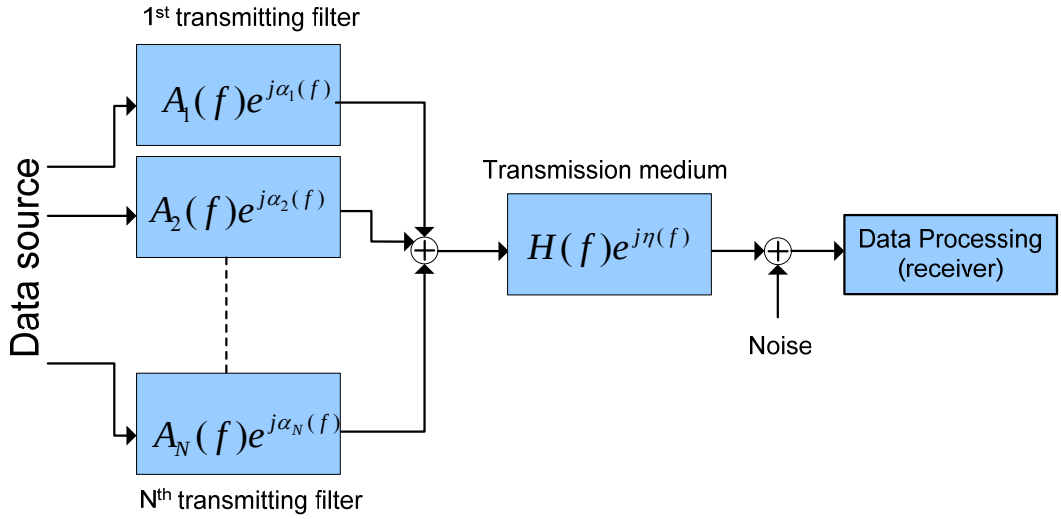

Fig. 2.4: Chang OFDM system with transmitting filters.

Instead of applying filter banks, block of oscillators and mixers at the transmitter and receiver for each subcarrier at discrete frequencies; OFDM can be implemented using inverse fast Fourier transformation (IFFT) at the transmitter and FFT at the receiver. Thus, simplified channel equalization techniques can be used. Salz of Bell Labs [20] used the first proposal of FFT to generate the orthogonal signals in 1969.

Figure 2.5 represents a typical OFDM signal of five subcarriers in both time and frequency domains. Figure 2.5 (a) shows the OFDM signal in a time domain where all subcarriers have the same phase and amplitude, but in practice each subcarrier may have different amplitude and phase. The OFDM subcarriers orthogonality can be presented in the frequency domain as shown in Fig. 2.5 (b). The OFDM spectrum contains five subcarriers which is a convolution of a group of Dirac delta function located at the subcarrier frequencies

with a spectrum of an ideal square pulse (windowing function). The square pulse spectrum is a sinc function. Obviously, the neighboring subcarriers (sinc spectra) are overlapped with each other. The power of an adjacent subcarrier equals to zero at the central frequency of the maximum of each specific subcarrier spectrum.

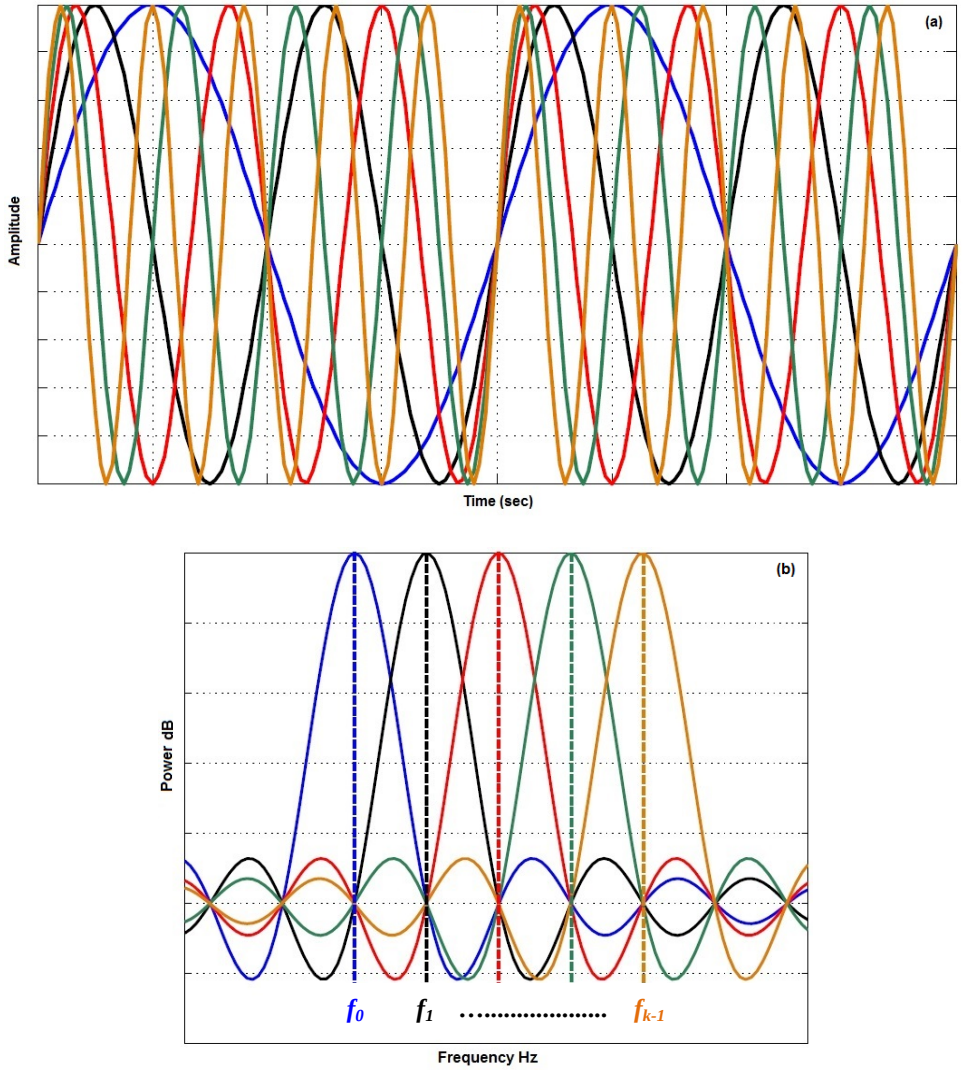

Fig. 2.5: OFDM symbol with 5 subcarriers (a) in time domain; (b) in frequency domain.

The major advantage of OFDM technique is increasing the spectrum efficiency. It is realized by overlapping the neighboring subcarriers with each other in the frequency domain. So, the subcarriers will be orthogonal if the dot product of two signals equals to zero. Orthogonal means that there is an accurate mathematical relationship between the frequencies of the different subcarriers in the system (Appendix A).

2.4 OFDM System Design

The main idea of OFDM is that the input high bit rate serial data are converted to the low bit rate parallel block of bits which are transmitted over a number of overlapped subcarriers. In OFDM system design, the following parameters must been taken into consideration

1. The number of subcarriers N_{sc}.
2. The guard time between OFDM symbols to prevent ISI.
3. The frequency spacing Δf to prevent the frequency offset.
4. Symbol duration T_s.
5. The modulation type.

Figure 2.6 shows the basic block diagram of wireless OFDM transmission system. At the transmitter, a symbol rate R_s is generated from a pseudorandom binary sequence (PRBS). The serial data rate is converted to low data rate (R_s/N_{sc}) parallel blocks of bits, where N_{sc} is the number of parallel data paths. The blocks of bits contain information symbols of N_{sc} subcarriers. The information symbols are mapped by suitable modulation format such as quadrature amplitude modulation (QAM) or quadrature phase shift keying (QPSK). By IFFT, one obtains N_{sc} orthogonal subcarriers with equally spaced frequencies Δf.

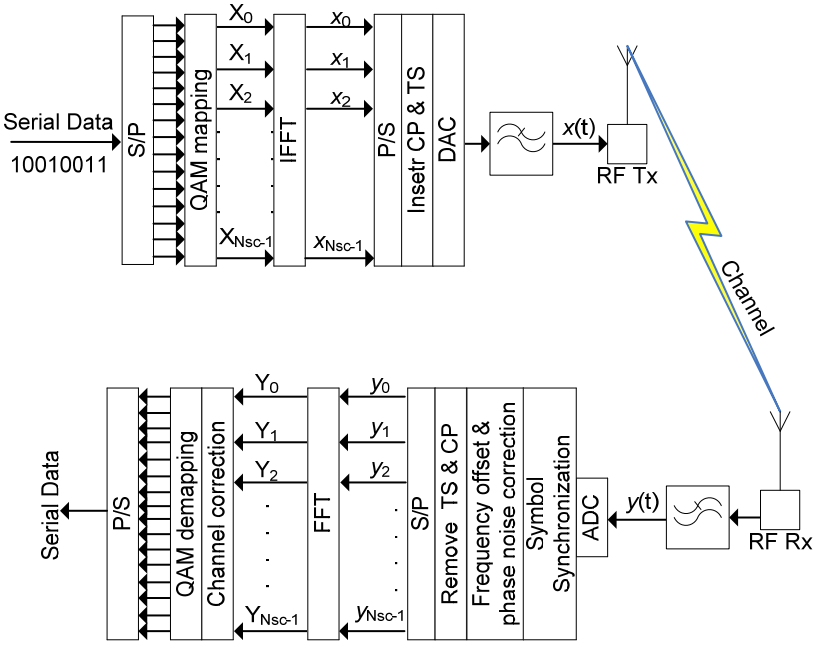

Fig. 2.6: Wireless OFDM transmission system.

The IFFT size determines the numbers of subcarriers. Increasing the IFFT size makes the signal less susceptible to ISI between OFDM symbols and reduces the overhead of guard interval. Its drawbacks are the increased processing complexity at the transmitter and receiver. Moreover, it increases the sensitivity to the phase noise. As long as the OFDM signal is a special case of multicarrier technique like FDM, it consists of a sum of N_{sc} channel number with the carrier frequencies $f_0, f_1, f_2, \ldots\ldots f_{N_{sc}-1}$, each transmitted FDM signal can be represented as

$$x_k(t) = A_k(t)e^{j(\omega_k t+\emptyset_k(t))} \tag{2.1}$$

where k is channel index from 0 to N_{sc}-1, $A_k(t)$ is amplitude of transmitted complex data at the k^{th} channel , ω_k is the angular frequency and $\emptyset_k(t)$ is the phase at k^{th} channel. The pulse shape function is dropped to simplify the equation. The combined FDM signal can be written as

$$x(t) = \sum_{k=0}^{N_{sc}-1} A_k(t)\, e^{j(\omega_k t+\emptyset_k(t))} \tag{2.2}$$

The FDM signal uses non-overlapped technique with broader bandwidth because of spacing between consecutive channels. While, OFDM signal uses overlapping technique with orthogonal subcarrier. To provide the orthogonality in between each two consecutive subcarriers, the following condition should be set

$$\omega_k = \omega_0 + k\frac{2\pi}{T_s} = 2\pi(f_0 + k\Delta f) \tag{2.3}$$

where f_0 is the lowest subcarrier frequency and Δf is the OFDM subcarrier spacing frequency. For each symbol, the subcarriers amplitude and phase depend on the frequency of that particular subcarrier; so it can be rewritten as $A_k(t) => A_k$ and $\emptyset_k(t) => \emptyset_k$. Thus, the complex continuous OFDM signal can be rewritten as

$$x(t) = \sum_{k=0}^{N_{sc}-1} A_k\, e^{j(\omega_k t+\emptyset_k)} \tag{2.4}$$

Filter banks, block of oscillators and mixers at the transmitter and receiver to generate subcarrier at discrete frequencies has been applied in the early version of OFDM technique.

Using IFFT at the transmitter and FFT at the receiver, OFDM can be implemented in digital domain and the system complexity is largely reduced.

Due to the subcarrier frequencies are uniformly spaced in the frequency domain; for simplicity, assume $f_0 = 0$. Then, if the signal is sampled at sampling frequency $\frac{1}{T_s}$, the resulting OFDM signal is expressed as

$$x(nT_s) = \sum_{k=0}^{N_{sc}-1} A_k e^{j\emptyset_k} e^{j2\pi k\Delta f nT_s} \tag{2.5}$$

The OFDM signal is analyzed to N_{sc} samples over a period of one data symbol. Thus, we have a relationship of $t = N_{sc}T_s$. The general form of IFFT is

$$g(nT_s) = \frac{1}{N_{sc}} \sum_{k=0}^{N_{sc}-1} G(\frac{n}{N_{sc}T_s}) e^{j\emptyset_k} e^{\frac{j2\pi nk}{N_{sc}}} \tag{2.6}$$

From Eq. (2.5), the term $A_k e^{j\emptyset_k} = X_k$ is a definition of the signal in the sampled frequency domain, and $x(nT_s)$ is a time domain signal. Eq. (2.5) and Eq. (2.6) are equal if

$$\Delta f = 1/(N_{sc} \times T_s) \tag{2.7}$$

By multiplying constant $\frac{1}{N_{sc}}$ in Eq. (2.5), where N_{sc} is a power of two. Then, Eq. (2.5) of one OFDM symbol becomes the same as the equation of the N-point IFFT

$$x_n = x(nT_s) = \frac{1}{N_{sc}} \sum_{k=0}^{N_{sc}-1} X_k e^{\frac{j2\pi nk}{N_{sc}}} \tag{2.8}$$

The IFFT is fast and very efficiently algorithm for implementing an inverse discrete Fourier transforms (IDFT) operation. It decreases the processing complexity at the transmitter and receiver. The N point discrete Fourier transforms (DFT) requires N^2 complex multiplications and $N^2 - N$ complex adder. It requires a complex signal processing at the transmitter and receiver. Using radix-2 method to realize FFT, the complex multiplication decreases to $\frac{N}{2}\log_2 N$ and complex adder decreases to $N \log_2 N$. The complex multiplication can be decreased to $\frac{3N}{8}\log_2 N$ by using radix-4, while the complex adder is still the same of radix-2 [21]. Through the dissertation, uppercase represents frequency domain variables and

lowercase represents time domain variables. A comparison of the number of complex multipliers and adders is shown in Table 2.1.

	Complex multiplications	Complex adder
DFT	N^2	$N^2 - N$
FFT using radix-2	$\frac{N}{2}\log_2 N$	$N \log_2 N$
FFT using radix-4	$\frac{3N}{8}\log_2 N$	$N \log_2 N$

Table 2.1: Computional cost.

The FFT/IFFT is used to compute the frequency and the time component of a sampled signal assuming that the signal is periodic [22]. From this feature, the signal in the time domain must repeat continually. Then, the signal spectrum repeats periodically in the frequency domain. After IFFT, the complex vector x is then converted back into a serial data stream.

As mentioned in Section (2.2), wireless channels are strongly affected by multipath propagation. The received signal will contain different waves with various time delays t_d. The signals overlap each other which produce ISI. OFDM is a very effective technique to deal with such problem. To avoid ISI between OFDM symbols, a guard time T_g is inserted for each OFDM symbol [15]. The guard time must be selected larger than multipath delay time as

$$T_g > t_d \tag{2.9}$$

The guard time can be formed by two methods. The first one, the guard time contains zeros “no signal”. Therefore, it introduces ICI, as the orthogonality among the subcarriers will be lost when multiple of the time delayed OFDM signals are received. To compensate for ICI, a CP is inserted. The CP is formed by copying the last N_g samples of each OFDM symbol to the beginning of the same symbol as shown in Fig. 2.7. The T_g can be represented in samples N_g as

$$N_g = f_s \cdot T_g \tag{2.10}$$

where f_s is the sampling frequency of digital-to-analog converter (DAC). The CP produces overhead due to it contains redundant information. To minimize the overhead, a good selection of minimum T_g is required. The CP overhead ε_{cp} can be written as [23]

$$\varepsilon_{cp} = N_g \; / \; N_{sc} \tag{2.11}$$

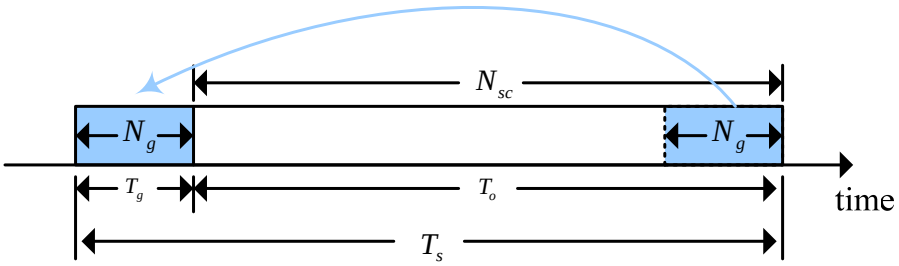

Fig. 2.7: OFDM symbol showing the cyclic prefix.

The total OFDM symbol duration can be written as

$$T_s \; = \; T_g + \; T_0 \tag{2.12}$$

where T_0 is detection window "observation period" which is used to generate OFDM signal from IFFT. T_S is the total OFDM symbol duration which consists of the cyclic prefix and the observation period. It should be noted that a large IFFT size reduces the CP overhead. Suitable values for ε_{cp} are 0.125 [11] and 0.0625 [13, 24, 25] which are used in optical OFDM systems.

Figure 2.8 represents the effect of CP to prevent ISI among OFDM symbols induced by multipath propagation. There are two consecutive OFDM symbols with the two subcarriers. Figure 2.8(a) shows that the two subcarriers are aligned at the transmitter. Figure 2.8(b) shows the same OFDM subcarriers at the receiver, where one subcarrier is received on time and the other delayed by t_d. A detection window is selected which contains a complete OFDM symbol for the second subcarrier. Due to the channel dispersion, the delayed subcarrier has crossed the period boundaries causing interference between neighboring OFDM symbols "ISI". Moreover, the delayed subcarrier is incomplete, so the orthogonality among subcarriers is lost leading to ICI. Figure 2.8(c) shows adding of CP by copying the last samples of each OFDM symbol to the beginning of the same symbol with a guard time T_g. Figure 2.8(d) shows the OFDM signal with CP at the receiver. Assuming that the

signal has crossed the same channel dispersion, the same detection window is chosen containing a complete OFDM symbol for the second subcarrier.

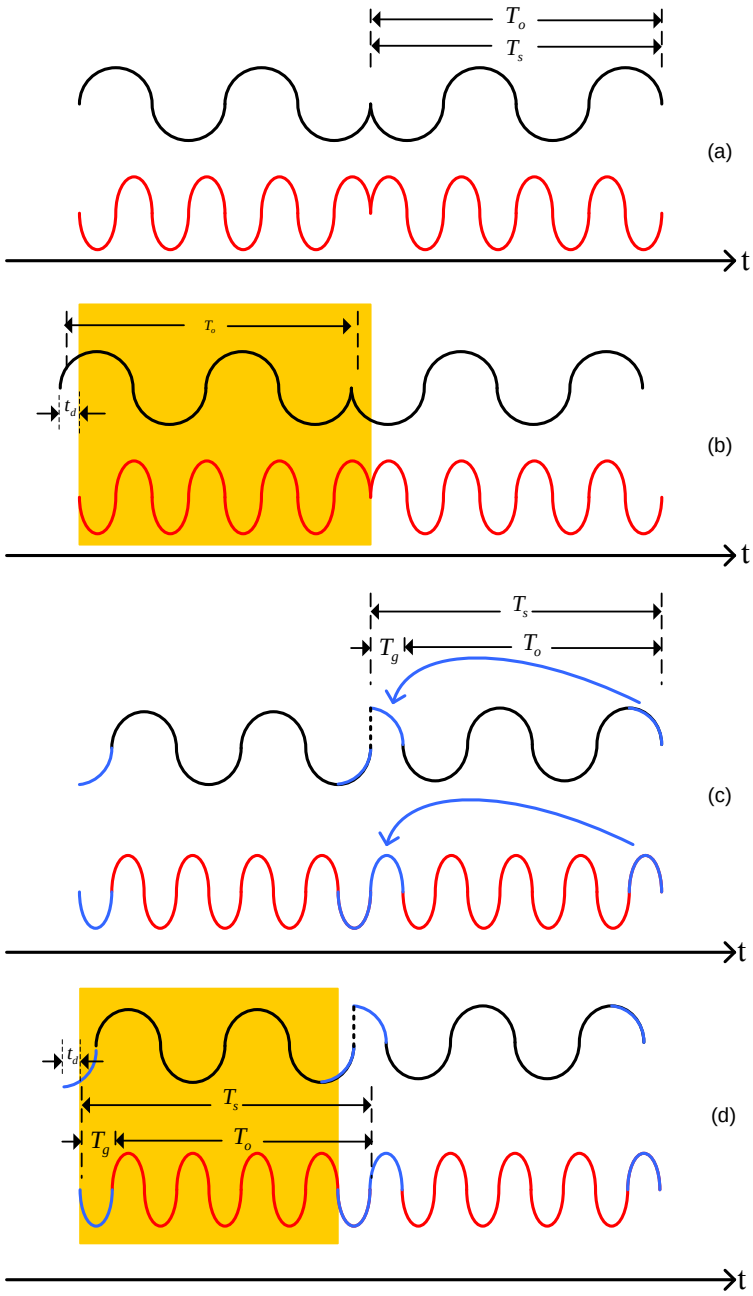

Fig. 2.8: OFDM signal with CP effect.

It can be noticed that a complete OFDM symbol for the delayed subcarrier is also selected in the detection window. A proportion of CP has moved into the detection window, replacing the similar part that has moved out. Hence, the OFDM symbol for the delayed

subcarrier is similar of the transmitted subcarrier with a phase shift. The phase shift can be mitigated using channel estimation.

Training symbols are another important overhead. It is required in OFDM systems to perform symbol synchronization. The synchronization is an important task stage which is performed in the receiver side. In wireless coherent systems, it requires transmitter and receiver local oscillators have exactly the same carrier frequency and phase. Moreover, an accurate sampling clock to recover the transmitted signal effectively. In reality, the synchronization between the transmitter and receiver is mismatched most of the time. Even with perfect matching, an additional phase offset in the LO is provided by an unknown propagation delay between the transmitter and receiver [26]. All of such impairments degrade the system performance. OFDM systems are more sensitive to the synchronization errors. Synchronization can be classified into timing synchronization and frequency synchronization. Synchronization errors in OFDM systems occur due to:

1. Symbol timing offset: refers to the error when the start of the observation period of the received OFDM symbol is determined improper. It introduces ISI.
2. Sampling clock offset: refers to the sampling clock error between the transmitter and receiver sampling rates.
3. Frequency offset: loses the orthogonality among the OFDM subcarriers leading to produce ICI.
4. Phase offset: introduces an additional phase rotation due to ICI and CPE in the received symbols.

Then the received OFDM signal needs three stages of synchronization before the estimated symbol can be decided correctly.

1. Symbol Synchronization: determines the start of the observation period of the received OFDM symbol.
2. Sampling clock synchronization: performs clock recovery.
3. Frequency and phase compensation: estimates and compensates the frequency and phase offset between the transmitter and receivers LOs.

Training symbol is proposed for symbol synchronization. One of the common training symbols for symbol synchronization was proposed by Schmidl and Cox [27]. The approach

consists of two identical data sequences that form a preamble or pilot sequence as shown in Fig. 2.9.

As the two data sequences have the identical data, therefore, synchronization can be achieved by correlating between sequential symbols. The same training symbol is furthermore used to estimate the coefficients for the channel correction and perform the channel correction.

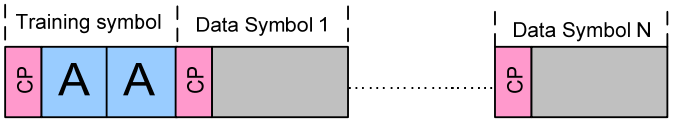

Fig. 2.9: OFDM signal structure with Schmidl's training sequence.

The major drawback of the method is causing timing uncertainty. Other efficient algorithms were proposed to improve synchronization such as the delay and correlate algorithm [28], maximum likelihood (ML) synchronization algorithm [29] and minimum mean squared error (MMSE) algorithm [30]. It is preferable to increase the number of data symbols between each training symbols to reduce the overhead. The training overhead ε_{ts} can be expressed as [23]

$$\varepsilon_{ts} = N_{ts} \,/\, N_{sy} \tag{2.13}$$

where N_{ts} is the number of OFDM training symbols and N_{sy} is the number of OFDM symbols.

Finally, the information symbols after inserting training symbols are serialized and converted to analog electrical signal, using DAC. Then, the analog OFDM signal passes a low-pass filter (LPF) "anti-alias filter" to suppress aliasing due to the sampling process of DAC.

At the receiver, the received OFDM signal is digitized in an analog to digital converter (ADC). After symbol synchronization is performed, the frequency and phase noise between the transmitter and receiver LOs need to be compensated. The cyclic prefix and training symbols are removed. Then, the digital serial signal is converted to complex parallel data blocks using a serial to parallel (S/P) converter. By FFT the OFDM signal is converted back to the frequency domain. The estimated received OFDM signal after FFT becomes

$$Y_{ik} = H_{ki}X_{ik} + N_{ik} \tag{2.14}$$

where Y_{ik} is the received OFDM data symbols of the k^{th} subcarrier in the i^{th} OFDM symbol, H_{ki} is the channel transfer function in the frequency domain , X_{ik} is the transmitted data symbols and N_{ik} is an adaptive white Gaussian noise (AWGN). Channel correction "tap equalizer" is required to estimate and mitigate the effect of channel dispersion that gives the frequency selective fading channels. The estimation is performed by comparing the original training symbols with the received one. The transmitted OFDM symbols can be recovered correctly from the received symbols by multiplying Eq. (2.11) by $1/H_{ki}$. Each subcarrier can be estimated as

$$\hat{X}_{ik} = \frac{Y_{ik}}{H_{ki}} = X_{ik} + \frac{N_{ik}}{H_{ki}} \tag{2.15}$$

A disadvantage of a single tap equalizer is shown in Eq. (2.13). If H_{ki} is very small, the noise effect is increased.

Finally, each QAM symbol is demodulated by QAM de-mapping. It produces parallel data. The parallel data can be converted to serial data by parallel to serial (P/S) conversion and the bit error-ratio (BER) is calculated. Any OFDM systems have overhead due to cyclic prefix and training symbols. Therefore, the actual data rate R_{net} (net data rate) after coding is lower than the nominal data rate R before coding. Taking into account overhead of forward error correction (FEC) ε_{FEC} which induced from FEC code, cyclic prefix and training symbols. The net data rate R_{net} can be expressed as

$$R_{net} = R \times \frac{1}{(1+\varepsilon_{FEC})} \times \frac{1}{(1+\varepsilon_{cp})} \times \frac{1}{(1+\varepsilon_{ts})} \tag{2.16}$$

2.5 OFDM Advantages and Disadvantages

A comparison of advantages and disadvantages between OFDM and single carrier systems is always necessary when comparing both systems. The OFDM system has the following key advantages; it is less sensitive to channel distortions which introduce ISI than single carrier systems at same data rates. The channel equalization complexity in the receiver is reduced dramatically by using IFFT at the transmitter and FFT at the receiver. Instead of applying filter banks, block of oscillators and mixers at the transmitter and receiver for each subcarrier at discrete frequencies in the multicarrier system. Therefore, channel equalization in OFDM

systems becomes simpler than channel equalization in the single carrier systems. OFDM technique provides high spectrum efficiency by using overlap.

On the other side, OFDM has some disadvantages compared with the signal carrier system. OFDM depend on the orthogonality among subcarrier signals. Therefore, OFDM is more prone to the synchronization errors than single carrier systems. The most important drawbacks of OFDM are the high sensitivity to frequency offset and phase noise which lead to ICI. The phase noise will be explained in Chapter 4 in more details. Another important drawback is the high PAPR. The PAPR is the ratio of the peak power of the transmitted signal to the average power. For high PAPR, many of components in the transmitter and receiver must have a wide dynamic range for linear region, especially the power amplifier in the transmitter. At high input power, the transmitter amplifier will work into the saturation region that causing the nonlinear amplification of large amplitude signals. To avoid the nonlinear region, the amplifier must work much lower than the amplifier saturation power. Thus, it reduces the amplifier efficiency. Many algorithms have been proposed to overcome high PAPR such as clipping the OFDM signal [31, 32] and peak power reduction method [33, 34]. In the optical OFDM transmission systems, the optical power amplifier has a wide linear range due its slow response time [5]. Although, PAPR still exists in the optical communications systems due to the optical fiber nonlinearity [35, 36].

The exact general BER formula for single carrier systems of M-QAM signals is presented in [37, 38] as

$$BER_{M-QAM} = \frac{\sqrt{M}-1}{\sqrt{M}\,\log_2\sqrt{M}}\,erfc\left(\sqrt{\frac{3\log_2 M \cdot SNR}{2(M-1)}}\right) \tag{2.17}$$

where SNR is signal to noise ratio which measures the ratio between the transmitted signal power and background noise power. Intuitive, the BER performance decreases by increasing modulation levels "M", thus 4-QAM has better BER performance than 64-QAM. In [38], the authors explored that the performance of OFDM systems increase by increasing the number of orthogonal subcarriers. The general BER expression for M-QAM OFDM systems is described in [39] as

$$BER_{M-QAM,OFDM} = \frac{\sqrt{M}-1}{\sqrt{M}\,\log_2\sqrt{M}}\,erfc\left(\sqrt{\frac{2^{\sqrt{N}}-1}{2^{\sqrt{N}-1}}\cdot\frac{3\log_2 M \cdot SNR}{2(M-1)}}\right) \tag{2.18}$$

where N is the number of orthogonal subcarriers. The authors assumed that the general BER expression for M-QAM OFDM systems follows the BER expression of bi-orthogonal signals with lack of evidence. They did not reveal the conditions under which the formula was found. Furthermore, cyclic prefix is not taken into account.

To measure the BER for M-QAM single carrier system and M-QAM OFDM system over AWGN channel, a numerical simulation is implemented. The simulation BER for M-QAM single carrier system and M-QAM OFDM system is shown in Fig. 2.10. The generation and analysis of the single carrier/OFDM system with M-QAM constellations and the system performance are simulated using Matlab.

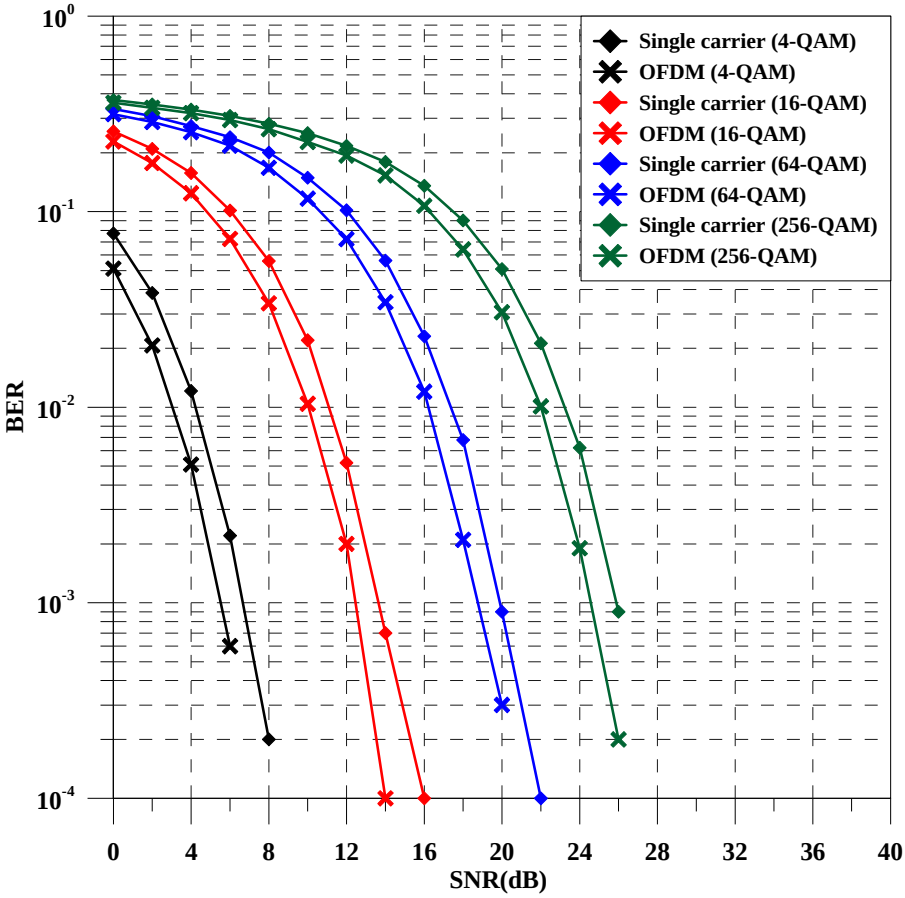

Fig. 2.10: OFDM & Single carrier BER performance.

A basic simulation of M-QAM single carrier system and M-QAM OFDM system over AWGN channel with the following parameters, the bit stream was mapped to 4-QAM, 16-QAM, 64-QAM and 256-QAM. A square root raised cosine filter with a roll-off factor of 0.2 is used for pulse shaping and filter the main signal. Moreover for OFDM signal, an

IFFT/FFT size of 64 is used with 48 data subcarriers. 16 zeros are inserted to generate a guard band between OFDM sidebands. CP of 12.5% of the symbol length is set.

The required SNR for a BER of 10^{-3} is 5.5 dB and 6.7 dB for 4-QAM-OFDM and single carrier system with 4-QAM modulation, respectively. The OFDM can improve SNR by 1.2 dB compared the single carrier systems. By increasing the modulation level up to 64 (64-QAM), The OFDM improves the SNR at a BER of 10^{-3} by 1.1 dB compared to the single carrier systems. The simulation results reveal that using OFDM systems, the SNR can be improved more than using the single carrier systems. The cyclic prefix overhead reduces the sensitivity of OFDM system about 0.5 dB.

Chapter 3: Optical OFDM Systems

3.1 Introduction

The technology of OFDM has been applied for widespread use in wireless communication due to its advantages. However, it has been applied to the optical communications since 2001 by few groups. Chapter 3 provides the difference between the OFDM in wireless communication and optical fiber communication. The advantages of optical OFDM are also presented in Section 3.2. The optical OFDM systems can be classified into three approaches according to the detection scheme. Section 3.3 represents the internal structure of optical OFDM systems and the different existing approaches. Then, Section 3.4 elaborates and compares the performance of the three existing optical OFDM systems in more details. A PDM configuration of CO-OFDM transmission system is shown. Moreover, the required digital signal processing algorithms for frame synchronization, frequency offset compensation and channel estimation are elaborated in Section 3.5. Finally, Section 3.6 provides a square root raised-cosine windowing function of OFDM spectra which is suggested to enhance the efficiency of CO-OFDM systems.

3.2 The Difference between RF-OFDM and Optical OFDM Systems

The main advantage of OFDM technique in wireless communication systems is mainly referred to the fact that the radio communication channels are strongly affected by frequency selective fading channel. OFDM technique is less prone to channel distortions. In the fiber optical communication systems, there is no frequency selective fading occurs. The loss of the fiber produces an equally distributed attenuation over frequency. Therefore, the advantage of using OFDM in the optical communication systems refers to other strengths but not to its robustness against frequency selective fading. The following differences have significant consequences for OFDM design [5, 40].

In wireless OFDM systems, an electrical signal is used to carry the data. The electrical signal can be bipolar which have both positive and negative values. The systems use LO at the receiver side for coherent detection. It use wireless channels which can be modeled as linear time-variant model. The channels are strongly affected by multipath propagation. Also, the moving of the users produces Doppler frequency which has an effect on the systems. The

wireless channel does not have any nonlinearity effect. The nonlinearity occurs in the power amplifier.

In direct detection optical OFDM systems, the intensity of the optical signal is used to carry the data and therefore the signal is unipolar with only positive values [40]. The system can use either coherent detection with laser LO at the receiver side or direct detection without laser LO for signal detection. It uses optical fiber which is more simply modeled in the frequency domain for the two polarization components which are phase dispersion and Jones matrix. The phase dispersion is according to the fiber chromatic dispersion. While Jones matrix represents the effect of PMD and polarization dependent loss (PDL). The optical fiber nonlinearity has a significant effect on the system performance. The optical power amplifier has a wide linear range due its slow response time [5].

Optical OFDM is simply adaptable to high speed transmission and higher level modulation formats. It reduces digital signal processing (DSP) implementation of the transmitter and receiver and relaxes the clock recovery requirements. Furthermore, oversampling can be realized in OFDM by leaving unmodulated subcarriers (adding zeros) at high frequencies. Hence, a spectral gab is generated between the OFDM signal and the aliasing which is generated by the sampling process. Therefore, Optical OFDM decreases the ADC sampling rates requirements compared optical single carrier systems. The ADC often uses 2 times oversampling in case of single carrier receiver [41], while the minimal practical oversampling reaches 1.5 times [42]. Using the DDO-OFDM transmission systems, the authors in [24] use the ADC with 1.25 times oversampling. Moreover, CO-OFDM offers the great advantage for mitigation linear impairments such as CD and PMD of the optical links.

On the other hand, the optical OFDM systems require DACs and ADCs for the generation and detection of the OFDM signal with the high data rates. The development of these DACs and ADCs are complex and expensive [43]. Additionally, high sensitivity to phase noise induced by transmitter and LO lasers.

3.3 Optical OFDM Systems

The optical OFDM systems can be classified into three approaches according to the detection scheme. The approaches are DDO-OFDM was first investigated in 2006 by Lowery. Shieh investigates CO-OFDM in 2006 to mitigate CD. In 2007, Shieh also proved that CO-OFDM can mitigate PMD. In 2008, Xu investigated SCO-OFDM system. It modifies CO-OFDM in

so far as it extracts the optical carrier from the optical OFDM signal at the receiver for coherent interference.

An increasing number of papers on the simulation and experimental analysis for high data rate optical OFDM have been published. For DDO-OFDM, simulation results of 10 Gbps over 4000 km transmission standard single mode fiber (SSMF) were presented in [10]. While an experimental results of 24 Gbps over 800 km transmission SSMF were reported in [24]. For the early CO-OFDM systems, the transmission of 10 Gbps over 3000 km SSMF was simulated in [11]. Experimental results of 8 Gbps transmission over 1000 km SSMF are reported in [44]. While, the transmission of 25.8 Gbps over 4160 km SSMF was demonstrated in [23]. Simulation results of 100 Gbps back-to-back transmission are reported in [45]. For SCO-OFDM, simulation results of 10 Gbps back-to-back transmission are reported in [13]. While, demonstration results of 15.3 Gbps over 81.4 km transmissions are presented in [25]. High speed transmission with 100 Gbps [46, 47] and 1 Tbps [48, 49] for long haul transmission had been demonstrated.

3.3.1 Internal structure

This section represents the design concepts used in the three systems with the main differences between them. The block diagram of three existing optical OFDM back-to-back transmission have four main blocks as follows:

- RF-OFDM-transmitter (Tx).
- RF-to-optical (RTO) up-converter.
- Optical-to-RF (OTR) down-converter.
- RF-OFDM-receiver (Rx).

The RF-OFDM-Tx and RF-OFDM-Rx are common parts between the three existing systems while the RTO up-converter and OTR down-converter blocks differ.

A very important assumption for the OFDM systems is the linearity in modulation and demodulation [50]. Transfer characteristic curves for both optical intensity and optical field (I/Q) components against the input voltage are displayed in Fig. 3.1. In the direct detection, the transfer curve of MZM is the optical intensity versus the input voltage, whereas the transfer curve of MZM in case of coherent detection is optical field against the input voltage. A linear RTO up-converter and linear OTR down-converter can be obtained in principle by biasing Mach Zehnder modulator (MZM) at optimal point which is quadrature point in case

of optical intensity or null point in case of optical field. It is required in order to obtain a linear transformation between RF signal and optical signal [11, 51, 52].

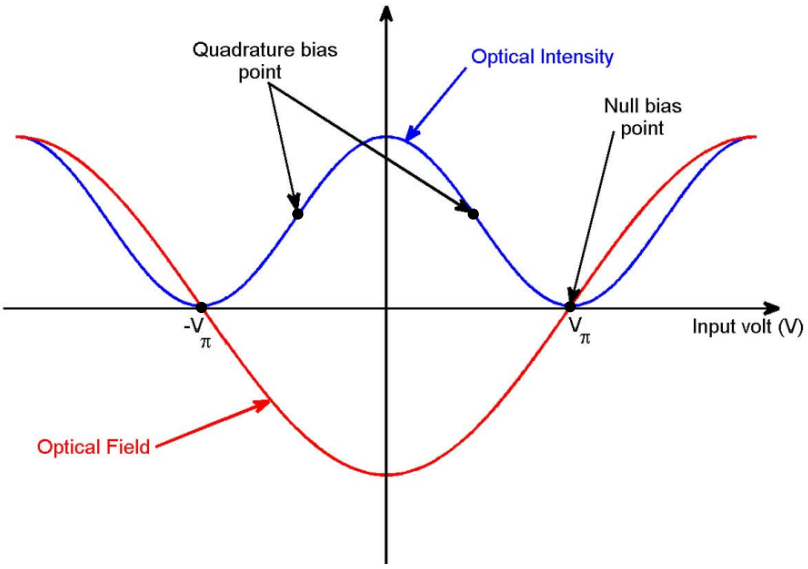

Fig. 3.1: Transfer characteristic curve of MZM.

3.3.1.1 RF-OFDM-Tx

The first common block diagram in the optical OFDM systems is the RF-OFDM-Tx which is used to generate the electrical OFDM signal. The input high-bit-rate (R_s) serial data are converted to low-bit-rate (R_s/N) parallel blocks of bits where N is the number of parallel data paths. The blocks of bits contain information symbols of N_{sc} "subcarriers". The information symbols are mapped by QAM onto N_{sc} orthogonal carriers with equally spaced frequencies.

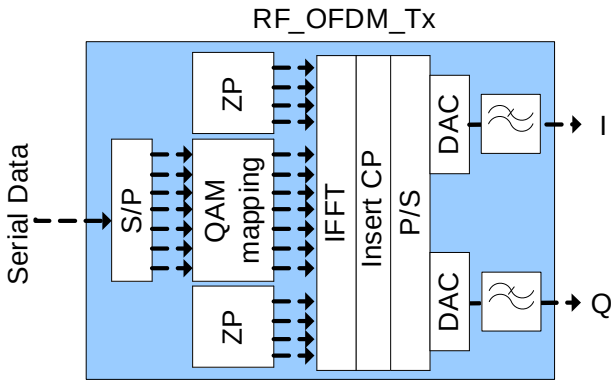

Fig. 3.2: The schematic of an electrical OFDM transmitter.

To avoid aliasing due to the sampling process of DAC, zero padding (ZP) is needed. It shifts the aliases away from the OFDM signal. Different methods of ZP will be explained in Section 4.4.3. By IFFT, one obtains the time-domain OFDM signal. The IFFT size determines by the numbers of subcarriers and the numbers of ZP. The ZP may be inserted in the middle of the IFFT sequence or at its edges. Usually half of the input IFFT sequence is used for ZP while the other half is used for subcarriers. The IFFT size usually lies between 128 [44] and 2048 [53]. Increasing the IFFT size makes the signal less susceptible to ISI between OFDM symbols. Its drawbacks are the increased processing complexity at the transmitter and receiver and the increased sensitivity to laser phase noise in case of coherent detection.

The CP is an effective method to avoid the ISI between OFDM symbols. The last N_g samples of each OFDM symbol are copied to the beginning of the same symbol to generate the CP. The CP contains redundant information which produces overhead. A good selection of short guard time T_g is required to reduce the overhead. In the optical OFDM, the minimum T_g used to compensate all ISI caused by CD and differential group delay (DGD) can be written as [11]

$$T_g \geq DGD_{max} + \Delta f \cdot N_{sc} \cdot |D| \cdot \frac{c}{f_c^2} \tag{3.1}$$

where DGD_{max} is the maximum DGD which can be approximated about 3.5 times of the mean PMD in typical fiber installations, Δf is the subcarrier spacing, D is the total amount of CD, c is the speed of light and f_c is the optical carrier frequency.

Finally, the information symbols at the output of IFFT are serialized and converted to analog electrical signal, using a DAC. A raised cosine filter with a roll-off factor of 0.2 removes the alias and filters the main OFDM signal. Rx-OFDM-Tx block is common for the three optical OFDM systems.

3.3.1.2 RTO up-converter

The second block diagram in the optical OFDM systems is the RTO up-converter which is used to convert the OFDM signal from the electrical domain to the optical domain. In order to transform the RF signal linearly to an optical signal two different configurations can be

applied in the transmitter [51]. In the block diagram, the dash line represents the electrical signals while the solid line represents the optical signals.

- Intermediate frequency (IF) conversion architecture

The first configuration of RTO up-converter is shown in Fig. 3.3. The OFDM baseband signal is up-converted to an IF in the electrical domain, and then the new RF-OFDM signal is up-converted to the optical domain using one MZM. The optical OFDM signal has double side bands (DSB). Due to the symmetry of the optical OFDM spectra at both sides of the optical carrier, one must suppress one of the sidebands and optical carrier by an optical band-pass filter (OBPF), to get the desired spectral efficiency. The efficiency of the architecture depends on the performance of the OBPF being used. It is more suitable for DDO-OFDM [10].

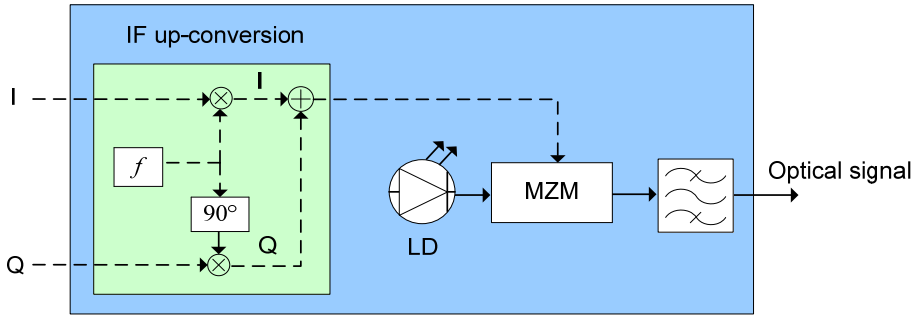

Fig. 3.3: The schematic of RTO up-converter based on an electrical IF up-conversion.

- Direct up-conversion architecture

It uses an optical IQ-MZM which consists of two null biased MZMs with a 90° phase difference between them as shown in Fig. 3.4. The real and imaginary components of the baseband OFDM signal are up converted directly to only one optical signal.

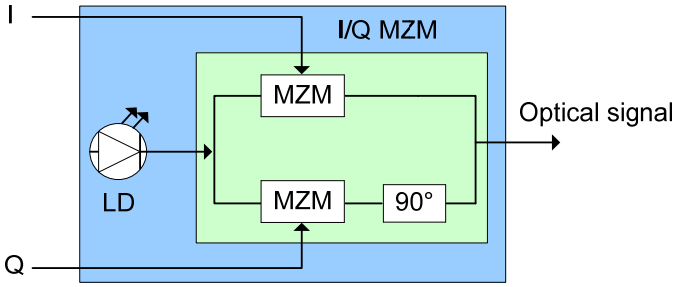

Fig. 3.4: The schematic of RTO up-converter based on direct up-conversion.

The output field of one MZM modulator is 90° shifted in respect to the other tributary to form a quadrature modulator when combining the modulated output. There is no DSB problem, nor is an OBPF required. The need for precise adjustment of three bias voltages is the main disadvantage of such architecture. It is more suitable for CO-OFDM and SCO-OFDM systems [11, 13].

3.3.1.3 OTR down-converter

The OTR down-converter is the third block diagram in the optical OFDM systems. It is used to down convert the OFDM signal from the optical domain to the electrical domain. The receiver must linearly convert the optical signal to an RF signal, which reverses the previous operation. Two different configurations can also be applied. DDO-OFDM system uses only IF conversion architecture while SCO-OFDM system use normally down-converter architecture.

- IF conversion architecture

After transmission of the optical OFDM signal through the fiber link, the photodiode (PD) down-converts the optical signal to an electrical IF signal. After splitting I/Q components of RF-OFDM signal, the RF-OFDM baseband signal is obtained by mixing with 0° and 90° phases at the IF as shown in Fig. 3.5. Such architecture is always preferred for DDO-OFDM systems [10].

The PD can be modeled as a square law detector. It generates a shot noise from the incoming photons producing a current impulse. The shot noise can be modeled as a Gaussian distribution [54]. Also, a thermal noise is generated by the electrical components which are connected to the PD. The thermal noise is also modeled as a Gaussian distribution.

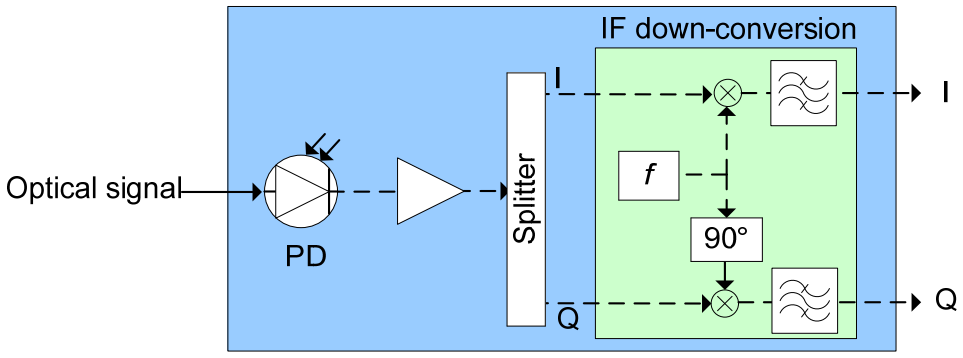

Fig. 3.5: The schematic of OTR down-converter based on an electrical IF down-conversion in DDO-OFDM system.

The output of PD consists of a direct current (DC) component, OFDM subcarriers and a second order nonlinearity term which requires to be suppressed. The second ordered terms are called unwanted terms. If the guard band between the optical carrier and the OFDM band is wide, the unwanted terms will fall out of the OFDM spectrum, without causing performance degradation. If the optical OFDM spectrum is located close to the optical carrier, the unwanted terms are located inside the OFDM spectrum, causing performance degradation. The DC component can be easily suppressed by a DC block. The OFDM subcarriers term is the data to be recovered and the nonlinear term should be eliminated. Several methods are developed to decrease the effect of the unwanted term.

Coherent and self coherent optical OFDM systems can use either the IF conversion architecture or direct down-conversion architecture.

- IF conversion architecture

At the receiver, the optical OFDM signal is first pulsed with the LO laser to 3-dB coupler. Then it down-converted using a pair of balanced detectors to obtain the I/Q components of RF baseband OFDM signal at IF. By using an electrical I/Q demodulator, the real and imaginary components are retrieved as shown in Fig. 3.6(a) for CO-OFDM systems.

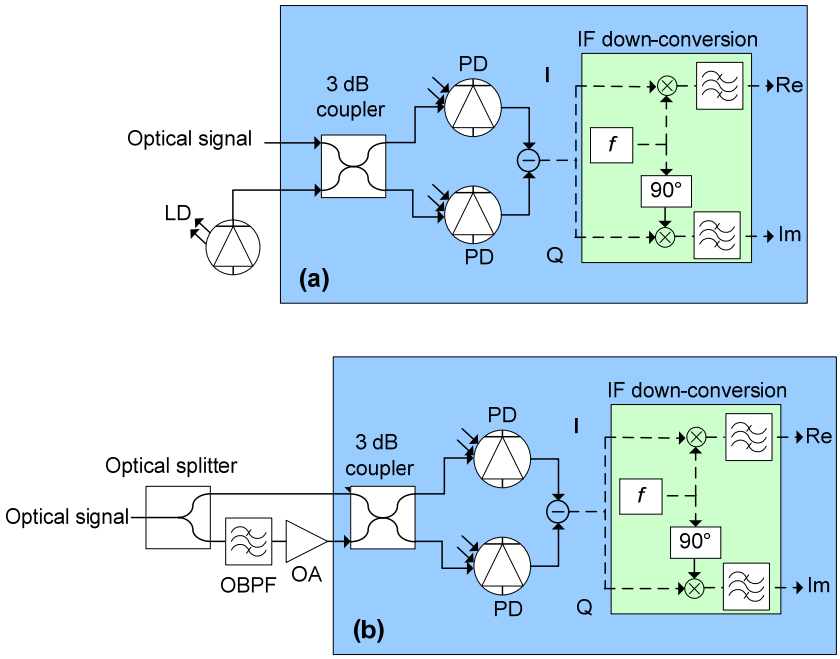

Fig. 3.6: The schematic of OTR down-converter based on an electrical IF down-conversion in (a) CO-OFDM system; (b) SCO-OFDM system.

In SCO-OFDM systems, optical splitter splits the received optical OFDM signal into two paths. One of the splitting signals is passed through OBPF to extract the optical carrier and then is amplified using optical amplifier (OA) as shown in Fig. 3.6(b).

- Direct down-conversion architecture

At the receiver, The optical OFDM signal mixes with the LO laser and down-converts using an optical 90° hybrid and two pairs of balanced detectors to obtain the I/Q components of the baseband OFDM signal as shown in Fig. 3.7(a). Such architecture is normally used in CO-OFDM systems [51]. In SCO-OFDM systems, instead of using LO laser at the receiver side, the received optical OFDM signal is split into two portions by an optical 3-dB (or similar) coupler. One flows directly to an optical 90° hybrid for direct down-conversion as shown in Fig. 3.7(b). The other is passed through OBPF which extracts the optical carrier, so it looks like homodyne detection.

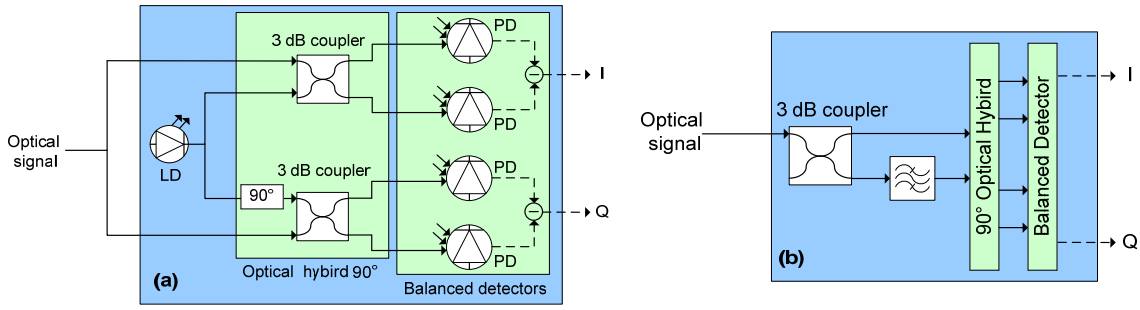

Fig. 3.7: The schematic of OTR down-converter based on direct down-conversion in (a) CO-OFDM system; (b) SCO-OFDM system.

Since the two interfering optical signals come from the same laser source, their polarization and phase noise are identical. Therefore the complexity of DSP is decreased. Furthermore, no LO is required at the receiver.

3.3.1.4 RF-OFDM-Rx

Finally, RF-OFDM-Rx reverses the operation of RF-OFDM-Tx as shown in Fig. 3.8. The real and imaginary components of RF-OFDM signal are digitized in ADCs. Phase noise of transmitter laser and LO need to be compensated in CO-OFDM systems. While, DDO-OFDM systems and SCO-OFDM systems are homodyne detection. Therefore, no phase noise compensation is required at the receiver. For polarization division multiplexing, both

DDO-OFDM and SCO-OFDM transmission systems require polarization controller. Therefore, the receiver side will be more difficult to control optical carrier power. The digital serial signal is converted to complex parallel data blocks using an S/P converter, and the CP is removed. By FFT, the OFDM signal is converted back to the frequency domain. After removal of ZP, each QAM symbol is demodulated by QAM de-mapping. It produces parallel data. The data can be converted to serial data by P/S conversion.

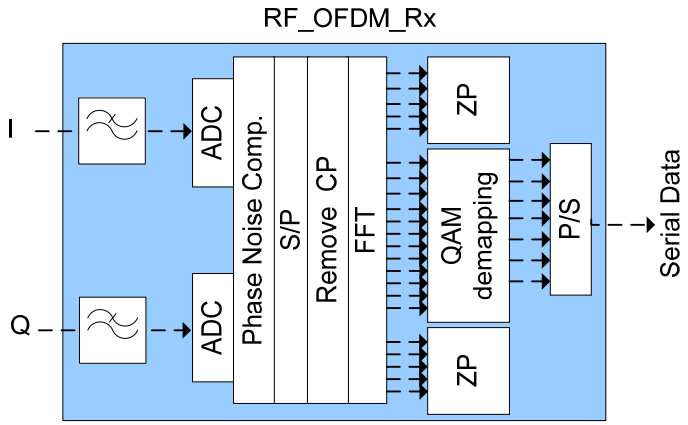

Fig. 3.8: The schematic of an electrical OFDM receiver.

Such block is also common for three optical OFDM systems. From the block diagrams which were explained until now, optical OFDM systems always use RF-OFDM-Tx and RF-OFDM-Rx blocks as a common parts while it change the RTO up-conversion and OTR down-conversion blocks.

3.3.2 DDO-OFDM

There are salient differences between DDO-OFDM and CO-OFDM; DDO-OFDM is more suitable for short distance and inexpensive applications as it requires fewer components at the transmitter and receiver than CO-OFDM. Whereas, it needs a guard band between the optical carrier and the OFDM band to avoid inter-modulations in the photodiode [10]. Therefore, it increases the bandwidth requirements and decreases the spectral efficiency. Moreover, it measures only the amplitude of the optical signal.

Polarization division multiplexing is more difficult in DDO-OFDM systems due to guard band between the optical carrier and OFDM sidebands. It is difficult to control the optical carrier's polarization at the receiver [59].

3.3.3 CO-OFDM

CO-OFDM combines two main benefits of coherent detection and OFDM. Moreover, it achieves the best performance in receiver sensitivity, spectral efficiency, robustness against PMD and CD. However, it requires the highest complexity in the receiver design. CO-OFDM is suitable for long haul transmission with high-bit-rate. To achieve high performance for CO-OFDM, it requires a transmitter laser and LO laser with a particularly narrow linewidth ($\Delta\nu$) and an effective DSP. The receiver involves extra signal processing for phase and frequency estimation to compensate the phase noise and frequency offset between transmitter laser and LO. Therefore, CO-OFDM systems will be more expensive than DDO-OFDM systems. Moreover, CO-OFDM systems allow detecting phase, frequency and the amplitude of the transmitted signal.

3.3.4 SCO-OFDM

SCO-OFDM system is a modification of CO-OFDM system in the OTR down-converter block at the receiver side. It extracts the optical carrier from the optical OFDM signal at the receiver for coherent interference. Therefore, SCO-OFDM systems use the same RTO up-conversion architecture as in CO-OFDM system. The direct up/down-conversion scheme is normally used in SCO-OFDM systems [13, 25].

For Polarization division multiplexing, an optical controller is used to adjust the OFDM and optical carrier power before the polarization diversity coherent receiver.

Polarization division multiplexing for the optical OFDM systems will be presented in details in Section 3.5.

3.4 Simulation Setup and Results of Optical OFDM Systems

The first performance analysis between the three existing optical OFDM systems is investigated [55]. The generation and analysis of the OFDM signal are simulated, using VPItransmissionMaker™ V8.5. An OFDM signal with data rate of 20 Gbps is generated from PRBS of length 2^{13}-1. The bit stream was converted from serial to parallel, then mapped with 4-QAM (QPSK). An IFFT/FFT size of 1024 is used with 512 OFDM subcarriers. 512 zeros are inserted at both edges of the IFFT. A CP having 12.5% (128 samples) of the symbol length is added. A square root raised cosine filter with a roll-off

factor of 0.2 filters the main OFDM signal. A laser with 1 MHz linewidth is used to generate a continuous signal at 193.1 THz. It is modulated with the OFDM signal in a null-biased IQ-MZM for CO-OFDM or SCO-OFDM systems. In contrast, for the DDO-OFDM system $f_{IF} =$ 12 GHz is used to shift an optical OFDM signal band above the optical carrier as shown in Fig. 3.9. The frequency shift allows inter-modulations distortion of the photodiode to fall into it [10]. It increases the bandwidth of the channel and decreases the spectrum efficiency. In the DDO-OFDM system, the total bandwidth will equal to $(\frac{N_{sc}}{N_{FFT}} \times f_s) + f_{IF} =$ 22 GHz where $f_s = 20$ GS/s is the sampling rate. Moreover, the bandwidth exceeds by 2 GHz due to the roll-off factor. The data rate will be $\frac{N_{sc}}{N_{FFT}+N_{cp}} \times log_2^M \times f_s = 17.8$ Gbps. where M is the QAM modulation level. Therefore, the spectral efficiency will be 0.74 bit/s/Hz.

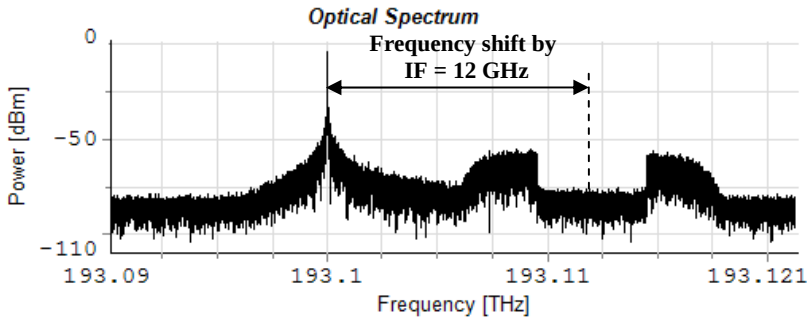

Fig. 3.9: Optical OFDM spectrum at Tx for DDO-OFDM.

A MZM up converts the RF OFDM signal to the optical domain. The guard band is not needed in CO-OFDM or SCO-OFDM systems as shown in Fig. 3.10, because both sidebands are homodyne for SCO-OFDM systems or heterodyne for CO-OFDM systems, where I and Q components are available. Increasing the number of zero padding leads to the more reduction in spectral efficiency and bit rate. For both of the CO-OFDM and SCO-OFDM systems, the bandwidth will equal to $\frac{512}{1024} \times 20\text{G} \times 1.2 = 12$ GHz. The data rate will be $\frac{512}{1024+128} \times 2 \times 20\text{G} = 17.8$ Gbps. Therefore the spectral efficiency will be 1.5 bit/s/Hz.

To test the optical signal to noise ratio (OSNR) performance, noise is added to control the received OSNR. The main drawback of the coherent reception is the tough requirement on laser linewidth. Equal laser linewidth for transmitter and LO lasers are assumed. In [13], the authors compared SCO-OFDM systems with CO-OFDM systems and investigated their

performance. CO-OFDM system has better performance than SCO-OFDM system. They mentioned also the bandwidth of the OBPF which extracts the optical carrier at the receiver.

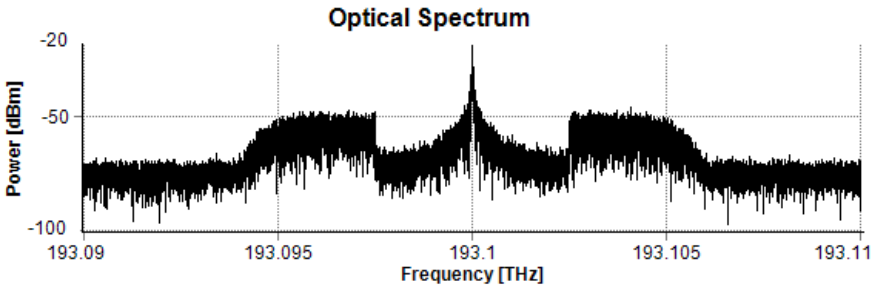

Fig. 3.10: Optical OFDM spectrum at Tx for CO-OFDM and SCO-OFDM.

The quality of the extracted optical carrier is reduced by amplified spontaneous emission (ASE), and the larger the filter bandwidth, the more noise passes with the optical carrier. Therefore, a narrow bandwidth filter will improve the performance of SCO-OFDM systems. But the authors did not provide any result about a low-bandwidth filter. In the dissertation, the performance of SCO-OFDM systems with different filter bandwidths are given and compared to CO-OFDM system.

Figure 3.11 presents the back-to-back BER performance as a function of OSNR for laser linewidth ($\Delta\nu$) = 1MHz, received optical power (ROP) = 0 dBm.

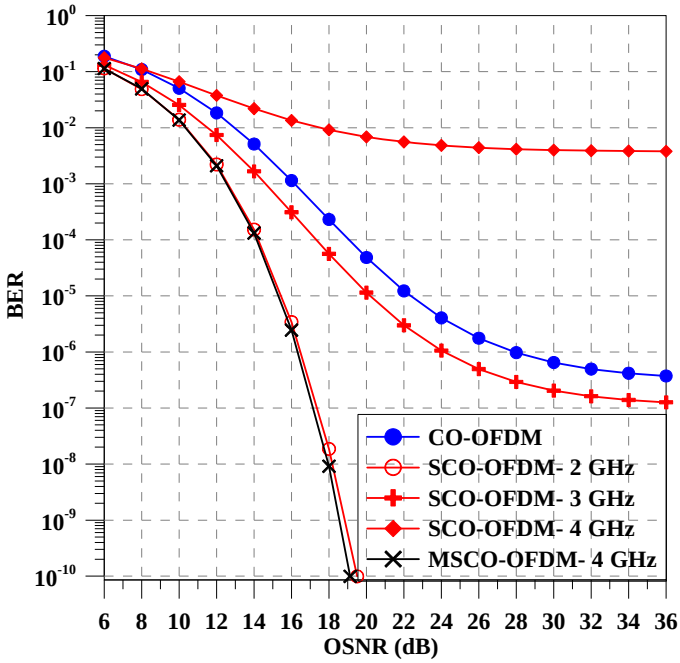

Fig. 3.11: BER versus OSNR for SCO-OFDM with different OBPF bandwidth.

The OBPF bandwidth in SCO-OFDM is varied from 2 to 4 GHz. The required OSNR for a BER 10^{-3} is 12.6 dB and 16.1 dB for SCO-OFDM with 2 GHz OBPF width and CO-OFDM, respectively. SCO-OFDM therefore improves the OSNR by 3.5 dB. At an increased bandwidth of 3 GHz, the required OSNR for a BER 10^{-3} is increased to 14.6 dB for SCO-OFDM. So, the OSNR improvement is decreased to 1.5 dB due to the more ASE noise passes with the extracted optical carrier. For 4 GHz bandwidth, a BER of less than 10^{-3} cannot be obtained. Performance of SCO-OFDM is obviously improved by reduced the OBPF width. So, the OSNR improvement is decreased to 1.5 dB due to the more ASE noise passes with the extracted optical carrier. The performance of SCO-OFDM system at 2 GHz bandwidth can be achieved by a modified the system design with a narrow optical band-stop filter (OBSF) as shown in Fig. 3.12. It removes the optical carrier from the optical OFDM signal before the optical 90° hybrid. So, the effect of weak optical carrier will be eliminated. Compared with SCO-OFDM at 2 GHz bandwidth of OBPF, the modified SCO-OFDM (MSCO-OFDM) with 4 GHz bandwidth of OBPF requires 12.5 dB OSNR for a BER 10^{-3}. Therefore, the MSCO-OFDM can achieve 0.1 dB OSNR improvement.

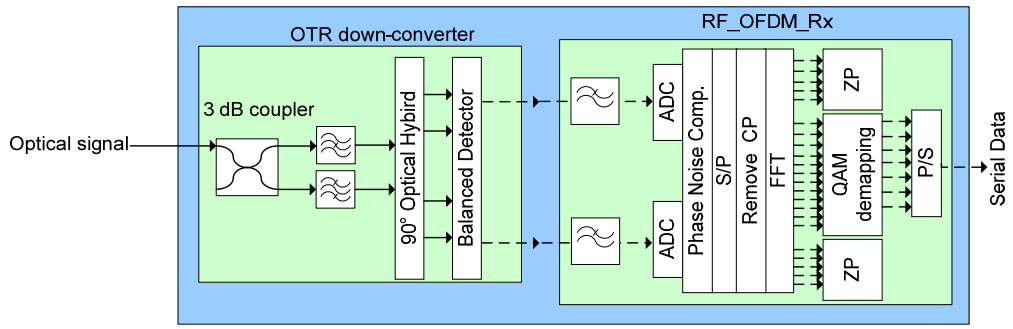

Fig. 3.12: Block diagram of MSCO-OFDM receiver.

The influence of OSNR on the BER is shown in Fig. 3.13 for back-to-back configuration. The BER is simulated for $\Delta\nu$ = 1MHz, ROP = 0 dBm and 2 GHz bandwidth of OBPF for SCO-OFDM. The required OSNR for BER of 10^{-3} is 12.6 dB, 16.1 dB and 26.4 dB for SCO-OFDM, CO-OFDM and DDO-OFDM respectively. Compared with DDO-OFDM, CO-OFDM can improve OSNR by 10.3 dB. An additional 3.5 dB OSNR benefit can be achieved with a SCO-OFDM system which means 13.8 dB OSNR improvement compared with DDO-OFDM. The performance of SCO-OFDM overcomes the performance of CO-OFDM and DDO-OFDM.

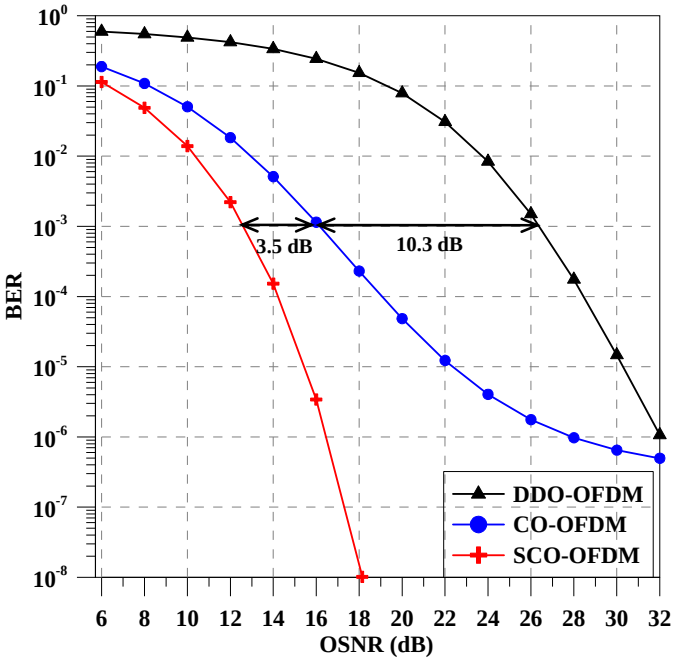

Fig. 3.13: OSNR versus BER for different optical OFDM systems.

Figure 3.14 shows the BER performance of varying Δν at 0 dBm ROP and 25 dB OSNR. At Δν of 1 MHz, the BER is 3.85×10^{-3}, 2.59×10^{-6} and 7.22×10^{-7} for DDO-OFDM, CO-OFDM and SCO-OFDM respectively.

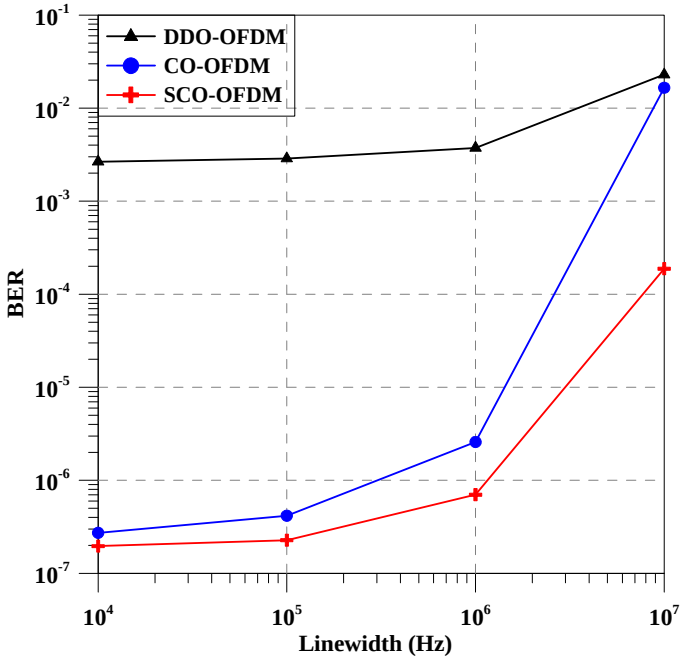

Fig. 3.14: BER versus laser linewidth for different optical OFDM systems.

Increased laser linewidth brings CO-OFDM performance close to that of DDO-OFDM, while SCO-OFDM is not as much affected and performs better than these two, even at 10 MHz linewidth.

The effect of varying ROP at 25 dB OSNR and 1 MHz linewidth for DDO-OFDM, CO-OFDM and SCO-OFDM back-to-back transmission is shown in Fig 3.15. The ROP is varied from −40 dBm to 10 dBm. From the simulation results, a BER 10^{-3} can be achieved at a ROP of −26.1 dBm and −26 dBm for SCO-OFDM and CO-OFDM, respectively. While the BER performance for DDO-OFDM indicates that 25 dB OSNR is not sufficient to transmit with a BER 10^{-3}, increased ROP does improve the BER as shown in Fig. 3.15. It can be clearly observed that SCO-OFDM has a good tolerance to laser linewidth and the highest system performance compared to the others approaches. However, the dissertation will focus on CO-OFDM system.

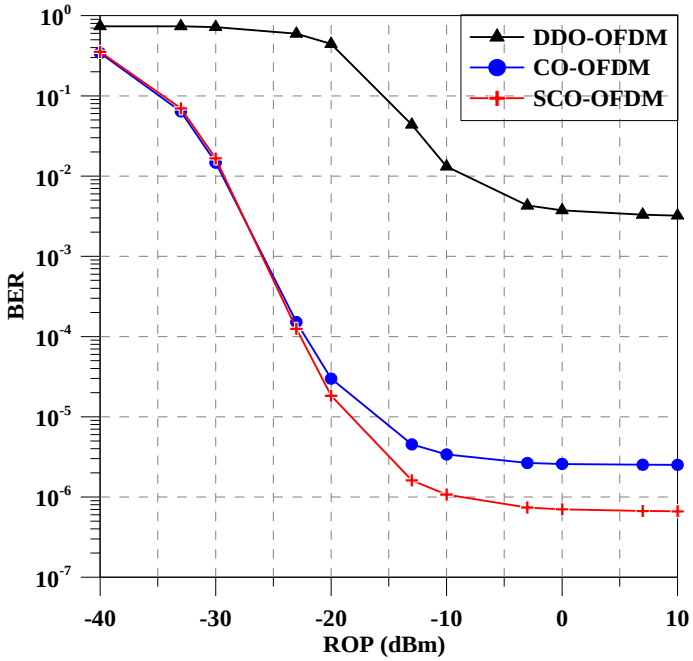

Fig. 3.15: BER versus ROP for different optical OFDM systems.

Table 3.1 summarizes the differences between the various approaches in optical OFDM systems.

	DDO-OFDM	CO-OFDM	SCO-OFDM
Distance	Short	Long	Long
Data rate	Low	High	High
Complexity	Simple	Complex	Complex
Requirements	Guard band	Transmitter laser and LO with narrow linewidth	Narrow OBPF
Cost	Inexpensive	Expensive	Expensive
Spectrum efficiency	0.74 b/s/Hz	1.5 b/s/Hz	1.5 b/s/Hz

Table 3.1: Comparison between various optical OFDM systems.

3.5 Polarization Division Multiplexing (PDM)

In wireless communication systems, multiple-input and multiple-output (MIMO) is used to describe a wireless communication system with multiple transmit antennas and multiple receive antennas. MIMO is used to increase data throughput, improve the system performance and spectrum efficiency [56, 57]. Signals in the wireless channels suffer from multipath fading; therefore, MIMO is combined with OFDM [58]. In optical communication systems, MIMO techniques are applied successfully in SSMF by transmitting and receiving separate data on orthogonal polarizations. MIMO is called polarization multiplexing [40].

PDM is more difficult in DDO-OFDM systems due to guard band between the optical carrier and OFDM sidebands. It is difficult to control the optical carrier's polarization at the receiver [59]. The authors used DDO-OFDM system with a single optical OFDM transmitter and two optical OFDM receivers [60, 61] to compensate the effect of PMD in the DDO-OFDM systems. In [62], the authors proposed the first experimental PDM-DDO-OFDM system using two optical carriers at orthogonal polarization with guard band 25 GHz. They recovered two orthogonal polarization OFDM sidebands using two photodiodes followed by MIMO channel estimation and equalization methods. While, the drawbacks of this technique are large guard band between orthogonal optical carriers; it will decrease the spectrum efficiency and increase the complexity of the DSP at the receiver. Moreover, the polarization controller is required.

In SCO-OFDM transmission systems, PDM concept is used to transmit optical carrier orthogonal polarized to the OFDM sidebands. For detection the orthogonal components,

polarization beam splitter and OBPF are used to separate the optical carrier and OFDM sidebands components and then the separated OFDM sidebands and optical carrier are optically amplified. An optical controller is used to adjust the OFDM and optical carrier power before the polarization diversity coherent receiver [63, 64]. The drawback of these methods is that the spectral efficiency is decreased compared by the conventional SCO-OFDM technique.

The concept of PDM is approximately simple in CO-OFDM systems as the optical carrier polarization in the receiver can be controlled simply. Fig. 3.16 shows the PDM-CO-OFDM system which is unknown also as 2×2 MIMO-CO-OFDM system [65, 66]. At the transmitter, two optical OFDM signals are generated and multiplexed onto orthogonal polarizations by polarization beam combiner (PBC). At the receiver, polarization beam splitter (PBS) splits the optical received signal into two random polarizations. Two coherent detectors are used one for each polarization. The optical polarization controller is not required. The MIMO processing is used to de-rotate the polarization and separate two OFDM signals.

The major advantages of using the 2×2 MIMO-CO-OFDM configuration compared to single polarization configuration which is known as single input dual output are:

1. The channel capacity and spectral efficiency are doubled compared to the single polarization CO-OFDM transmission systems.
2. The channel capacity increment will not be affected by PMD due to the PMD impact can be simply handled with channel and phase estimation [12, 67].
3. The dynamic polarization tracking at the receiver is not required due to using polarization coherent diversity receiver.

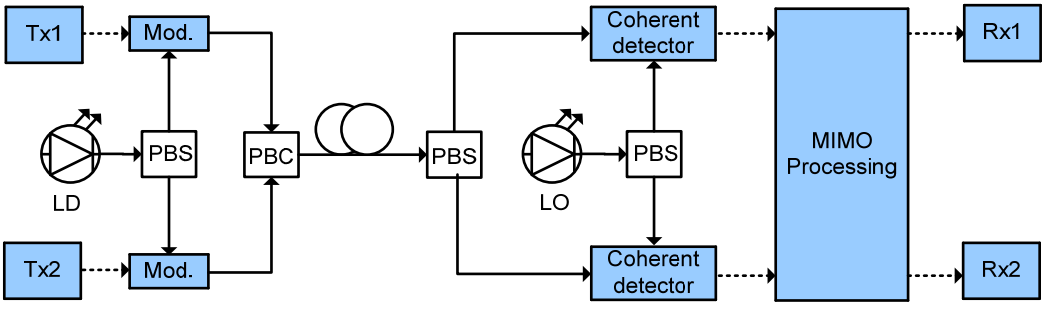

Fig. 3.16: The architecture of PDM-CO-OFDM system using MIMO processing concept.

During the MIMO processing stage, it is required to perform time and frequency synchronization, channel estimation, phase estimation and other processes of recovering baseband signal. It is necessary to explain some important stages of MIMO Processing in detail below:

1. Timing synchronization: It is important to align the starting point of the OFDM frames to avoid ISI. One of the common training symbols for frame synchronization was proposed by Schmidl [27]. A training symbol (TS) with two identical data sequences in time domain is inserted at the beginning of each OFDM frame. TS contains N samples which equals the number of samples in the OFDM symbol. Therefore, each data sequence has length of $\frac{N}{2}$ samples. The samples are generated by inserting a pseudo random sequence at even subcarriers and inserting zero at odd subcarriers. At the receiver, the starting sample of OFDM frame is achieved by searching for the data sequences which are identical and calculating the correlation peak between the two sequences. The timing metric function $M(d)$ can be written as

$$M(d) = \frac{|R_{cor}(d)|^2}{(R(d))^2} \tag{3.2}$$

where $R_{cor}(d)$ and $R(d)$ are the correlation function of the received signal in the time domain and the received energy for the second data sequence of TS, respectively, $R_{cor}(d)$ can be given by

$$R_{cor}(d) = \sum_{i=0}^{N/2-1} r^*(d+i).r(d+i+N/2) \tag{3.3}$$

$$R(d) = \sum_{i=0}^{N/2-1} \left|r(d+i+N/2)\right|^2 \tag{3.4}$$

where $r(d)$ is the received signal in the time domain with zero phase shift and zero frequency offset. The maximum value of the timing metric points to TS starting. Since TS length is known, the starting sample of the OFDM frame can be determined. The main drawback of Schmidl scheme is that the correlation peak has plateau because of channel effect and ASE which causes timing uncertain [5].

To overcome this drawback, a simple and effective frame synchronization algorithm is proposed by Puntsri [68, 69, 70]. The proposed technique uses TS with 1

and -1 in at the beginning of OFDM frame. At the receiver, the received data which includes TS is correlated with the known TS to find the maximum correlation peak. The cross-correlation can be written as

$$R_{cor}(d) = \sum_{i=d-L}^{d} C_{IQ}(i) r_{IQ}(d+i) \tag{3.5}$$

where $C_{IQ}(i)$ and $r_{IQ}(d+i)$ are the I and Q components of known TS and received signal, respectively. L is the length of TS code. The maximum value of the correlation function represents the starting samples of the OFDM frame which can be given by

$$M_{max}(d) = \max\left(R_{cor}(d)^2\right) \tag{3.6}$$

The square of the correlated function is used to avoid the negative values. The correlation peak is very sharp without any plateau as shown in Fig. 3.17. In the dissertation, all simulation setups use this technique for frame synchronization.

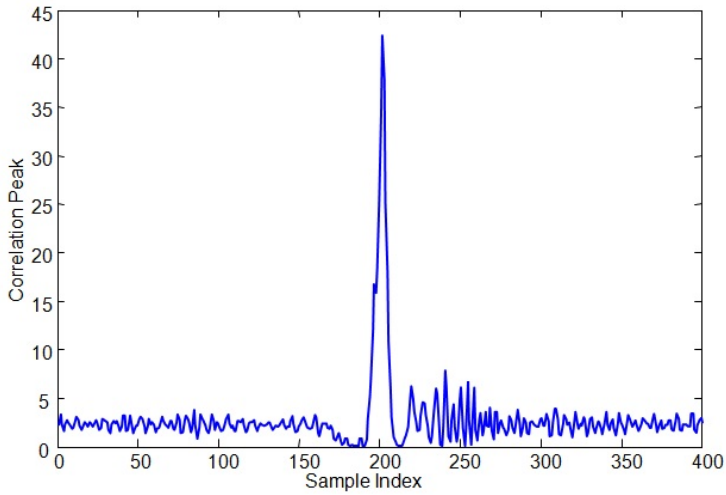

Fig. 3.17: Correlation peak of frame synchroniation algorithm.

2. Frequency synchronization: Frequency offset in the OFDM systems loses the orthogonality among the OFDM subcarriers, which leads to ICI and hence degrades the system performance. The simplest method to estimate and compensate the frequency offset is Schmidl approach. The frequency offset can be written as

$$\hat{f}_{off} = \frac{\Delta f}{\pi}.\arg\left(R_{cor}(d)\right) \tag{3.7}$$

where $\hat{f}_{off}$ is the estimated frequency offset, Δf is frequency spacing between subcarriers and $\arg\left(R_{cor}(d)\right)$ is the angle of correlation function in radian [5, 27]. Then, the received signal can be mitigated as

$$\hat{y}_{ik} = y_{ik}.e^{-j2\pi\hat{f}_{off}t} \tag{3.8}$$

where $\hat{y}_{ik}\ and\ y_{ik}$ are the frequency offset compensated and received OFDM symbols of the k^{th} subcarrier in the i^{th} OFDM symbol, respectively. In the dissertation after frame synchronization, Schmidl approach is used for frequency offset compensation in all simulation setup.

3. Phase estimation: different methods of phase noise estimation and compensation techniques will be presented in details in Chapter 4.
4. Channel estimation: After successful achievement of OFDM frame, frequency synchronization and phase noise compensation, the OFDM signal after FFT stage can be written as

$$R_{ik} = H_{ik}T_{ik} + N_{ik} \tag{3.9}$$

where R_{ik} and T_{ik} are the received and transmitted OFDM symbols of the k^{th} subcarrier in the i^{th} OFDM symbol, respectively. H_{ik} is the channel transfer function and N_{ik} is random noise. For the sake of simplicity, i and k subscripts will be dropped. By using PDM, the transmitted and received signals of the two polarizations are given in the forms of Jones vector by

$$\begin{aligned} \boldsymbol{T} &= \begin{bmatrix} T_x \\ T_y \end{bmatrix} = \begin{bmatrix} E_{in,x}(t) \\ E_{in,y}(t) \end{bmatrix} = \begin{bmatrix} E_{in,0x}e^{j\emptyset_{in,x}} \\ E_{in,0y}e^{j\emptyset_{in,y}} \end{bmatrix} \\ \boldsymbol{R} &= \begin{bmatrix} R_x \\ R_y \end{bmatrix} = \begin{bmatrix} E_{out,x}(t) \\ E_{out,y}(t) \end{bmatrix} = \begin{bmatrix} E_{out,0x}e^{j\emptyset_{out,x}} \\ E_{out,0y}e^{j\emptyset_{out,y}} \end{bmatrix} \end{aligned} \tag{3.10}$$

where $E_{out,x}$, $E_{out,y}$, $E_{in,x}$ and $E_{in,y}$ are the output and the input electrical fields of the two polarizations with relative amplitudes ($E_{0x}, E_{0y)}$ and relative phases ($\emptyset_x, \emptyset_y$), respectively.

The fiber transmission Jones matrix describing the chromatic dispersion and the polarization effects is

$$\boldsymbol{H} = e^{j\emptyset_D(f)}\boldsymbol{J} = \begin{bmatrix} H_{xx} & H_{xy} \\ H_{yx} & H_{yy} \end{bmatrix} \tag{3.11}$$

where $\emptyset_D(f)$ is the phase dispersion due to chromatic dispersion and $\boldsymbol{J}$ is the Jones matrix of the fiber link. Vectors and matrices are donated by bold symbols. Therefore, the estimated transmitted signals can be expressed as

$$\widehat{\boldsymbol{T}} = \boldsymbol{H^{-1}R} \tag{3.12}$$

It is essential to estimate the channel parameters at the receiver. Different techniques are used for channel estimation; zero forcing (ZF) method is commonly used by multiplying the received signal with the inverse of the channel matrix to obtain the estimated value of the transmitted signal [67]. Minimum mean-squared-error (MMSE) algorithm is used for higher performance but it requires more computational complexity. For channel estimation, Jansen [66] uses time-multiplexed training symbols where each training symbol consists of two consecutive pilot symbols with orthogonal polarizations as shown in Fig. 3.18. By transmitting TS one after the other, the orthogonality between the transmitters is recognized. At the receiver after FFT stage, the channel estimation can be computed by comparing the received and transmitted training symbols.

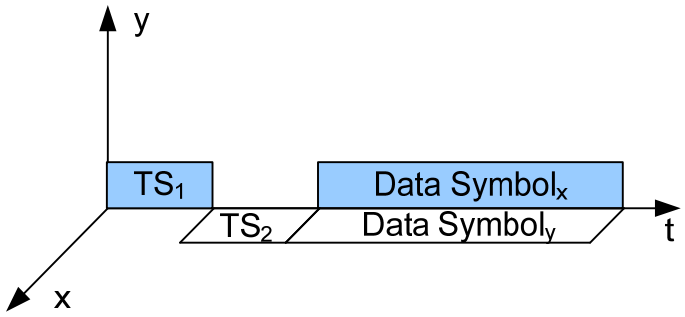

Fig. 3.18: Time multiplexed training symbols and OFDM symbols.

Using TS_1, the following channel parameters can be estimated as

$$\begin{bmatrix} R_x \\ R_y \end{bmatrix} = \begin{bmatrix} H_{xx} & H_{xy} \\ H_{yx} & H_{yy} \end{bmatrix} \cdot \begin{bmatrix} T_x \\ 0 \end{bmatrix} \tag{3.13}$$

From Eq. 3.13, the two channel parameters can be written as

$$\begin{aligned} R_x &= H_{xx}\, T_x \rightarrow H_{xx} = {R_x}/{T_x} \\ R_y &= H_{yx}\, T_x \rightarrow H_{yx} = {R_y}/{T_x} \end{aligned} \tag{3.14}$$

Using TS_2, the other channel parameters can be expressed by

$$H_{xy} = {R_x}/{T_y}, \quad H_{yy} = {R_y}/{T_y} \tag{3.15}$$

Using the inverse of the calculated channel matrix and the received symbols in Eq. (3.12), the estimated transmitted OFDM symbols in the two polarizations can be estimated. The presented technique is used in all simulation setups in the dissertation.

3.6 Pulse Shaping for CO-OFDM Systems

FFT is used to perform spectral analysis of a signal assuming that the signal is periodic [22]. However, most of the signals are not strictly periodic due to phase transitions caused by modulation, therefore the FFT does not estimate the frequency components accurately and an error is present, known as leakage "spectral spreading". The leakage spreads the energy from a single frequency over a wide frequency range. Figure 3.19(a) displays the rectangular shaped of three OFDM subcarriers. While, the phase transitions effect on three OFDM subcarriers is shown in Fig. 3.19(b). A windowing function is applied to minimize the effects of the spectral spreading as shown in Fig. 3.19(c). The windowing function modifies the signal in the time domain by forcing it to zero at both ends and to become periodic in the time domain. Windowing is also used for designing finite impulse response (FIR) filters.

The authors in [8, 71] used the windowing of OFDM symbols to minimize the sensitivity to linear distortion. Windowing shapes only the cyclic prefix samples and remains the original part of the signal unchanged. The system performance was not affected by such windowing. Therefore, it will not be used further.

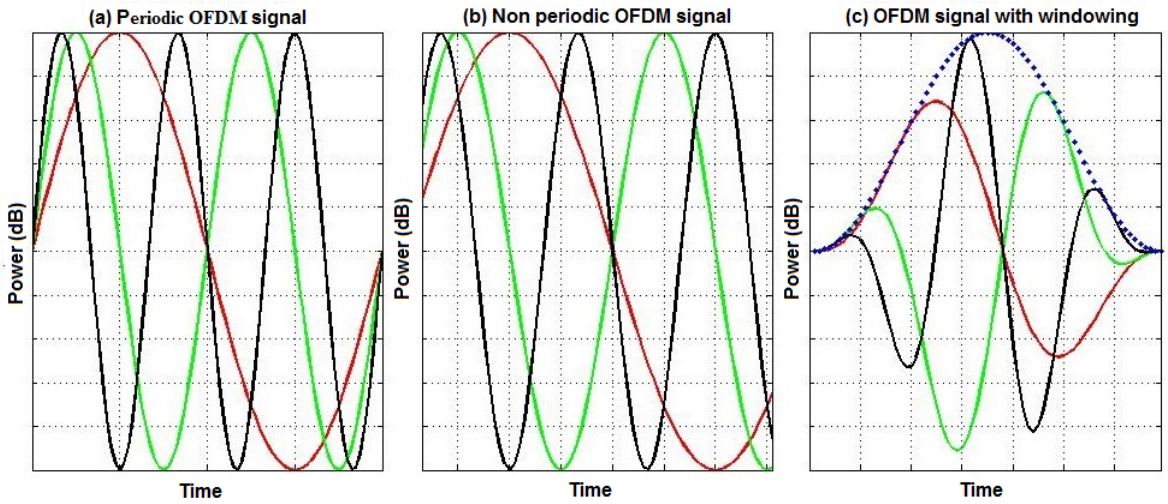

Fig. 3.19: OFDM signal with rectangular and non-rectangular windowing.

The authors in [72, 73] used windowing of OFDM symbols to compensate frequency offset in the system. Frequency differences between local oscillators at the transmitter and receiver generates frequency offset. After the OFDM signal is cyclically extended, then the whole signal is shaped with windowing function [74].

Applying a rectangular time window with a sinc function in the frequency domain of OFDM symbols has a very important drawback. It lets OFDM suffering from its high side-lobes which makes the out-of-band spectra fall off slowly. The side-lobes increase the OFDM signal bandwidth and reduce the spectral efficiency.

The side-lobe power and the transition width are two main parameters which determine the performance of the window function. The transition width measures the width of the first lobe (main lobe) to the first null. There is a contrast between side-lobe power and the transition width of the window function as reducing the side-lobe power, increasing the transition width. Figure 3.20 displays the rectangular, raised-cosine and square root raised-cosine windowing functions. The rectangular windowing has transition width lower than the raised-cosine and square root raised-cosine windowing. But, the rectangular windowing has a higher side-lobe power. From [2], the spectrum of the rectangular pulse can be defined as

$$P_{rec}(f) = sinc(fT) \tag{3.16}$$

while the raised cosine spectrum can be expressed as

$$P_{RC}(f) = sinc(fT)\frac{\cos(\pi\alpha fT)}{1-(2\alpha fT)^2} \tag{3.17}$$

where α is the roll off factor and $0 \leq \alpha \leq 1$. Finally, the frequency response of square root raised cosine pulse is

$$P_{SRRC}(f) = \frac{(4\alpha fT)\,cos[(1+\alpha)\pi fT] + sin[(1-\alpha)\pi fT]}{\pi fT[1-(4\alpha fT)^2]} \tag{3.18}$$

Since the multiplication and convolution are dual operations. Filtering techniques can be used instead of windowing. When windowing is used, a multiplication is done in frequency domain. In contrast, when applying the filtering in the time domain means the convolution is used. A ‘‘better than’’ raised-cosine, raised cosine (RC) and rectangular windowing have been compared in wireless OFDM [75].

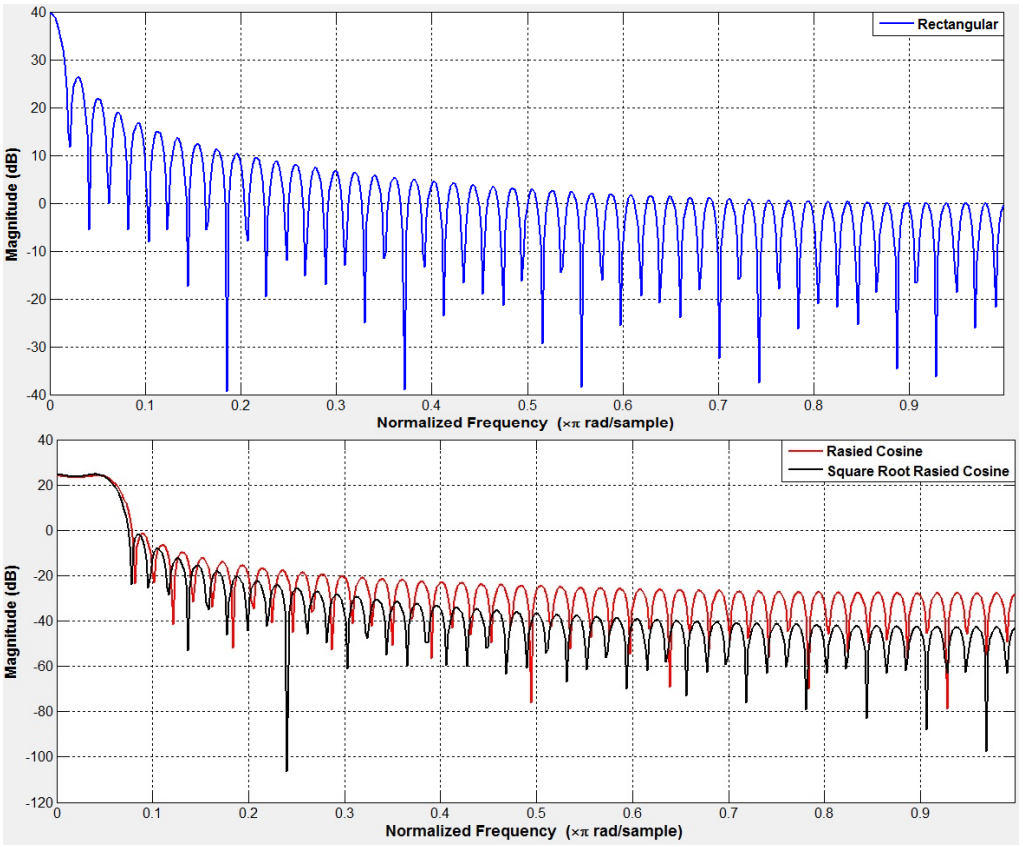

Fig. 3.20: Spectrum of rectangular, rasied-cosine and square root rasied-cosine windowing.

The ‘‘better than’’ raised-cosine pulse reduces ICI due to frequency offset between the transmitter and receiver LO. The simulation results show that the OFDM systems with rectangular pulse shape always has greater ICI power than provided by either the RC or the ‘‘better than’’ RC pulse shape. Using the RC windowing in CO-OFDM systems, the out-of-band suppression is enhanced compared to the conventional rectangular window [76]. A square root raised-cosine (SR-RC) windowing in CO-OFDM system is provided and examined. Simulation results are compared with those of RC and rectangular windowing [77].

3.6.1 Simulation setup and results of pulse shaping for CO-OFDM systems

The generation and analysis of the OFDM signal and the system performance are simulated using VPItransmissionMaker™ V8.7. Figure 3.21 shows the schematic of the CO-OFDM transmission system with windowing function which uses to enhance the system performance. An IFFT/FFT size of 512 is used with 480 OFDM subcarriers carrying 4-QAM

modulation in one polarization with a nominal data rate of 40 Gbps. 32 zeros are padded at both edges of the OFDM symbol. The zeros generate a guard band between OFDM sidebands. CP of 6.25% (32 samples) of the symbol length is set with a guard time of $(\frac{32}{20\ G})$ which equals to 1.6 ns. Subcarrier frequency spacing is $(\frac{20\ G}{512})$ which equals to 39.0625 MHz. From Eq. 3.1, the delay spread of SSMF can be calculated as $(39.0625\text{M} \times 480 \times 16\ \text{ps/nm.km} \times 80\ \text{km} \times \frac{3\times10^8}{(193.12\times10^{12})^2})$ which equals to 0.2 ns. Moreover, DCF is used to fully compensate for dispersion, after each span. The information symbols are serialized and converted to analog electrical signals by DACs at a sample rate of 20 GS/s. LPF is used as a substitute for pulse shaping (windowing function) with roll-off factor of 0.2. OFDM have bandwidth of 22.5 GHz and the data rate will be 35.3 Gbps. Therefore, the spectral efficiency will be 1.56 bit/s/Hz for single polarization transmission system. A laser with 100 kHz linewidth is modeled to generate a continuous signal at 193.1 THz. It is modulated with the OFDM signal in a null-biased IQ-MZM for CO-OFDM. Equal linewidths for transmitter and LO lasers are assumed. The LO power is assumed to have 0 dBm.

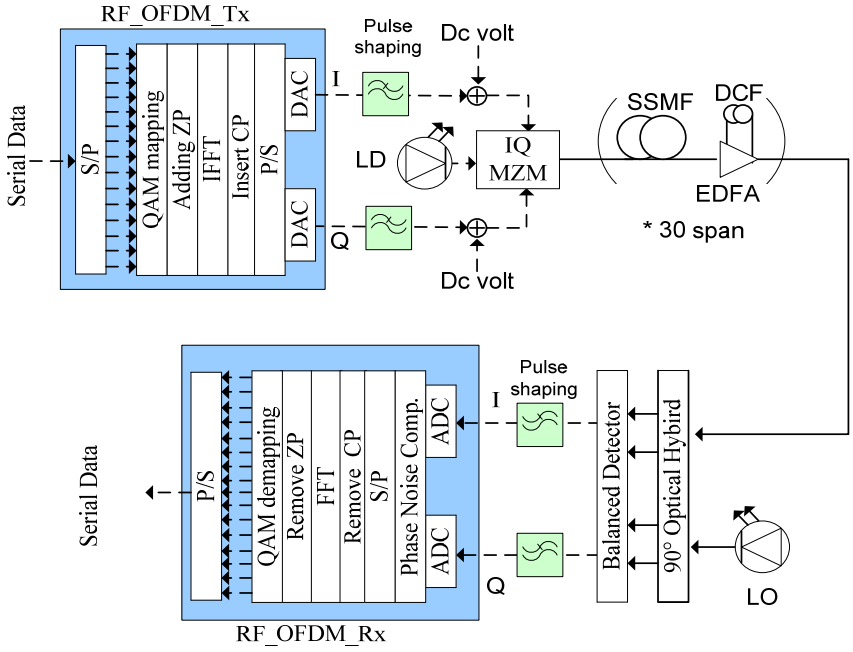

Fig. 3.21: Simulation setup of 40 Gbps CO-OFDM over 2400 km using pulse shaping.

The transmission line consists of 30 fiber spans. Each of them comprises 80 km of SSMF. The SSMF has an attenuation of 0.2 dB/km, a dispersion of 16 ps/nm/km, a

dispersion slope of 0.08 ps/nm^2/km. After each span, the fiber loss is compensated by a double-stage EDFA with a noise figure of 4 dB. Between each EDFA's stages, there is 16 km of dispersion compensating fiber (DCF) with a dispersion of −80 ps/nm/km; thereby forming a fully periodic dispersion map. The DCF launch power is 6 dB lower than the launch power of SSMF to decrease the effect of DCF nonlinearity. Phase noise is mitigated by RFP based phase noise compensation [78]. An optimal pilot-to-signal ratio (PSR) value of 5.2 dB is used. A 4th order 35 MHz Butterworth LPF is used at the receiver side to extract the RFP signal. Different windowing schemes for CO-OFDM systems using the rectanglar, the SR-RC and the RC with a roll-off factor of 0.2 are compared.

Figure 3.22 shows the BER performance as a function of OSNR. The BER is simulated for laser linewidths of 100 kHz and ROP of 0 dBm. The required OSNR for BER of 10^{-3} is 10.7 dB, 11.1 dB and 11.8 dB using the SR-RC, the RC and the rectangular windowing, respectively. The SR-RC window can improve OSNR by 1.1 dB compared to the rectangular window, and about 0.4 dB compared to the RC window.

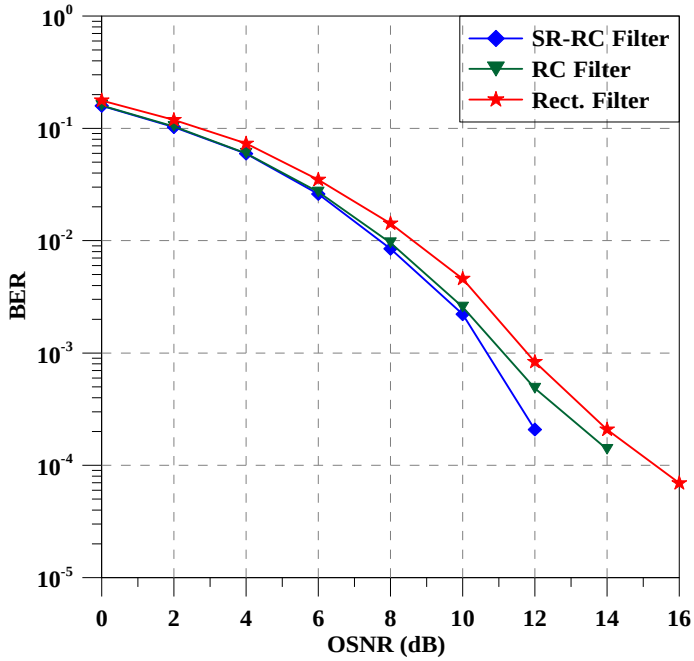

Fig. 3.22: BER versus OSNR of different pulse shaping in CO-OFDM systems.

Figure 3.23 shows the system Q of the received data as a function of individual laser linewidth at 12 dB of OSNR and 0 dBm ROP. The system Q for linewidths of 100 kHz is

10.95 dB, 10.4 dB and 9.05 dB using the SR-RC, the RC and the rectangular windowing, respectively.

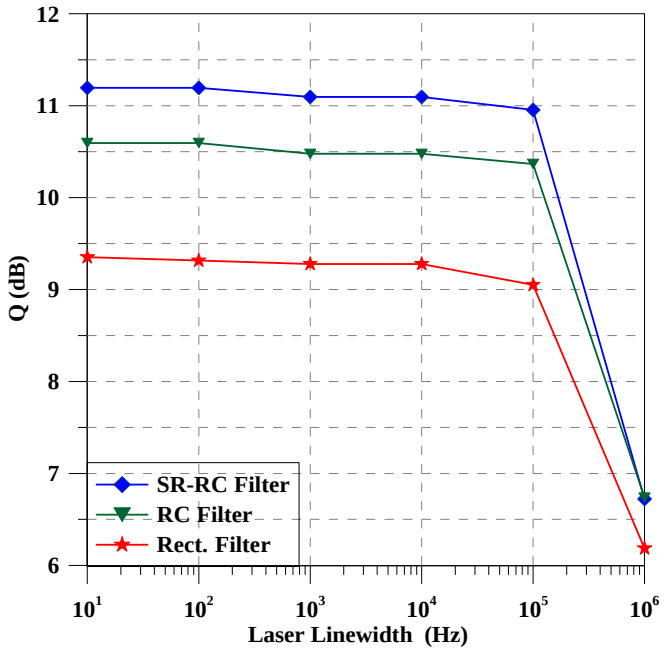

Fig. 3.23: System Q factor versus laser linewidth of different pulse shaping in CO-OFDM systems.

In all schemes, Q decreases for laser linewidths beyond 100 kHz. Compared to the rectangular windowing, the SR-RC can improve the Q factor by 1.9 dB and the RC windowing about 1.35 dB, respectively. Increasing the laser linewidth up to 1 MHz leads to an almost equal performance of RC windowing and SR-RC windowing while the performance of using rectangular windowing is worst. Generally, the OFDM symbols with SR-RC windowing outperform RC and rectangular windowing. The out-of-band suppression is effectively increased when SR-RC windowing function is used.

The schematic of the PDM-CO-OFDM transmission system with pulse shaping is shown Figure 3.24 shown. The same simulation setup is used for PDM-CO-OFDM transmission system with 4 training symbols every 50 OFDM data symbols, these training symbols are inserted to the head of OFDM frame at the transmitter. The training symbols of 8% overhead are used for frame synchronization, frequency offset compensation and channel estimation as explained in Section 3.5. While in the single polarization transmission systems, the data rate will be 32.7 Gbps. Hence, the spectral efficiency will be 1.45 bit/s/Hz. At the receiver side, the optical, the received optical signal is split into *x*-polarization (*x*-pol.) and *y*-polarization

(*y*-pol.) by a PBS and then fed into polarization diversity coherent receiver. Each polarization signal is mixed with LO inside an optical 90° hybrid.

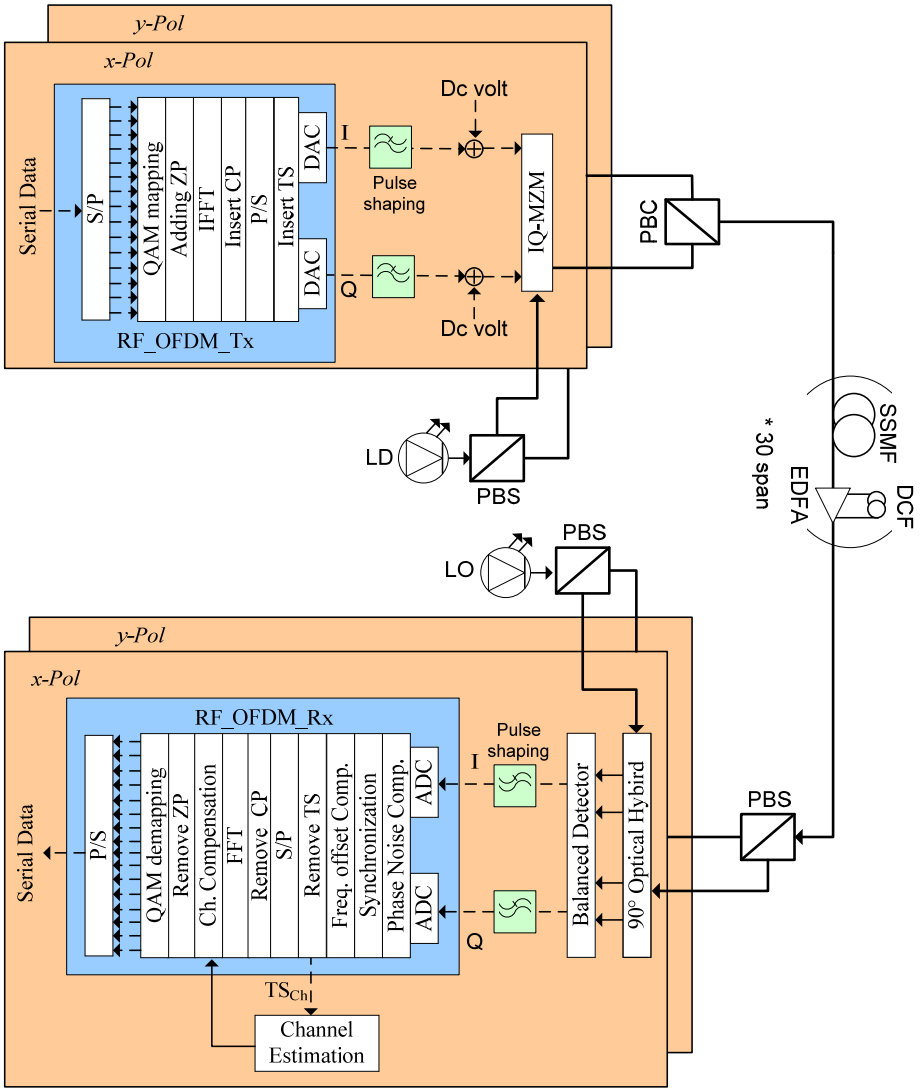

Fig. 3.24: Schematic of the PDM-CO-OFDM transmission system using pulse shaping.

Two balanced photo detectors at each branch are used to detect the I/Q components. After passing through LPF, the RF signals from the balanced detectors are sampled with ADCs. At the receiver, the digital signal processing involves frame synchronization using Puntsri approach [68, 69, 70], the frequency offset is mitigated using Schmidl method and the laser phase noise is compensated using RFP technique. All TS are removed and the channel training symbols are used for channel estimation as explained in Section 3.5. The CP is removed and the OFDM signal is converted back to the frequency domain using FFT. The

channel compensation is applied to derotate the polarization of the received symbols. Finally, each QAM symbol is demodulated by QAM de-mapping and BER is computed. The nominal bit rate is doubled, therefore it becomes 80 Gbps. But, the net bit rate will be $\frac{480}{512+32} \times 2 \times 20G \times \frac{1}{1+0.08} \times 2$ which equals to 65.4 Gbps. Subsequently, the spectral efficiency will be 2.9 bit/s/Hz.

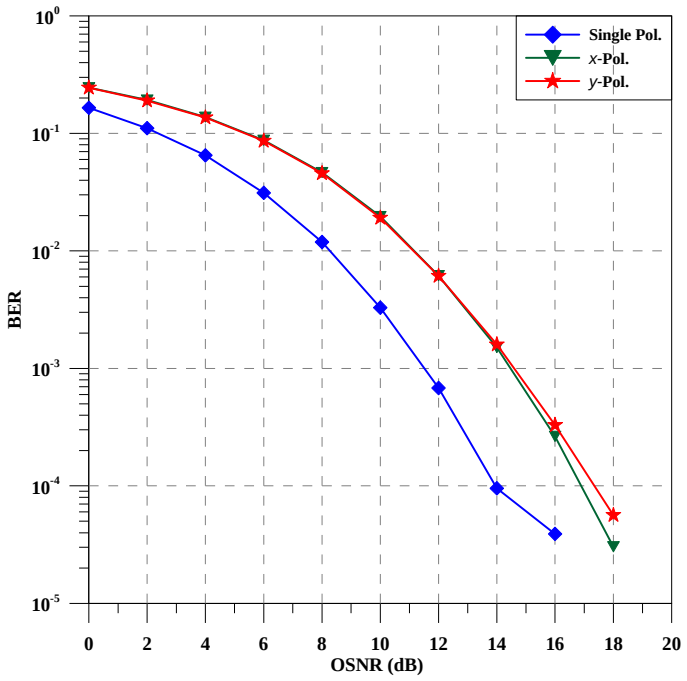

Fig. 3.25: BER versus OSNR for single and PMD CO-OFDM systems using SR-RC windowing.

The influence of OSNR on the BER for using SR-RC pulse shaping is shown in Fig. 3.25. The BER is simulated for each laser linewidths of 100 kHz and ROP of 0 dBm. The required OSNR for BER of 10^{-3} can be observed at 11.51 dB for 4-QAM single polarization. The OSNR requirement for PDM transmission system is increased about 3 dB which is theoretical penalty to reach 14.46 dB and 14.59 dB for *x* and *y* polarizations, respectively.

Chapter 4: Phase Noise Compensation

4.1 Introduction

Phase noise effects must be taken into account when studying the performance of CO-OFDM transmission systems. One drawback of CO-OFDM is the high sensitivity to phase noise. Phase noise in CO-OFDM transmission system is not only generated by transmitter laser and receiver local oscillator (LO), but also by nonlinear optical fiber transmission [79]. Optical amplifier noise also deteriorates phase estimation. Thus, phase noise reduces the received signal quality. As long as phase noise is a vital aspect in the design and analysis the performance of CO-OFDM systems, phase estimation plays an important role in a communication receiver. The receiver needs an extra effective DSP to estimate and compensate the phase noise. In this chapter, the principles of laser and nonlinear phase noise are briefly explained in Section 4.2 and Section 4.3, respectively. Then, Section 4.4 will introduce several popular laser and nonlinear phase noise compensation approaches. The simulation studies of different proposed laser and nonlinear phase noise compensation methods are investigated and compared. Furthermore, simulation results for single-polarization CO-OFDM systems and 2×2 MIMO-CO-OFDM systems using the proposed algorithms are elaborated in Section 4.5.

4.2 Laser Phase Noise

The investigation of the phase noise impact on system performance is important. Phase noise has to be estimated for an optimal approach and its effect to the system has to be compensated. The phase noise contributions in CO-OFDM transmission are generated from [79]:

1. Nonlinear optical fiber transmission produces a nonlinear phase noise. The nonlinear phase noise comes from the interaction of amplified spontaneous emission (ASE) with OFDM signal by self-phase modulation (SPM), cross-phase modulation (XPM) and four-wave mixing (FWM) [80].
2. Transmitter laser and receiver LO cause common phase error (CPE) which affects the phase of the subcarriers. It rotates the constellation points, and inter-carrier interference (ICI) which is a complex value generated from laser phase drift, is added to each phase

of the subcarriers and appears as a Gaussian noise. The mathematical description for CPE and ICI will be represented in Eq. (4.9) and Eq. (4.11), respectively.

3. Optical amplifiers generate ASE which degrades the efficiency of the amplifier. The effect of ASE can be described as an additive white Gaussian noise (AWGN).

The ideal carrier for optical communication is a light wave with constant amplitude, frequency and phase. Unfortunately, the ideal carrier cannot be produced. Laser phase noise describes the fluctuations in the phase of the laser output which increase the laser linewidth and decrease optical coherence length. The laser phase noise is assumed to be Wiener process with a zero-mean and variance

$$\sigma^2 = 2\pi\Delta\nu T_s \tag{4.1}$$

where $\Delta\nu$ is the phase noise linewidth of transmitter and LO lasers and T_s is the symbol period. Equation (4.1) indicates that phase noise increases with time. The laser linewidth describes the laser phase noise which expresses the -3-dB of the power density spectrum of the laser.

For clarity, the laser phase noise in the received OFDM signal consists of two components. A random noise component that can be treated as AWGN and a constant component produced from laser phase drift that modifies all the subcarriers uniformly. Section 4.2 focuses on the phase noise induced by transmitter laser and receiver LO.

The electrical baseband OFDM signal is generated from the RF-OFDM transmitter as mentioned in Section 3.3. The RTO up-converter is used to shift the baseband OFDM signal to the optical domain using IQ-MZM. From [5, 50], the optical transmitted OFDM signal $E_t(t)$ can be written as

$$E_t(t) = e^{j(2\pi f_{ld1} t + \emptyset_{ld1})} x_{ik} \tag{4.2}$$

where f_{ld1} and $\emptyset_{ld1}$ are the frequency and phase noise of the transmitter laser, respectively. x_{ik} is the transmitted OFDM symbols of the k^{th} subcarrier in the i^{th} OFDM symbol, the transmitted optical signal $E_t(t)$ passes through an optical fiber with an impulse response h_{ik}. Therefore, the received optical signal $E_r(t)$ becomes

$$E_r(t) = e^{j(2\pi f_{ld1} t + \emptyset_{ld1})} x_{ik} \otimes h_{ik} \tag{4.3}$$

where $\otimes$ is convolution operator. The optical OFDM signal mixes with the LO laser and down-converts using an optical 90° hybrid and two pairs of balanced detectors. The received electrical signal can be expressed as

$$y_{ik} = e^{j(2\pi f_{off} t + \emptyset_i(n))} . r_{ik} \quad (4.4)$$

$$r_{ik} = x_{ik} \otimes h_{ik} \quad (4.5)$$

where $f_{off} = f_{ld1} - f_{ld2}$ and $\emptyset_i(n) = \emptyset_{ld1} - \emptyset_{ld2}$ are the frequency offset and the phase noise offset between the transmitter laser and LO. Assuming that f_{off} is zero and a generated ASE noise from EDFA is inserted in the system. The received OFDM signal will be

$$y_{ik} = e^{j\emptyset_i(n)} . (x_{ik} \otimes h_{ik}) + n_{ik} \quad (4.6)$$

Assuming perfect frame and frequency synchronization, the OFDM signal is demodulated after FFT stage. Therefore, the received OFDM signal in the frequency domain is given by

$$Y_{ik} = I_{i0} H_{ik} X_{ik} + ICI + \mathrm{N}_{ik} \quad (4.7)$$

where X_{ik} and $\mathrm{Y_{ik}}$ are transmitted and received signal respectively for k^{th} subcarrier in i^{th} OFDM symbol, H_{ik} is the transfer function of the transmission channel response, N_{ik} is a random noise. The first and second terms represent the CPE and ICI distortion terms in the received OFDM signal, respectively. The expression of both terms can be found in details in [81, 82]. As I_{ik} is the FFT of $e^{j\emptyset_i(n)}$ which can be given by

$$I_{ik} = \frac{1}{\mathrm{N}_{sc}} \sum_{n=0}^{\mathrm{N}_{sc}-1} e^{j\emptyset_i(n)} e^{\frac{-j2\pi nk}{\mathrm{N}_{sc}}} \quad (4.8)$$

I_{i0} is a CPE coefficient which can be obtained if $k = 0$ in Eq. (4.8) as

$$I_{i0} = \frac{1}{\mathrm{N}_{sc}} \sum_{n=0}^{\mathrm{N}_{sc}-1} e^{j\emptyset_i(n)} \quad (4.9)$$

The CPE is a constant value during the same OFDM symbol and leads to constant phase rotation for all of the subcarriers. Since the rotation is common, the phase noise can be estimated and compensated using pilots as described in [78, 79]. The ICI term can be represented as

$$ICI = \sum_{m=0;\, m \neq l}^{\mathrm{N}_{sc}-1} I_{i(m-l)} H_{im} X_{im} \quad (4.10)$$

where $I_{i(m-l)}$ is the ICI coupling coefficient between two subcarriers with distance of m subcarrier [50], it can be given by

$$I_{i(m-l)} = \frac{1}{\mathrm{N}_{sc}} \sum_{n=0}^{\mathrm{N}_{sc}-1} e^{j\emptyset_i(n)} e^{\frac{j2\pi n(m-l)}{\mathrm{N}_{sc}}} \qquad m \neq l \tag{4.11}$$

The ICI is the summation of the average of phase noise with a spectrum shift multiplied by each phase of the subcarrier of $\mathrm{N}_{sc} - 1$ which acts as a random noise. When the laser linewidth is greater, the ICI effect will be dominated over the CPE effect. Because of its random nature, the ICI effect is difficult to compensate. In [79], the authors assumed that OFDM frames must be short to that set the phase error effect is common within an OFDM symbol. Then, they could use their method to compensate ICI effect. But in [78], the authors assumed a random term for ICI which is more accurate. In the case of perfect phase noise estimation, phase noise dose not exist. Therefore, $I_{ik} = \delta(k)$ and Eq. (4.7) reduces to

$$Y_{ik} = H_{ki}X_{ik} + \mathrm{N}_{ik} \tag{4.12}$$

Figure 4.1(a) shows the combination of the ICI and the CPE effects on a 4-QAM OFDM signal after demodulation. The transmitter and LO lasers have a linewidth of 100 KHz. A rotation of the subcarriers and ICI effect can be shown. After compensating ICI and CPE, a perfect separated constellation points can be shown in Fig. 4.1(b).

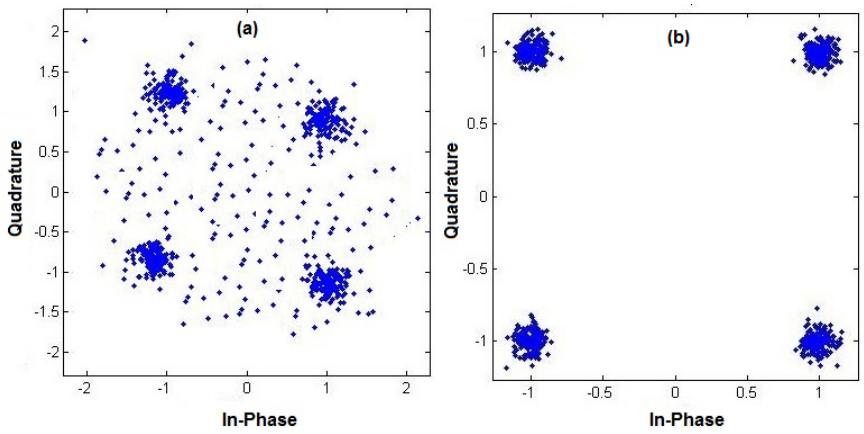

Fig. 4.1: Constellation diagram of the phase noise effect in the OFDM signal.

4.3 Nonlinear Phase Noise

An optical fiber transmits light a long its axis using the process of the total internal reflection. The fiber consists of a core enveloped by a cladding layer. The core refractive index must be greater than the cladding refractive index to reserve the optical signal in the core. Maxwell's equations are used to study the propagation of the optical field in the optical fiber at

transmission distance. The light wave in SSMF is represented by nonlinear Schrodinger equation (NLSE).

The optical fiber medium can be assumed as a linear medium when the lunch power is low. While in the long-haul fiber optic transmission system, the noise is accumulated by EDFAs along the fiber link. Therefore, the launch power must be increased to obtain high OSNR. The fiber nonlinearity becomes more significant by increasing the launch power. The nonlinear effects become problematic in long haul systems. Therefore, the system performance degrades. Fiber nonlinearities can be classified into two groups [5] as shown in Fig. 4.2. The analysis of the Kerr effect especially SPM is the main point of the dissertation.

The first group is Kerr effect which illustrates the proportionality of the refraction index on the light intensity. The fiber nonlinearities according to this group are classified into: SPM, XPM and FWM. The SPM is the main source of degradation in single channel systems. The XPM is related to the WDM systems. The variation of power of each optical channel is affected by the average power of all other channels leading to change in the refractive index.

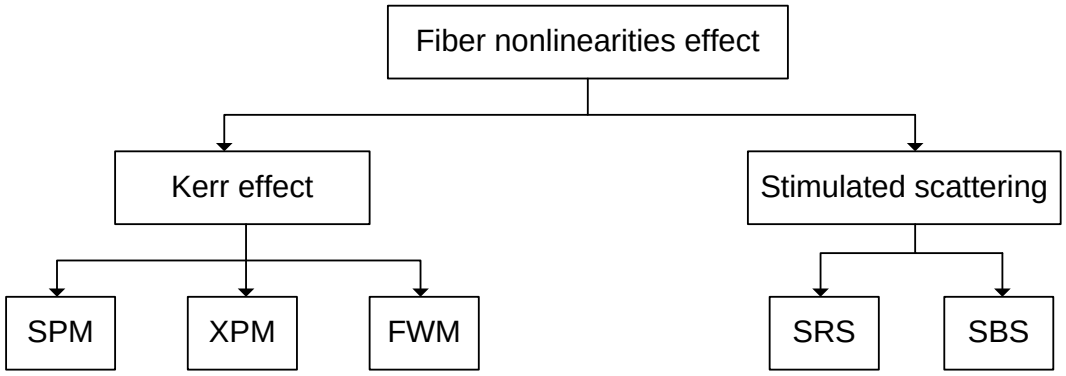

Fig. 4.2: Fiber nonlinearities classification.

Specifically, the refractive index is affected by all optical channels and causes nonlinear phase shift. The FWM is related also to the WDM systems. The interaction between different waves with different frequencies will generate a new wave with new different frequency. When the new wave locates in the other optical channels, it causes crosstalk between channels and degrades the system performance [83].

The second group is stimulated scattering effects which classified into stimulated Raman scattering (SRS) and stimulated Brillouin scattering (SBS). Simulated scattering is caused

due to the interaction of an optical wave with fiber molecules will transfer energy to the medium.

4.3.1 Kerr effect

In 1875, John Kerr discovered the optical Kerr effect. It represents the change in the refractive index of the fiber material to the optical power in the fiber. The change in the refractive index can be written as

$$n = n_0 + n_2 \frac{P}{A_{eff}} \tag{4.13}$$

where n_0 is refractive index for the linear effect, n_2 is the Kerr factor (second-order refractive index) with a value of $(2.2 - 3.4) \times 10^{-20}$ m^2/W, A_{eff} is the effective core area of the fiber and P is the launched power.

4.3.2 Self phase modulation

The propagation constant β is a function of refractive index.

$$\beta = \frac{2\pi n}{\lambda} \tag{4.14}$$

where λ is the wavelength. Thus, the propagation constant will be changed due to the variation in the refractive index as mentioned above.

$$\beta = \frac{2\pi n_0}{\lambda} + \frac{2\pi n_2}{\lambda A_{eff}} P = \beta_0 + \gamma P \tag{4.15}$$

where β_0 is the propagation constant for the linear effect and $\gamma = \frac{2\pi n_2}{\lambda A_{eff}}$ is the nonlinear coefficient with a value of 0.9–2.75 W^{-1} km^{-1} at 1550 nm [5].

The variation in propagation constants along the optical pulse leads to variation in phases in different portions of the pulse. Hence, the refractive index changes due to variations of power in the observed channel leading to the nonlinear phase shift of optical pulses (pulse distortion). By using $P = P_0 e^{-\alpha l}$ where P_0 is the initial launch power and α is the loss coefficient. The total nonlinear phase shift due to SPM after transmission distance L can be given by

$$\phi_{SPM} = \int_0^L [\beta - \beta_0] dz = \int_0^L \gamma P \, dz = \gamma P_0 \frac{1 - e^{-\alpha L}}{\alpha} = \frac{L_{eff}}{L_{Nl}} \tag{4.16}$$

where $L_{eff} = \frac{1-e^{-\alpha L}}{\alpha}$ is the effective length and $L_{Nl} = \frac{1}{\gamma P_0}$ is the nonlinear length. From Eq. (4.16), it can be observed that by decreasing L_{Nl} or increasing P_0, the nonlinear phase shift due to SPM can be enhanced.

4.4 Phase Noise Estimation Techniques

The objective of Section 4.4 is to provide enough background information about the phase noise estimation techniques. Three estimation methods are presented, the CPE (pilot-aided) phase estimation methods has been studied [79, 84]. Then Joint-SPM method is used to improve the SPM tolerance [85] in CO-OFDM transmission systems. Finally, the RFP based phase noise compensation is provided [78]. The RFP method avoids phase noise impairments at the receiver. To separate the RF tone completely from the OFDM spectrum, it is required to reserve a guard band between the RFP signal and the OFDM sidebands. Performance of the CPE and the RFP phase estimation methods have been compared [86]. Different RFP schemes to recover a clear RFP and improve the performance of the CO-OFDM system have likewise been studied and compared [87].

4.4.1 CPE (pilot-aided)

The CPE (pilot-aided) phase estimation method has been studied experimentally for a CO-OFDM transmission at 8 Gbps over 1000 Km SSMF [44, 84] with a small-sized FFT. Uniformly distributed pilots N_p are transmitted with the N_{sc} data subcarriers of the OFDM spectrum as shown in Fig. 4.3. In [84], the authors found that 5 pilots are suitable for effective phase estimation. At the receiver, the estimated laser phase drift is calculated by computing the average of the phase angle difference between the received and transmitted pilots for each symbol in the frequency domain. The estimated phase drift of the i^{th} OFDM symbol φ_i can be formally written as [44, 84]

$$\varphi_i = \arg\left(\frac{1}{N_p}\sum_{k=1}^{N_p}\{\, Y_{ik}^{p}.conj(X_{ik}^{p})\}\right) \tag{4.17}$$

where Y_{ik}^{p} is the received pilot subcarrier amplitude and X_{ik}^{p} is the transmitted pilot subcarrier amplitude of the k^{th} subcarrier in the i^{th} OFDM symbol and conj(.) is the complex conjugate.

The estimated transmitted data R_{ik} after the phase noise compensation can be given as

$$R_{ik} = Y_{ik} e^{-j\varphi_i} \tag{4.18}$$

The main drawback of such method is that the authors assume the OFDM frames must be short to set that the laser phase drift is common for all subcarriers within an OFDM symbol. Therefore, the CPE effect dominates over the ICI effect.

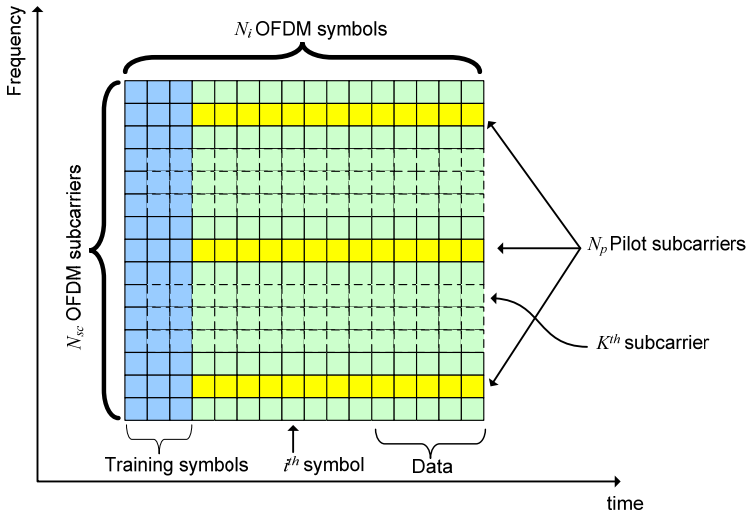

Fig. 4.3: OFDM frame in time & frequency domain.

To compensate nonlinear phase noise, the conventional CPE compensation technique requires more signal processing to be applicable for multi-span transmission [79, 88].

4.4.2 Joint-SPM

Joint-SPM (J-SPM) technique has been proposed to compensate fiber nonlinearities in OFDM transmission. It is an effective method for the compensation of SPM induced transmission impairments. The fiber nonlinearities can be compensated by an electronic post-compensation method based on digital signal processing [89] or using a combination of electronic pre- and post-compensation [90] which doubles the improvement of the received signal quality compared to pre- or post-compensation alone. In J-SPM technique, the electronic pre- and post-compensation is joined with inline dispersion compensated transmission to improve the fiber nonlinearities tolerance [85].

The fiber nonlinearities can be compensated by applying a negative phase shift to Eq. (4.13). The compensated phase noise $\phi_{SPM-comp}$ can be written as

$$\phi_{SPM-comp} = -\gamma P_0(t) L_{eff} \tag{4.19}$$

where γ is the fiber nonlinear coefficient, L_{eff} is the effective length of the fiber and $P_0(t)$ is the signal power. The compensated phase noise $\phi_{SPM-comp}$ is proportional to the signal power $P_0(t)$. In the existence of fiber dispersion, fiber nonlinearities can be mitigated based on digital signal processing at the transmitter, receiver, or both. Selecting a fully periodic dispersion map as shown in Fig. 4.4 can make the signal waveform changes during transmission adequately small to allow highly efficient J-SPM compensation.

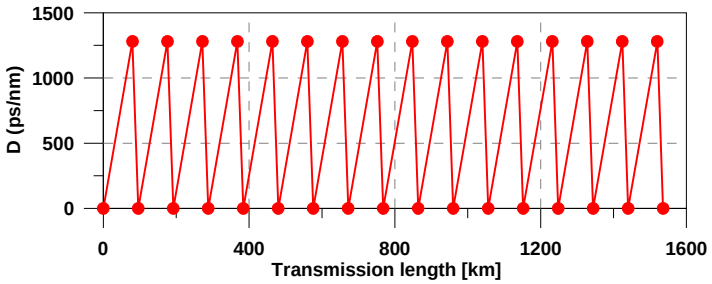

Fig. 4.4: A fully periodic dispersion map.

The J-SPM compensator is implemented after the IFFT at the transmitter side and previous to the FFT process at the receiver. The OFDM transmission system with J-SPM scheme is shown in Fig. 4.5. The drawback of the J-SPM technique is that it requires a priori knowledge of the fiber link parameters.

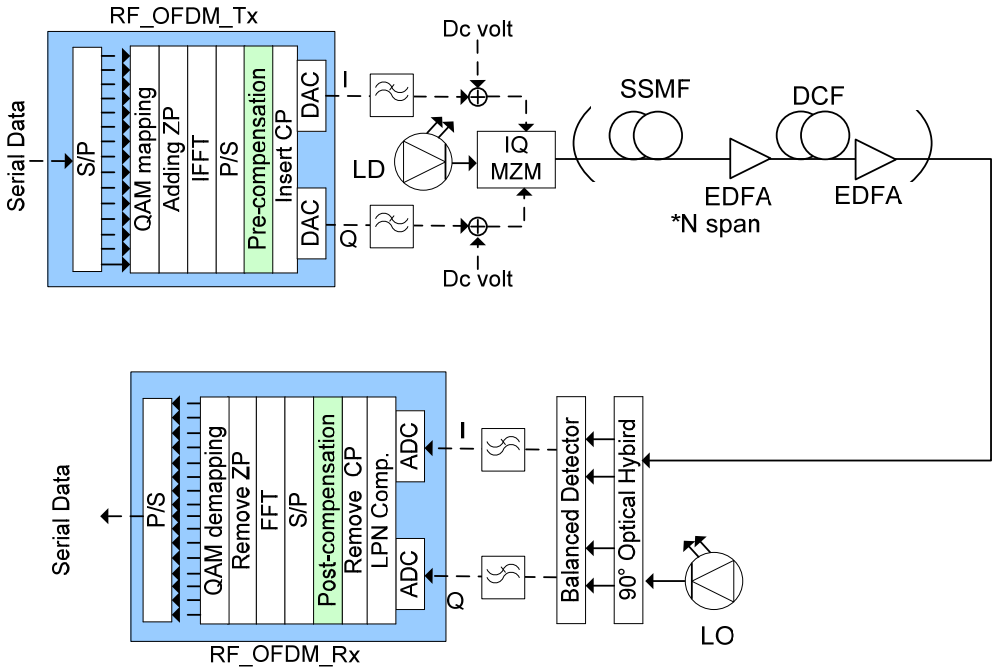

Fig. 4.5: CO-OFDM transmission system with J-SPM.

4.4.3 RFP

The RFP phase noise compensation technique is used to compensate for phase noise induced by transmitter laser and LO. It is able to compensate both ICI and CPE effect. It has been studied for a CO-OFDM transmission at 25.8 Gbps over 4160 km SSMF with 100 kHz laser linewidth [78].

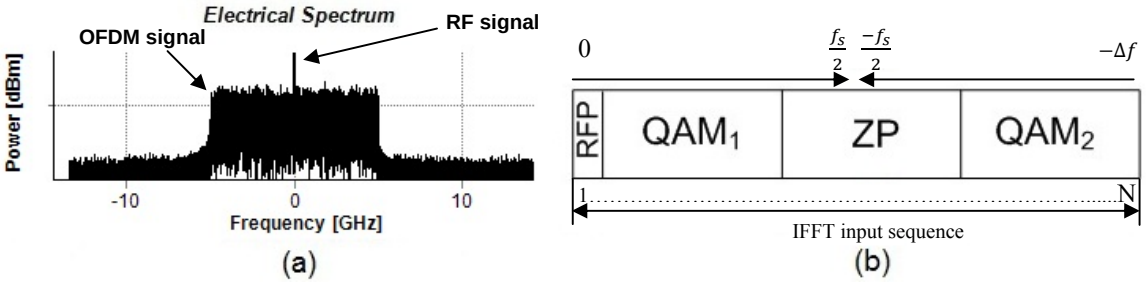

Fig. 4.6: (a) OFDM spectrum for the original RFP model; (b) IFFT input sequence configuration.

The laser phase noise can be compensated by inserting an RFP tone in the middle of the transmitted OFDM signal as shown in Fig. 4.6(a). The RFP tone is inserted by setting the first element on the OFDM symbol to 0 and applying a small DC offset in the I/Q components. The RFP tone will be the first input in the IFFT input sequence while zeros are inserted in the middle of IFFT input sequence as shown in Fig. 4.6(b). Therefore, the RFP tone will be affected by the phase noise and distorted in the same way as the whole OFDM signal. The zeros are padded to shift the alias which is generated by the sampling process away from the OFDM signal. This method will be referred as oversampling during the dissertation. At the receiver, the received RFP is selected by LPF. After a complex conjugation, it multiplies the received OFDM signal to compensate for any phase distortion as shown in Fig. 4.7.

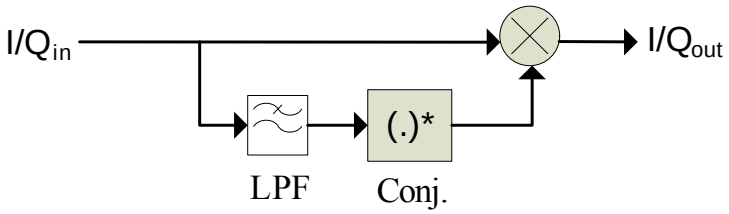

Fig. 4.7: The implementation of RFP phase noise compensator.

It is important to optimize the pilot-to-signal ratio (PSR). The PSR is the power ratio between electrical RFP signal and the average power of OFDM data subcarriers. For low

PSR, the filtered RFP is not accurate for estimating phase distortion due to the dominating ASE on the RFP tone. For high PSR, the OSNR between OFDM data and noise becomes small, which leads to worse performance.

In [86], the authors analyze and compare the CPE and RFP phase estimation methods. It is found that the RFP is more suitable for large laser linewidths and provided a fast phase dynamic. Moreover, it can compensate ICI. The main disadvantage of RFP method is that the residual received RFP is distorted by the received OFDM sidebands. The LPF cannot separate only RFP. Also, they used RF up-conversion to shift the electrical OFDM signal to high frequency in electrical domain before modulation which increases the bandwidth and decreases spectral efficiency. In [23, 78], the authors used an FFT with 256 points, 165 OFDM subcarriers and 90 zero padding (ZP) which are inserted in the middle of the OFDM subcarriers and 1 point as an RFP which inserted in the first element as shown in Fig. 4.6(b).

In [91], the authors use a 2% as guard band around the RFP to separate the clear RFP. The RF tone can be separated completely from the OFDM spectrum in [87, 92]. Zeros can be padded at both edges of the IFFT input sequence as shown in Fig. 4.8(b). Such configuration is called guard band. A LPF can simply separate the RFP as shown in Fig. 4.8(a). But the alias will not be removed as there is no oversampling.

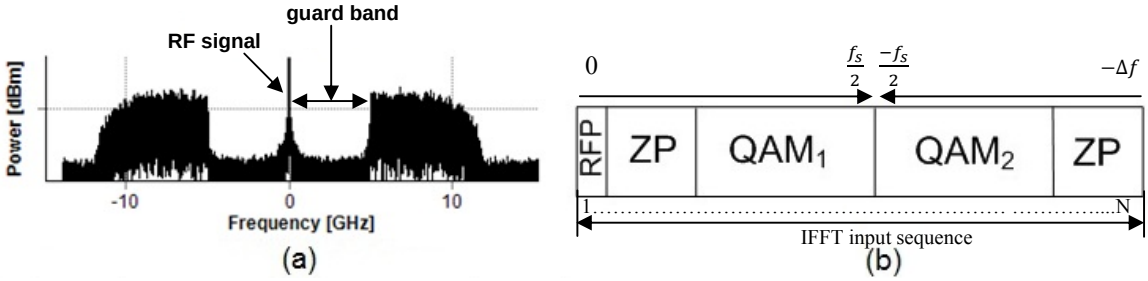

Fig. 4.8: (a) OFDM spectrum for guard band-RFP model; (b) IFFT input sequence configuration.

As a consequence, the RFP phase noise compensation model can be enhanced by removing the alias and separating the RFP from the OFDM sidebands. The zeros are inserted at both edges and in the middle IFFT input sequence as shown in Fig. 4.9(b). Band shifting and oversampling are combined. Such scheme is called enhancement-RFP (E-RFP) model. The LPF can simply separate a clear, undistorted RFP [87] as shown in Fig. 4.9(a).

The performance of the RFP algorithm depends on the bandwidth of the LPF, power of the pilot tone and number of padded zeros as the more zeros padding, the more reduction in spectral efficiency and bit rate.

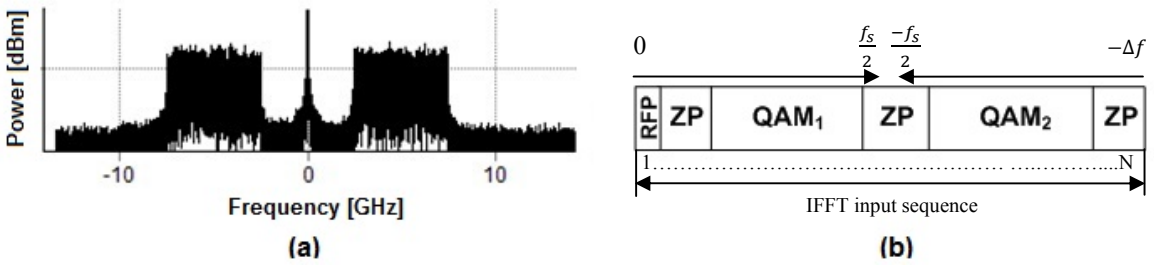

Fig. 4.9: OFDM spectrum for the E-RFP model; (b) IFFT input sequence configuration.

The RFP technique was also proposed for compensation of SPM and XPM in multiple OFDM channels for a 2000-km SSMF link with tap equalization [93]. The numerical results show that the RFP method increased the improvement of the nonlinear tolerance from 0.4 dB in a single channel system up to 0.5 dB for a WDM system. The small improvement indicates that the RFP scheme does not compensate for SPM effectively. The authors in [94, 95] proved that using SPM compensator with the RFP algorithm is more effective for SPM and XPM compensation. The simulation results show that the signal Q-factor is increased by 2.4 dB if SPM compensator is used.

4.4.3.1 Simulation setup of RFP approaches

The performance analysis of the original RFP scheme and the extended RFP schemes that overcome the drawbacks of the original RFP scheme has been investigated [87, 92]. Figure 4.10 shows the schematics of CO-OFDM transmission systems using the RFP phase noise compensation technique with direct up/down conversion architecture. The generation and analysis of the OFDM signal and system performance are simulated using Matlab™ and VPItransmissionMaker™ V8.5. The RFP, the guard band-RFP and the E-RFP phase noise compensation schemes have been applied to a CO-OFDM back-to-back transmission system.

An OFDM signal with a nominal data rate of 80 Gbps is generated from PRBS of length 2^{13}-1. The bit stream is converted from serial to parallel and then mapped with 16-QAM. An IFFT/FFT size of 1024 is used with 512 for the modulated data subcarriers and 512 ZP. The first channel is used to insert the RFP tone. In the RFP scheme, 511 zeros are padded from channel 258 to channel 768 of the FFT channels. While 511 zeros in the guard band-RFP scheme are inserted from channel 2 to channel 256 and from channel 769 to channel 1024. In the E-RFP scheme, 511 zeros are inserted from channel 2 to channel 128, from channel 385 to channel 640 and from channel 897 to channel 1024. A CP having 12.5% of the symbol

length is added. The information symbols are serialized and converted to analog electrical signal, using a DAC with a sample rate of 40 GS/s. A square root raised cosine filter with a roll-off factor of 0.2 removes the alias and filters the main OFDM signal. To insert the RFP tone, a small DC bias is inserted in the I and Q branches of the I/Q mixer to achieve an optimal PSR of 12.3 dB in back-to-back configuration. A laser with 100 KHz linewidth is assumed to generate a continuous signal at 193.1 THz. It is modulated with the OFDM signal in a small offset -biased IQ-MZM due to the insertion of RFP tone and ensure that the MZM modulator is driven in its linear field region. To test OSNR performance, ASE noise is added to deteriorate the received OSNR. An equal linewidths for transmitter and LO lasers are assumed.

At the receiver, the received optical signal and LO signal are fed directly into an optical 90° hybrid. The optical 90° hybrid is used for direct down-conversion to base-band signal. Two balanced photo-detectors in each branch are used to detect I/Q components. The OFDM signals from the balanced detectors are filtered using square root raised cosine filter with a roll-off factor of 0.2 and then sampled with ADCs. The phase noise compensation for the different applied RFP schemes is performed. The digital serial signal is converted to complex parallel data blocks using an S/P converter, and the CP is removed. Using FFT, the OFDM signal is demodulated. After removal of ZP, each QAM symbol is decoded by QAM de-mapping. The parallel data can be converted to serial data by P/S conversion.

4.4.3.2 Simulation results of RFP approaches

The influence of OSNR on BER is shown for 80 Gbps CO-OFDM back-to-back systems with direct up/down conversion using VPItransmissionMaker™ V8.5 and Matlab™ in Fig. 4.10. Using VPItransmissionMaker™ V8.5, a BER of less than 10^{-3} cannot be obtained for the RFP scheme. For the E-RFP and for the guard band-RFP phase noise compensation algorithms the required OSNR for a BER of 10^{-3} are 25 dB and 25.8 dB, respectively. Compared with the guard band-RFP scheme, the E-RFP can improve the OSNR by 0.8 dB. Using Matlab™, a BER of less than 10^{-3} cannot be obtained for the RFP scheme, while the required OSNR for a BER of 10^{-3} is 25 dB and 25.4 dB for the E-RFP and for the guard band-RFP phase noise compensation algorithms, respectively. The provided RFP approaches with frequency gap between the OFDM sidebands enhance the performance of the CO-OFDM systems with the standard RPF-based phase noise compensation [78].

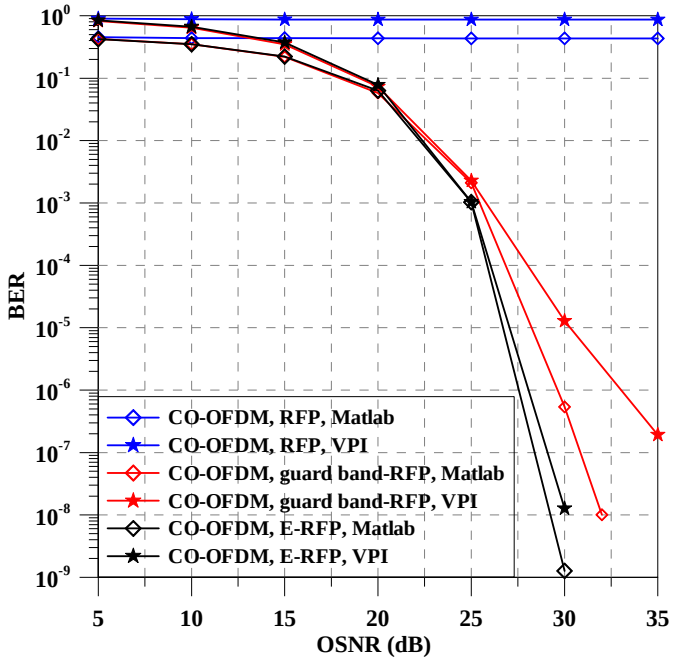

Fig. 4.10: BER versus OSNR of different RFP schemes in CO-OFDM systems using VPI and Matlab.

For 16-QAM, it is important to maintain a sufficiently broad guard band between the RFP tone and the OFDM spectrum to separate the RFP tone easily. The OSNR differences for the simulations result vary about 0.4 dB which increases with a higher OSNR. The increasing difference is due to the BER floor affecting VPItransmissionMaker™ results more than the Matlab™ results.

Figure 4.11 presents the BER performance as a function of OSNR for CO-OFDM transmission systems, one with a 20 GHz IF and the other with direct up/down conversion. Using VPItransmissionMaker™, a BER of less than 10^{-3} cannot be obtained with the RFP scheme for both architectures. With the E-RFP phase noise compensation algorithm, the required OSNR for a BER 10^{-3} is 25 dB and 25.3 dB for CO-OFDM systems with direct up/down conversion and with IF, respectively. So the direct up/down conversion improves the OSNR by 0.3 dB. When using the guard band- RFP method, the required OSNR for a BER of 10^{-3} is 25.8 dB and 32.5 dB for CO-OFDM with direct up/down conversion and with IF, respectively. So the OSNR improvement is increased to 6.7 dB. The advantages of direct-conversion architecture are (1) reduction of the required electrical bandwidth for transmitter and receiver, (2) cancellation of the requirements for image rejection filters in both transmitter and receiver.

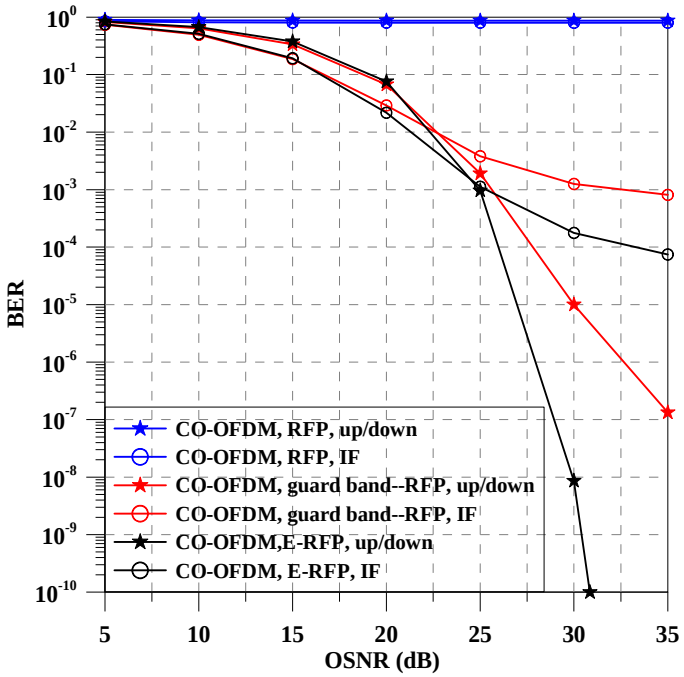

Fig. 4.11: BER versus OSNR of different RFP schemes in CO-OFDM systems with different architectures.

Figure 4.12 represents the influence of ROP on BER for 80 Gbps CO-OFDM transmission systems with direct up/down conversion at 35 dB OSNR and 100 KHz linewidth for the various RFP schemes. The ROP is varied from −40 dBm to 10 dBm.

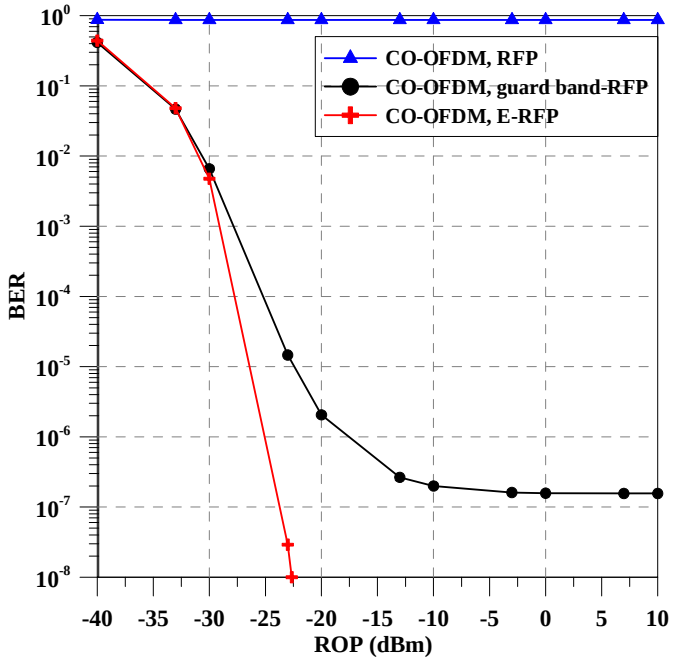

Fig. 4.12: BER versus ROP of different RFP schemes in CO-OFDM systems.

For the guard band-RFP and for the E-RFP phase noise compensation algorithm, the required OSNR for 10^{-3} BER are −27.85 dBm and −29.15 dBm, respectively. Compared with the guard band-RFP scheme, the E-RFP can improve the ROP by 1.3 dB. While the BER performance for the RFP scheme indicates that 35 dB OSNR is not sufficient to transmit with a BER 10^{-3}, increased ROP does improve the BER as shown in Fig. 4.12.

Figure 4.13 shows the BER performance with varying laser linewidth at 35 dB of OSNR and 0 dBm ROP. The RFP scheme cannot achieve a BER of 10^{-3}, while the E-RFP and the guard band-RFP phase noise compensation algorithms can reach a BER of 10^{-3} at 3.85 MHz and 1.85 MHz linewidth, respectively. Increased laser linewidth brings the E-RFP performance close to that of the guard band-RFP while the RFP performance is not as much affected. Our provided schemes perform better than the RFP scheme, even at 1 MHz linewidth.

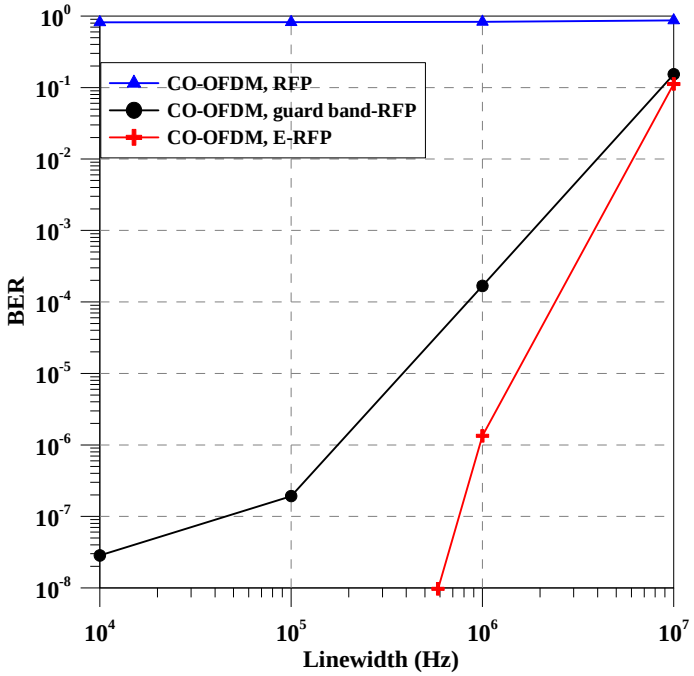

Fig. 4.13: BER versus laser linewidth versus ROP of different RFP schemes in CO-OFDM systems.

The provided RFP approaches with frequency gap between the OFDM sidebands enhance the performance of the CO-OFDM systems compared to the RPF phase noise compensation [78]. For 16-QAM, it is important to maintain a sufficiently broad guard band between the RFP tone and the OFDM spectrum to separate the RFP tone easily. For the three configurations, the OFDM bandwidth will be 24 GHz while the net bit rate for the

transmission system will be 71.1 Gbps. Therefore, the spectrum efficiency will be 2.96 bit/s/Hz.

4.5 Proposed Phase Noise Estimation Techniques

Section 4.5 presents new techniques for compensating the laser phase noise and mitigating the effect of the SPM induced by fiber nonlinearity. The first algorithm uses RFP phase noise compensation via CPE equalizer [96]. It uses the RFP technique in combination with the CPE method. A partial pilot filling (PPF) method is a new technique which is investigated to compensate the effect of laser phase noise [97, 98] and mitigate the effect of the SPM induced by fiber nonlinearity [99] in coherent optical OFDM. The PFF method uses linear interpolation between constant pilot frequencies. It has been shown experimentally [100] that the PPF technique can be validated in OFDM transmission systems. Finally, frequency domain dual compensators scheme for nonlinear phase noise mitigation is proposed for CO-OFDM long haul transmission systems [101]. The first compensator is similar to the CPE compensator. The second compensator estimates the phase noise of the remaining intermediate samples by linear interpolation using every two consecutive pilots [97, 98].

4.5.1 RFP-CPE

A CPE equalizer is combined with RFP compensator to mitigate the phase noise effect for CO-OFDM transmission system. The CPE scheme [84] effectively compensates for the CPE effect after using the E-RFP compensation method. A few uniformly distributed pilots are transmitted with the OFDM data subcarriers. Also, an RFP tone is inserted in the middle of the transmitted OFDM signal by setting the first element on the OFDM symbol to 0 and applying a small DC offset at the I/Q components. At the receiver, the phase noise is compensated in two stages [96]. The first stage uses the E-RFP phase noise compensation scheme in the time domain. After the OFDM signal is demodulated by an FFT, the second stage uses the CPE compensator in the frequency domain.

Figure 4.14(a) shows the electrical spectrum of I channel with higher aliasing product. After DACs, the aliasing will be removed by LPF as shown in Fig. 4.14(b). The RFP tone is inserted by setting the first subcarrier to 0 and inserting a small dc offset in the I and Q channels. The pilots and the RFP tone which are used for phase noise compensation can be seen.

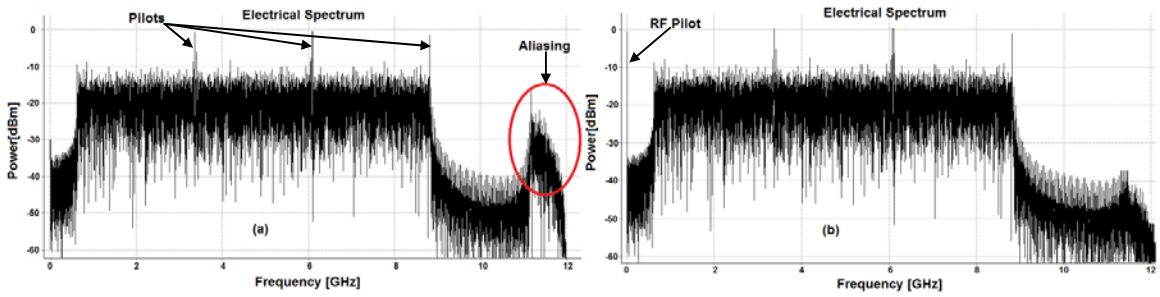

Fig. 4.14: Electrical OFDM spectrum with RFP & pilots.

4.5.1.1 Simulation setup of RFP-CPE approach

The generation and analysis of the OFDM signal and system performance are simulated using VPItransmissionMaker™ V9.0. Figure 4.15 shows the schematic of a CO-OFDM transmission system using the RFP-CPE phase noise compensation method. An OFDM signal with a nominal data rate of 40 Gbps is generated. The bit stream is converted from serial to parallel and then mapped with 4-QAM. The IFFT/FFT size is 512, for the processing of $N_{sc} = 414$ modulated data subcarriers. 60 zeros for oversampling are inserted at the middle of the IFFT input sequence to shift the alias which is generated by the sampling process away from the OFDM signal. A spectral gap of 32 zeros is inserted at both edges of IFFT input sequence and $N_p = 6$ pilots are reserved for RFP-CPE and CPE schemes. In case of the E-RFP scheme, for a fair comparison, 60 + 6 = 66 zeros for oversampling are used. A CP of 12.5 % of the symbol length is set. The information symbols are serialized. The electrical signal is sampled at a rate of 20 GS/s. A square root raised cosine filter with a roll-off factor of 0.2 removes the alias and filters the main OFDM signal. The OFDM bandwidth will be 19.7 GHz and the data rate will be 28.8 Gbps. Therefore, the spectral efficiency will be 1.45 bit/s/Hz. A laser with 100 kHz linewidth is modeled to generate a continuous signal at 193.1 THz. It is modulated with the OFDM signal in a small offset -biased IQ-MZM due to the insertion of RFP tone with an extinction ratio of 30 dB. To evaluate the OSNR performance, ASE noise is added to control the received OSNR. Equal linewidths for transmitter and LO lasers are assumed. The LO power is assumed to be 0 dBm.

The optical transmission link consists of 15 fiber spans. Each of them comprises 80 km of SSMF with an attenuation of 0.2 dB/km, a dispersion of 16 ps/nm/km, a dispersion slope of 0.08 ps/nm^2/km and a nonlinear coefficient (γ) 1.3 W^{-1}km^{-1}. After each span, the fiber loss is compensated by a double-stage EDFA with a noise figure of 4 dB. Between each EDFA's

stages, there is 16-km of DCF with a dispersion of −80 ps/nm/km; thereby forming a fully periodic dispersion map. The DCF launch power is 6 dB lower than the SSMF launch power to decrease the effect of DCF nonlinearity.

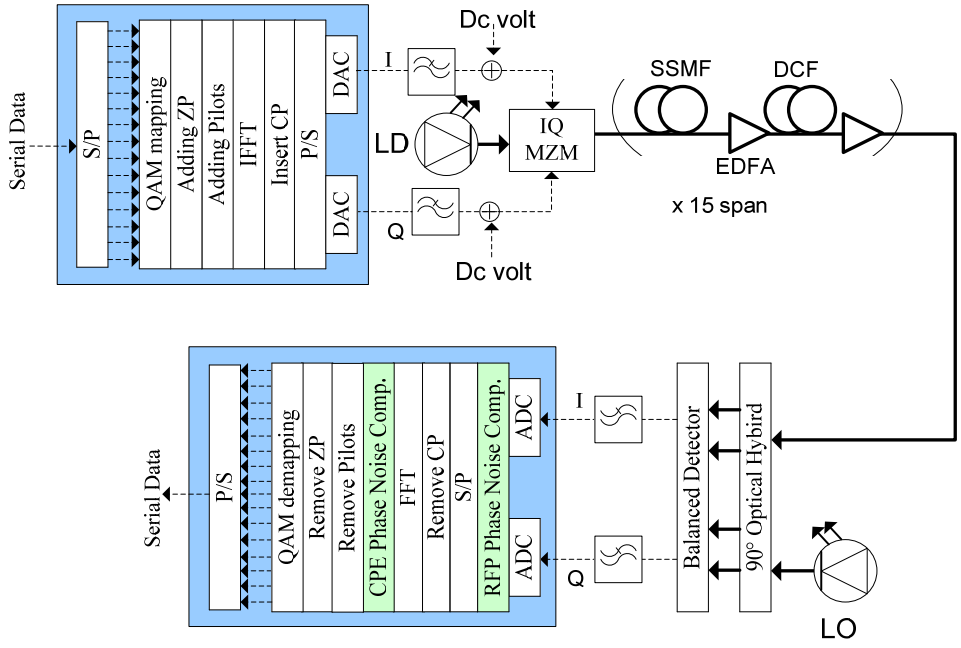

Fig. 4.15: Schematic for a CO-OFDM transmission system using the RFP-CPE compensators.

At the receiver, an I/Q homodyne detector is assumed. The OFDM signals from the balanced detectors are filtered by a LPF and then sampled with ADCs at a sampling rate of 20 GS/s. The phase noise is compensated in two stages. Firstly, the RFP compensator works in the time domain. Secondly, after an FFT the CPE compensator is utilized in the frequency domain.

4.5.1.2 Simulation results of RFP-CPE approach

The performances of the laser phase noise mitigation schemes are simulated and compared for CO-OFDM back-to-back transmission systems. A BER is simulated for each laser having a linewidth of 100 kHz and a ROP of 0 dBm. The E-RFP phase noise compensation models use the optimal PSR value of 6.45 dB, while the RFP-CPE scheme uses the optimal PSR value of 5.7 dB. A 4^{th} order 35 MHz Butterworth LPF is used at the receiver side to extract the RFP signal.

Figure 4.16 presents the BER performance as a function of OSNR. The required OSNR for BER of 10^{-3} is 8.7 dB, 9.7 dB and 9.5 dB for the RFP-CPE, the CPE and the E-RFP phase

noise compensation algorithms, respectively. The RFP-CPE can improve OSNR at a BER of 10^{-3} by 0.8 dB compared to the E-RFP and about 1.0 dB compared the CPE method.

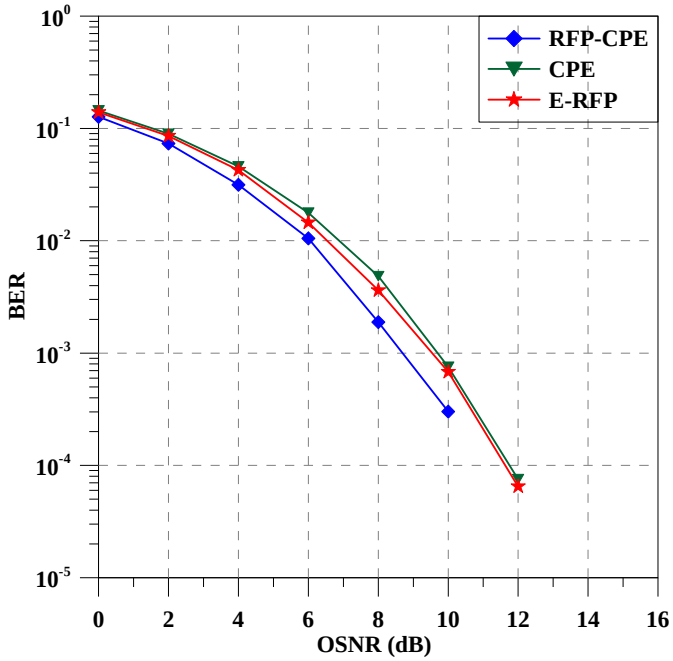

Fig. 4.16: BER versus OSNR of RFP-CPE, CPE and E-RFP schemes for CO-OFDM back-to-back systems.

Figure 4.17 shows the system Q factor of the received data as a function of individual laser linewidth at 9 dB of OSNR and 0 dBm ROP.

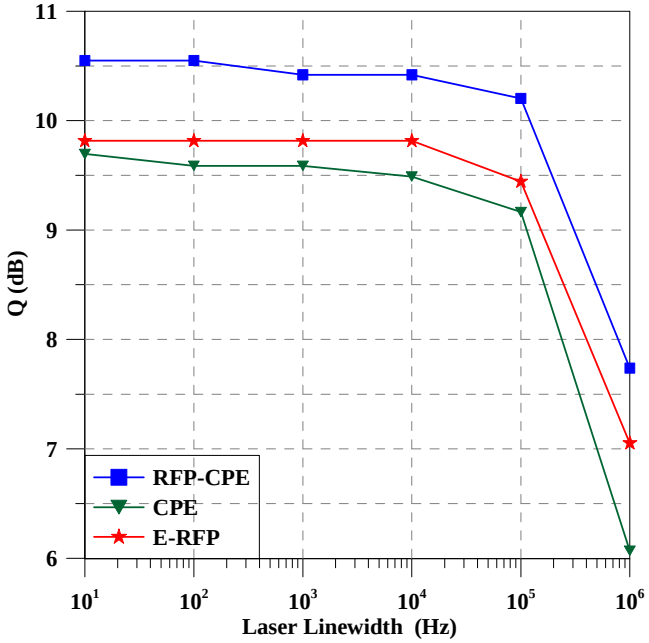

Fig. 4.17: System Q factor versus laser linewidth of RFP-CPE, CPE and E-RFP schemes for CO-OFDM back-to-back systems.

The system Q factor for a linewidth of 100 kHz is 10.2 dB, 9.16 dB and 9.44 dB for the RFP-CPE, the CPE and the E-RFP phase noise compensation algorithms, respectively. In all schemes, the Q factor decreases for laser linewidths beyond 100 kHz. The RFP-CPE scheme can improve the Q factor by 1.04 dB and 0.76 dB compared to the CPE and the E-RFP schemes, respectively. By increasing the laser linewidth up to 1 MHz, the RFP-CPE still shows the best performance.

In Fig. 4.18, the influence of ROP on the system Q factor is shown for 40 Gbps CO-OFDM transmission systems with 9 dB of OSNR and 100 kHz laser linewidth for the E-RFP scheme, CPE method and RFP-CPE model. The ROP is varied from −40 dBm to +10 dBm. Obviously, it is required automatic gain control in practice. By increasing the ROP, the Q factors of the received data improve until the ROP reaches −23 dBm, then they barely change. At 0 dBm ROP, the Q value for the RFP-CPE, CPE and E-RPF phase noise compensation algorithms are 10.2 dB, 9.16 dB and 9.44 dB, respectively. The RFP-CPE can improve the Q factor by 0.76 dB compared to the E-RFP scheme and about 1.04 dB compared to the CPE method. The RFP-CPE method shows a better sensitivity than the CPE method and E-RFP phase noise compensation.

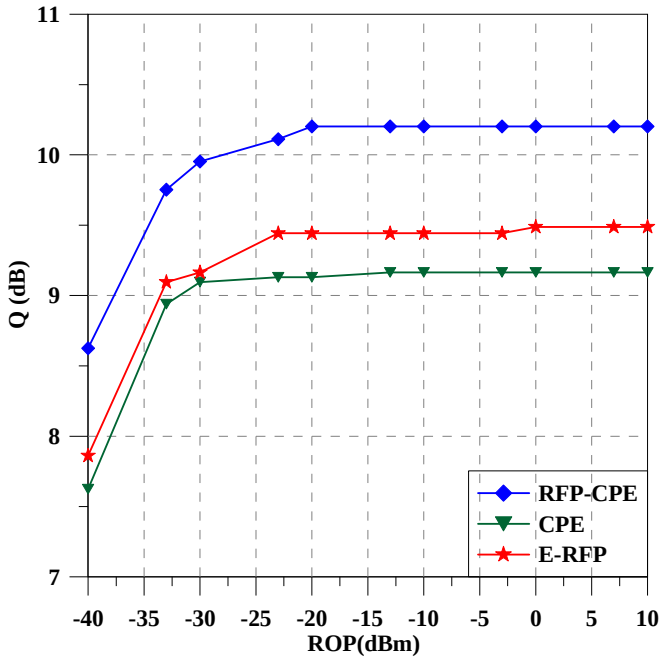

Fig. 4.18: System Q factor versus ROP of RFP-CPE, CPE and E-RFP schemes for CO-OFDM back-to-back systems.

The impact of SPM on a single channel configuration is investigated. The performances of the phase noise mitigation schemes are simulated and compared for CO-OFDM transmission systems due to fiber nonlinearity only. Ideal lasers without phase noise are assumed.

Figure 4.19 presents the BER performance as a function of OSNR for 40 Gbps CO-OFDM transmission systems over 1200-km SSMF with 0 dBm of ROP for the E-RFP, CPE and RFP-CPE models. The required OSNR for BER of 10^{-3} is 10.86 dB, 13.1 dB and 12.55 dB for the RFP-CPE, CPE and E-RFP phase noise compensation algorithms, respectively. The RFP-CPE improves the OSNR at a BER of 10^{-3} by 1.69 dB compared to the E-RFP and about 2.24 dB compared the CPE method. The simulation results show that the RFP-CPE scheme mitigates significantly the impact of SPM.

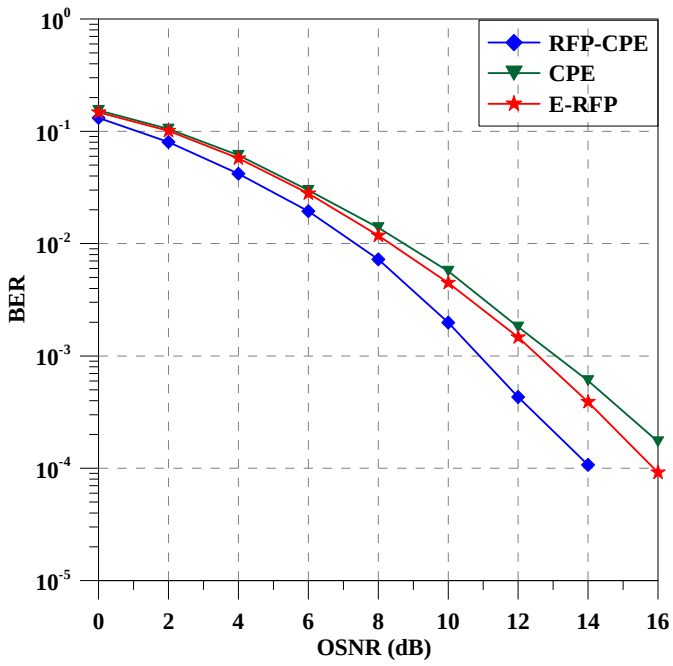

Fig. 4.19: BER versus OSNR of RFP-CPE, CPE and E-RFP schemes for CO-OFDM systems over 1200-km transmission.

Figure 4.20 shows the system Q factor as a function of fiber length with 11 dB OSNR and 0 dBm ROP. Over 1200 km, RFP-CPE gives about 0.6 dB and 1.1 dB improvement compared to the E-RFP and the CPE schemes, respectively. Again, it shows that the RFP-CPE significantly reduces the SPM penalty of the fiber.

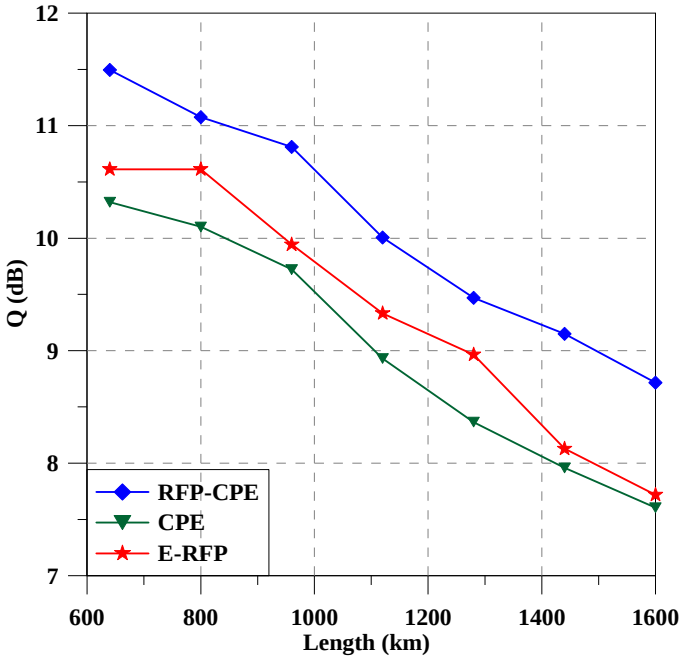

Fig. 4.20: System Q factor of RFP-CPE, CPE and E-RFP schemes for CO-OFDM systems versus fiber length.

Figure 4.21 presents the system Q factor as a function of the launch power for 40 Gbps CO-OFDM transmission systems over 1200-km SSMF with 0 dBm of ROP and 11 dB of OSNR for the E-RFP, the CPE and the RFP-CPE models.

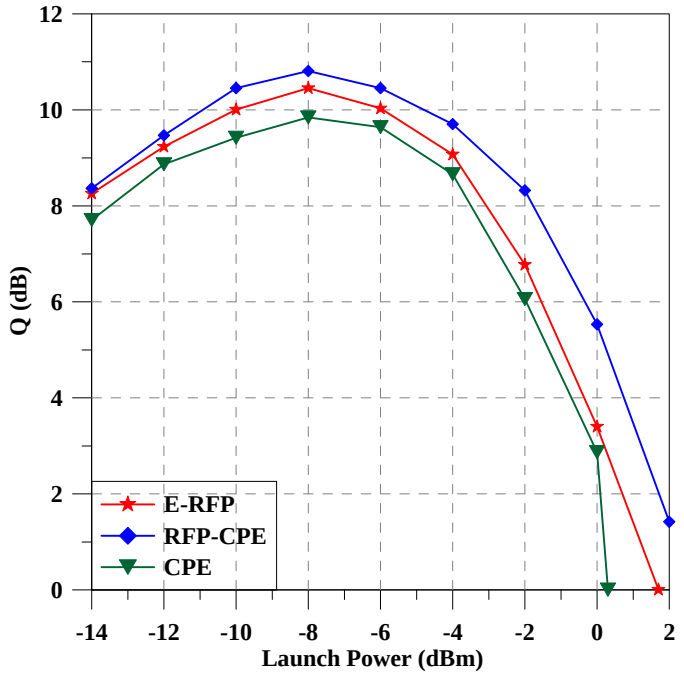

Fig. 4.21: System Q factor of RFP-CPE, CPE and E-RFP schemes for CO-OFDM systems versus optical launch over 1200-km transmission.

For low launch powers, the CPE decreased the performance by about 0.7 dB while RFP-CPE scheme improved performance for all powers. The nonlinearity limitation is above −10 dBm. At −8 dBm launch power when total nonlinearity is high, the RFP-CPE gives 1 dB and 0.4 dB improvement in Q-factor compared to the CPE and RFP schemes, respectively. The proposed scheme mitigates the effect of fiber nonlinearity very much.

Figure 4.22 shows the influence of ROP on the system Q factor for 40 Gbps CO-OFDM transmission systems with 11 dB OSNR, 0dBm ROP and −4 dBm launch power for the CPE scheme, the E-RFP method and the RFP-CPE model. The ROP is varied from −40 dBm to +10 dBm. An automatic gain control is required in practice. By increasing the ROP, the Q factors of the received data improve until the ROP reaches –20 dBm; then they barely change. At 0 dBm ROP, the Q value for the RFP-CPE, CPE and E-RPF phase noise compensation algorithms are 9.77 dB, 8.66 dB and 9.07 dB, respectively. The RFP-CPE can improve the Q factor by 0.7 dB compared to the E-RFP scheme and about 1.11 dB compared to the CPE method. The RFP-CPE method shows a better sensitivity than the E-RFP phase noise compensation and the CPE method.

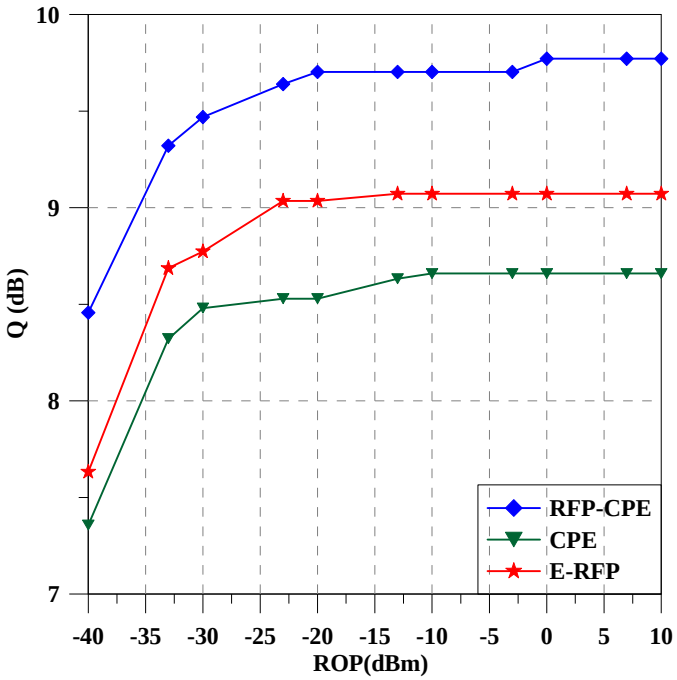

Fig. 4.22: System Q factor versus ROP of RFP-CPE, CPE and E-RFP for CO-OFDM systems over 1200-km transmission.

The same simulation parameters are used for PDM-CO-OFDM transmission system with 4 training symbols every 50 OFDM data symbols, these training symbols are inserted to the head of OFDM frame at the transmitter. The training symbols are used for frame synchronization, frequency offset compensation and channel estimation as explained in Section 3.5. Hence, the net bit rate will be 53.2 Gbps. Subsequently, the spectral efficiency will be 2.7 bit/s/Hz. While in the single polarization transmission systems, the data rate will be 26.6 Gbps. Hence, the spectral efficiency will be 1.35 bit/s/Hz.

At the receiver side, the optical, the received optical signal is split into *x*-polarization (*x*-pol.) and *y*-polarization (*y*-pol.) by a PBS and then fed into polarization diversity coherent receiver. After frame synchronization, the frequency offset is mitigated and the laser phase noise is compensated using RFP-CPE technique. The influence of OSNR on the BER for using RFP-CPE phase noise technique is shown in Fig. 4.23. The BER is simulated for each laser linewidths of 100 kHz and ROP of 0 dBm. A BER of 10^{-3} can be observed at OSNR of 12.4 dB for single polarization. The OSNR requirement for PDM transmission system is increased about 2.7 dB compared with the single polarization, which is theoretical penalty of 3 dB.

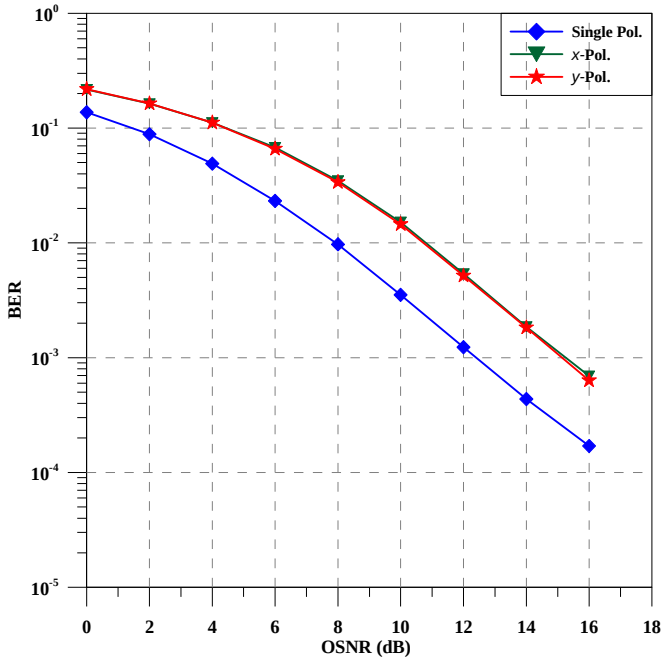

Fig. 4.23: BER versus OSNR for single and PMD CO-OFDM systems using RFP-CPE scheme.

4.5.2 PPF

The pilot-based compensation has been studied to estimate the channel response by interpolation in wireless OFDM [102]. The authors in [103] used the linear interpolation method to mitigate the ICI effects in time domain, to mitigate ICI by calculating the deterministic crosstalk from adjacent subcarriers from the variation of the CPE of following OFDM-symbols. The PPF technique for laser phase noise compensation in CO-OFDM transmission systems is investigated in [97, 98]. Also, it can be used to mitigate the effect of the SPM induced by fiber nonlinearity [99] in coherent optical OFDM. The performance of the PPF method is experimentally studied at sampling rate of 5 GS/s with laser linewidth of 150 kHz and 4-QPSK in 320-km CO-OFDM transmission systems [100]. The PPF scheme uses constant pilot frequencies for phase estimation to compensate laser phase noise based on linear interpolation.

A few N_p uniformly distributed pilots are transmitted with the N_{sc} subcarriers of the OFDM spectrum as shown in Fig. 4.24. A filling factor (FF) is defined as the number of pilots divided by total number of the subcarriers in each OFDM symbol which is equal to OFDM subcarriers plus pilots [104].

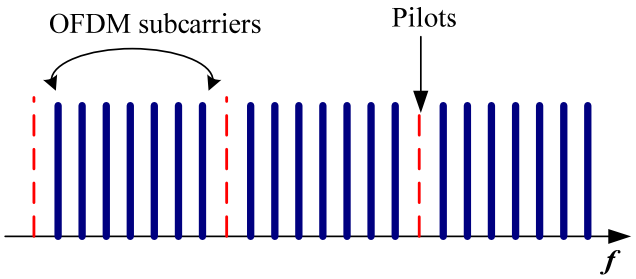

Fig. 4.24: OFDM symbol with distributed pilots at FF = 1/8.

Figure 4.24 shows the case of FF= 1/8 with one pilot before every seven OFDM subcarriers. At the receiver, after the OFDM signal is demodulated by an FFT. The PPF phase noise compensation is done in 3 steps:

1. Separation of pilots from OFDM data subcarriers.
2. Estimation of the remaining intermediate subcarriers amplitude by linear interpolation using amplitude of every two consecutive pilots P_{if} and P_{in} in the frequency domain for f^{th} and n^{th} subcarriers, respectively.

$$\hat{P}_{ik} = P_{if} + \frac{k-f}{n-f} \cdot \left(P_{in} - P_{if}\right) \qquad f < k < n \tag{4.20}$$

where $\hat{P}_{ik}$ is the estimated subcarrier amplitude of the k^{th} subcarrier which is located between the pilots P_{if} and P_{in} based on linear interpolation.

3. Complex conjugation of the estimated subcarrier amplitude and subsequent multiplication with the received OFDM signal which is given by

$$R_{ik} = Y_{ik} \cdot \frac{conj(\hat{P}_{ik})}{abs(\hat{P}_{ik})} \tag{4.21}$$

where $abs(\hat{P}_{ik})$ is the absolute value of the estimated subcarrier amplitude, R_{ik} is the estimated transmitted data after phase noise compensation and Y_{ik} is the received OFDM signal in frequency domain after FFT stage. k and i denote the subcarrier in frequency domain and OFDM symbol indices in time domain, respectively.

Several methods are used to compare the performance of the linear interpolation and mean value methods. The true and estimated values are compared to select the best method for estimating the missing values. Two performance indicators are used which are mean absolute error and root mean square error.

The mean absolute error (MAE) is calculated by

$$MAE = \frac{1}{N}\sum_{i=1}^{N}|E_i - T_i| \tag{4.22}$$

The root mean-squared error (RMSE) is evaluated by

$$RMSE = \left(\frac{1}{N}\sum_{i=1}^{N}[E_i - T_i]^2\right)^{1/2} \tag{4.23}$$

where N is no. of selected points, E_i and T_i are the estimated and true values of phase noise.

Both the MAE and RMSE range are starting from 0 and lower values of RMSE and MAE indicate the better performance of the method.

Figure 4.25 describes an example of random phase noise fluctuations with laser linewidth of 200 kHz for one OFDM symbol with 128 subcarriers. Furthermore, the CPE and PPF methods are used to estimate phase noise. Obviously, the CPE method calculates the mean phase noise for each OFDM symbol which is not accurate for the fast phase noise

fluctuations. On the other hand, the PPF estimation gives more accurate estimation due to the linear interpolation usage.

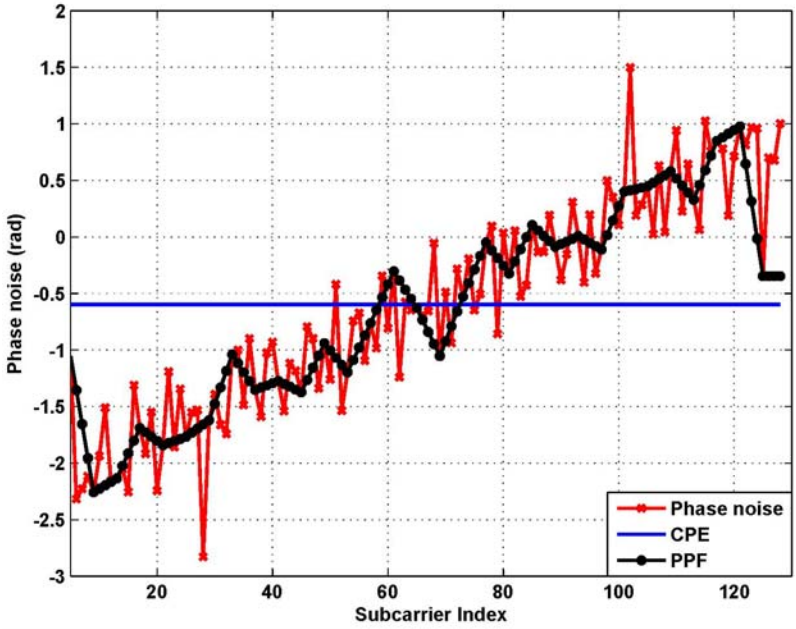

Fig. 4.25: Random phase noise variation over one OFDM symbol with CPE and PPF phase noise estimation.

From Table 4.1, the PPF method gives the smaller values for both the MAE and RMSE compared to the CPE method.

	MAE	**RMSE**
CPE	0.84	1.06
PPF	0.31	0.5

Table 4.1: Performance indicators of the CPE and PPF methods.

Using Matlab™, An OFDM signal with a nominal data rate of 40 Gbps is generated. The Data mapped with 4-QAM. An IFFT/FFT size of 512 is used with different numbers of OFDM subcarriers depending on the numbers of pilots. The information symbols are serialized and converted to analog electrical signals, using DACs with 20 GS/s sampling rate. A square root raised cosine filter with a roll-off factor of 0.2 removes the alias and filters the main OFDM signal. ASE noise is added to control the received OSNR. At the receiver, by an FFT the OFDM signal is demodulated. Phase noise compensated in the applied PPF schemes. After removal of the pilots, each QAM symbol is decoded by QAM de-mapping. BER is simulated for each laser having a linewidth of 100 kHz.

In Fig. 4.26, the performance of the PPF phase noise compensation is evaluated. The phase noise estimation is obtained with the PPF using linear interpolation and nearest neighbor methods. The nearest neighbor method estimates the phase of OFDM subcarriers as the phase of the nearest pilot. It cannot detect variations of the phase as a function of frequency. The alternative is the linear interpolation of OFDM subcarrier phases between the pilots. The influence of the OSNR on the BER is shown for 40 Gbps CO-OFDM back-to-back transmission systems at 100 kHz linewidth for FF = 1/16. The OSNR is varied from 0 dB to 14 dB. For PPF with linear interpolation and nearest neighbor method, the required OSNR for a BER of 10^{-3} are 7.5 dB and 8.5 dB, respectively. Compared with the nearest neighbor method, linear interpolation can improve the OSNR by 1.0 dB.

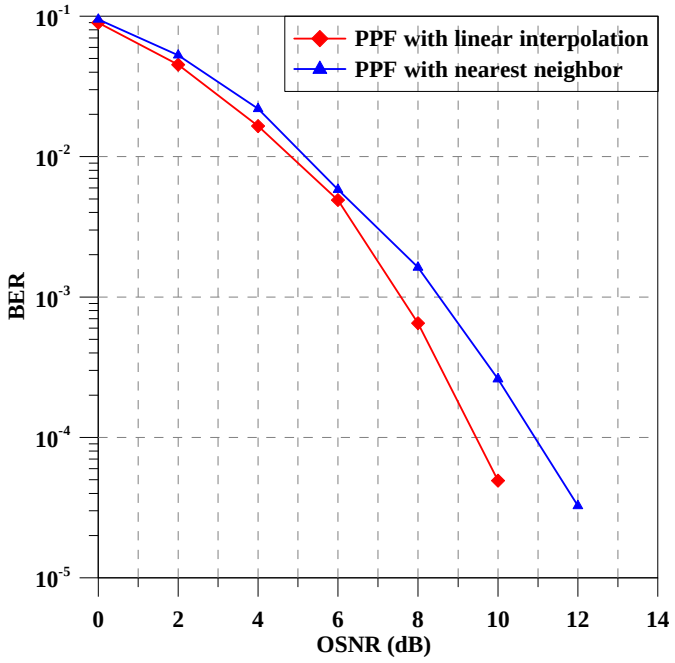

Fig. 4.26: BER performance versus OSNR in case of nearest neighbor and linear Interpolation.

Figure 4.27 shows the BER performance as a function of the number of pilots at three different OSNRs. Too few pilots are not suitable to compensate for the phase fluctuations. It can be seen that 32 pilots (FF = 1/16) are the best number of pilots for phase estimation. Increasing number of pilots, the BER performance is barely improved.

Figure 4.28 presents the BER performance as a function of OSNR at different FFs and the RFP compensation technique with 448 OFDM subcarriers and 64 zero padding [78] for 40 Gbps CO-OFDM back-to-back transmission systems at 100 kHz linewidth.

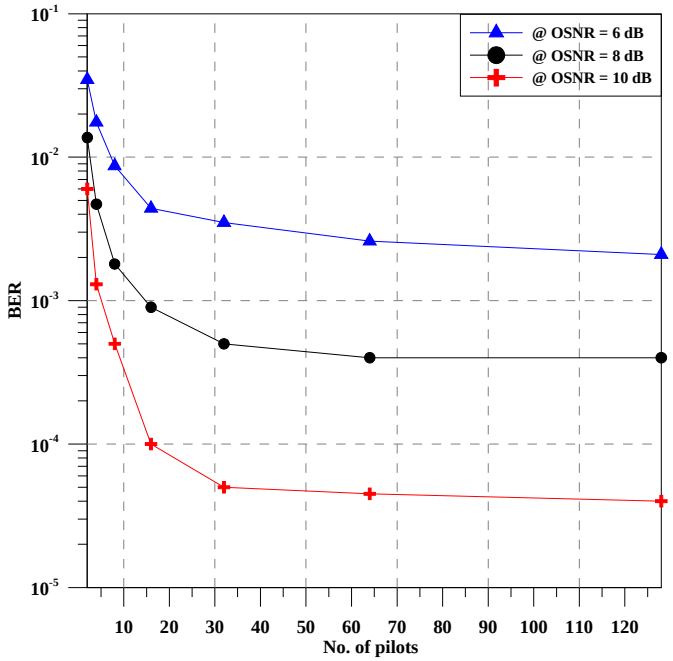

Fig. 4.27: BER performance versus number of pilots.

A BER of less than 10^{-3} cannot be obtained with the RFP method. The residual received RFP is distorted by the received OFDM sidebands. The LPF cannot separate only RFP. For PPF using linear interpolation with FF = 1/16, 1/32, 1/64 and 1/128, the required OSNR for a BER 10^{-3} is 7.5 dB, 7.0 dB, 7.0 dB and 6.9 dB, respectively.

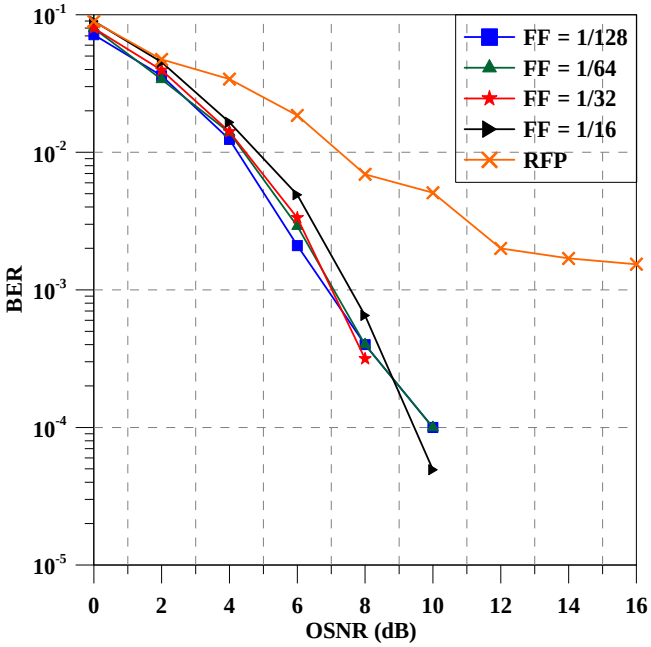

Fig. 4.28: BER versus OSNR for PPF with different FFs and RFP schemes.

Compared with FF = 1/16, PPF compensation scheme can improve the OSNR by 0.5 dB With FF = 1/32, 1/64 and about 0.6 dB using FF = 1/128.

4.5.2.1 Simulation setup of PPF approach

The generation and analysis of the OFDM signal and system performance are simulated using VPItransmissionMaker™ V9.0. Figure 4.29 shows the schematic of a CO-OFDM transmission system using PPF phase noise compensation method. An OFDM signal with a nominal data rate of 40 Gbps is generated. The bit stream is converted from serial to parallel and then mapped with 4-QAM. The IFFT/FFT size is 1024, for the processing of $N_{sc} = 954$ for modulated data subcarriers and 64 zeros for oversampling are inserted at the middle of the IFFT input sequence to shift the aliases which is generated by the sampling process away from the OFDM signal. For phase noise compensation $N_p = 6$ are reserved as a pilot in the PPF and CPE schemes. In case of the E-RFP, for a fair comparison, a spectral gap of 6 zeros is inserted around the RFP tone. A CP of 12.5 % of the symbol length is set. The information symbols are serialized. The electrical signal is sampled at a sampling rate of 20 GS/s. A square root raised cosine filter with a roll-off factor of 0.2 removes the alias and filters the main OFDM signal. OFDM have bandwidth of 22.5 GHz and the data rate will be 33.13 Gbps. Therefore, the spectral efficiency will be 1.47 bit/s/Hz for single polarization transmission system.

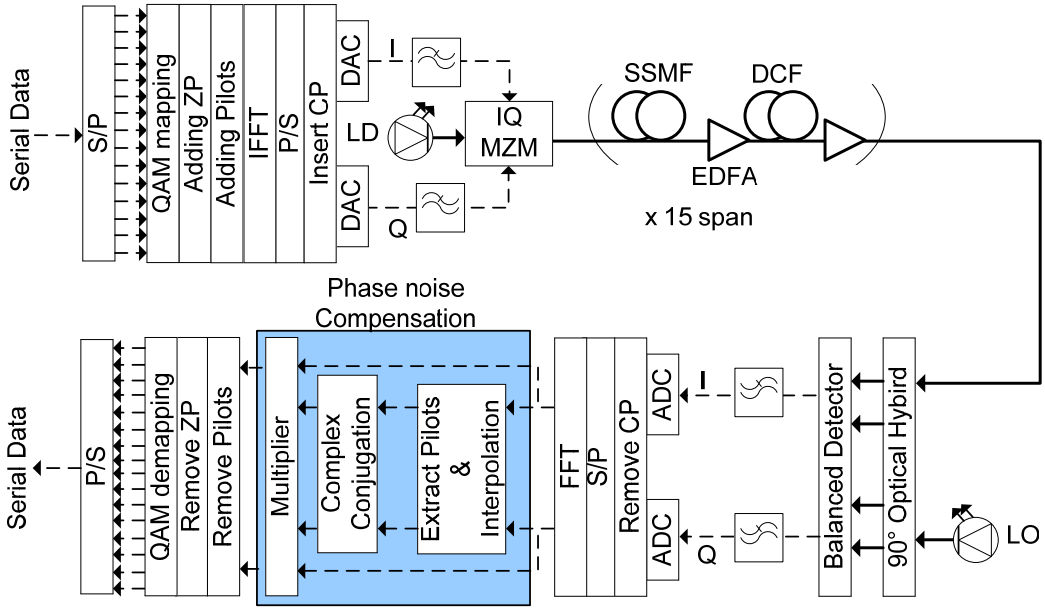

Fig. 4.29: Schematic for a CO-OFDM transmission system using PPF phase noise compensation.

A laser with 100 kHz linewidth is modeled to generate a continuous signal at 193.1 THz. It is modulated with the OFDM signal in a null-biased IQ-MZM with an extinction ratio of 30 dB. To evaluate the OSNR performance, ASE noise is added to control the received OSNR. Equal linewidths for transmitter and LO lasers are assumed. The LO power is assumed to be 0 dBm.

The optical transmission link consists of 15 fiber spans. Each of them comprises 80-km SSMF with an attenuation of 0.2 dB/km, a dispersion of 16 ps/nm/km and a dispersion slope of 0.08 ps/nm^2/km and a nonlinear coefficient (γ) 1.3 W^{-1}km^{-1}. After each span, the fiber loss is compensated by a double-stage EDFA with a noise figure of 4 dB. Between each EDFA's stages there is a 16-km of DCF with a dispersion of −80 ps/nm/km; thereby a fully periodic dispersion map is formed. The DCF launch power is 6 dB lower than the launch power of SSMF to decrease the effect of DCF nonlinearity.

At the receiver, an I/Q homodyne detector is assumed. The OFDM signals from the balanced detectors are filtered by a LPF and then sampled with ADCs at a sampling rate of 20 GS/s. The serial digital signal is converted to complex parallel data blocks by an S/P converter. An FFT demodulates the OFDM signal. Phase noise is compensated by the PPF scheme. After removal of the pilots, each QAM symbol is decoded by QAM de-mapping to produce parallel data. They can be converted to serial data by P/S conversion. Three schemes have been simulated: CO-OFDM with the E-RFP, CPE and PPF.

4.5.2.2 Simulation results of PPF approach

The performances of the laser phase noise mitigation schemes are simulated and compared for CO-OFDM back-to-back transmission systems. A BER is simulated for each laser having a linewidth of 100 kHz, OSNR of 11 dB and ROP of 0 dBm. The E-RFP phase noise compensation models use the PSR optimal value of 4.8 dB. A 4th order 35 MHz Butterworth LPF is used at the receiver side to extract the RFP signal.

The performance of the PPF phase noise compensation based on linear interpolation is simulated for different FFT size. Figure 4.30 (a) shows the influence of OSNR on the BER for the FFT size varied from 512 to 2048 at 100 kHz laser line-width, 0 dBm ROP and FF = 1/128. The PPF scheme is an effective method to compensate the laser phase noise with a high FFT size. With 2048 FFT, the PPF method can achieve a BER of 10^{-4}.

Figure 4.30(b) presents the BER performance as a function of OSNR. The required OSNR for BER of 10^{-3} is 9.6 dB, 10.0 dB and 10.7 dB for the PPF, CPE and E-RFP phase noise compensation algorithms, respectively. The PPF can improve OSNR at a BER of 10^{-3} by 1.1 dB compared to the E-RFP and about 0.4 dB compared the CPE method.

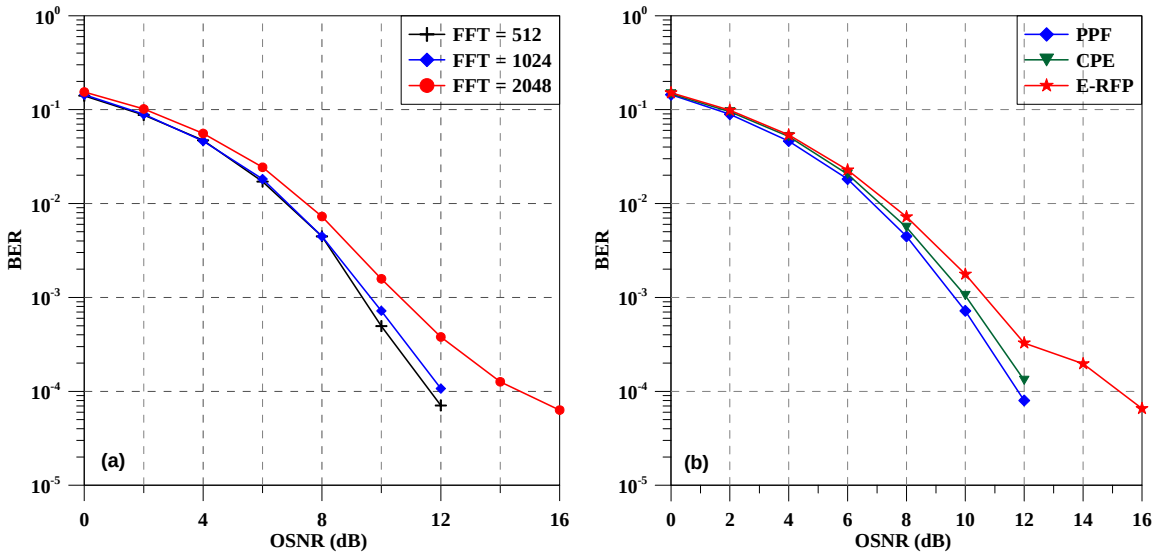

Fig. 4.30: BER performance versus OSNR for CO-OFDM back-to-back system (a) for PPF scheme with different FFT size; (b) for PPF, CPE and E-RFP schemes.

Figure 4.31 shows the system Q factor of the received data as a function of individual laser linewidth at 10 dB of OSNR and 0 dBm ROP. The system Q factor for a linewidth of 100 kHz is 10.06 dB, 9.76 dB and 9.3 dB for the PPF, CPE and E-RFP phase noise compensation algorithms, respectively. In all schemes, the Q factor decreases for laser linewidths beyond 100 kHz. The PPF scheme can improve the Q factor by 0.3 dB and 0.76 dB compared to the CPE and E-RFP schemes, respectively. By increasing the laser linewidth up to 1 MHz, the CPE performance is brought close to that of the E-RFP model whereas the PPF still shows the best performance. The PPF scheme performs better than the other schemes.

In Fig. 4.32, the influence of ROP on the system Q factor is shown for 40 Gbps CO-OFDM transmission systems with 10 dB of OSNR and 100 kHz laser linewidth for the E-RFP scheme, the CPE method and PPF model. The ROP is varied from −40 dBm to +10 dBm. Obviously, it is required automatic gain control in practice. By increasing the ROP, the Q factors of the received data improve until the ROP reaches −23 dBm, then they barely change.

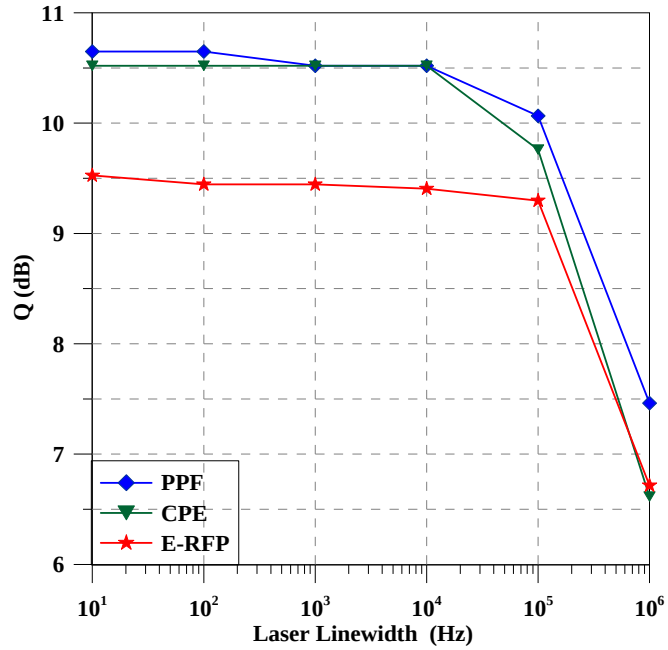

Fig. 4.31: System Q factor versus laser linewidth of PPF, CPE and E-RFP schemes for CO-OFDM back-to-back systems.

At 0 dBm ROP, the Q value for the PPF, CPE and E-RPF phase noise compensation algorithms are 10.06 dB, 9.76 dB and 9.3 dB, respectively. The PPF can improve the Q factor by 0.76 dB compared to the E-RFP scheme and about 0.3 dB compared to the CPE method.

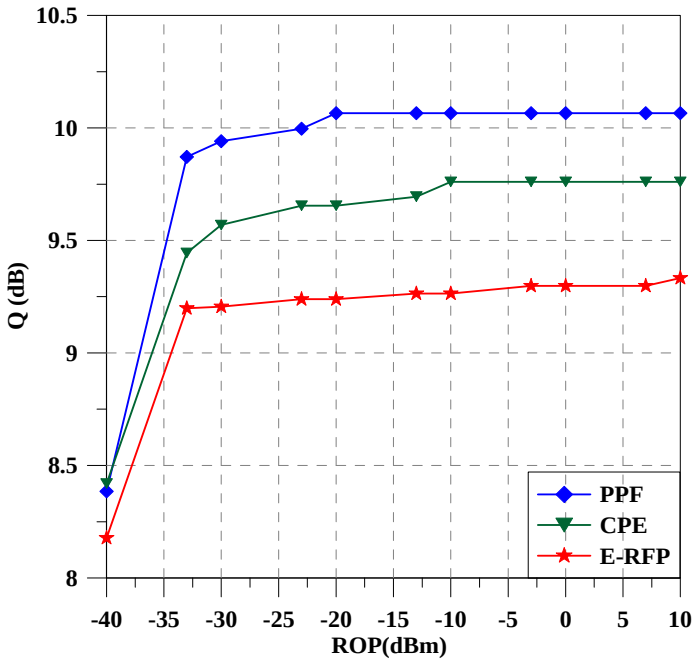

Fig. 4.32: System Q factor versus ROP of PPF, CPE and E-RFP schemes for CO-OFDM back-to-back systems.

The PPF method shows a better sensitivity than the E-RFP phase noise compensation and CPE method.

The impact of SPM on a single channel configuration is investigated. The performances of the phase noise mitigation schemes are simulated and compared for CO-OFDM transmission systems due to fiber nonlinearity only. Ideal lasers without phase noise are assumed. The J-SPM compensation technique is added to the study, for a fair comparison 64 + 6 = 70 zeros for over sampling are used.

Figure 4.33 presents the BER performance as a function of OSNR for 40 Gbps CO-OFDM transmission systems over 1200-km SSMF with -3 dBm of ROP for the E-RFP, CPE, Joint-SPM and PPF models. The required OSNR for BER of 10^{-3} is 10.44 dB, 11.46 dB, 12.44 dB and 13.17 dB for the PPF, J-SPM, CPE and E-RFP phase noise compensation algorithms, respectively. The PPF improves the OSNR at a BER of 10^{-3} by 2.73 dB compared to the E-RFP and about 2.0 dB compared the CPE method. The PPF also gives 1.02 dB improvement in OSNR compared to the J-SPM technique. The simulation results show that the PPF scheme mitigates significantly the impact of SPM.

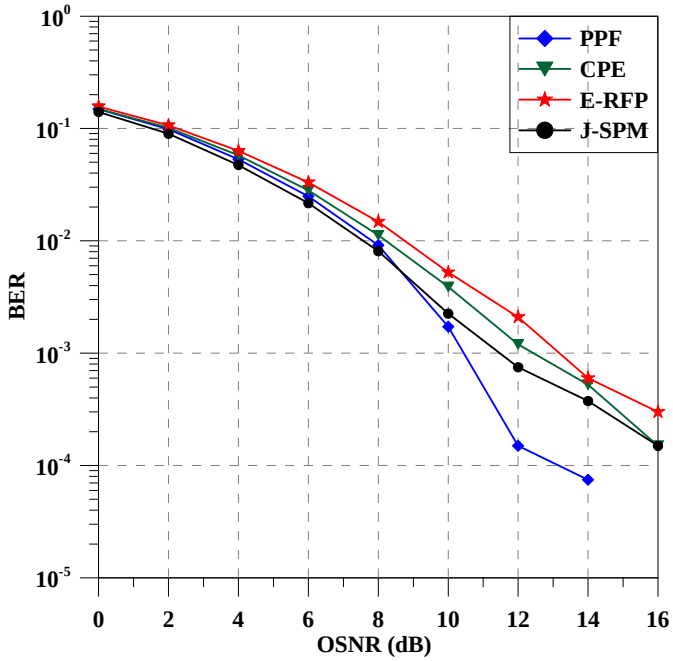

Fig. 4.33: BER versus OSNR of PPF, CPE, J-SPM and E-RFP schemes for CO-OFDM systems over 1200-km transmission.

Figure 4.34 shows the influence of ROP on the system Q factor for 40 Gbps CO-OFDM transmission systems with 11 dB OSNR and -4 dBm launch power for the CPE scheme, PPF

method, J-SPM technique and E-RFP model. The ROP is varied from −40 dBm to +10 dBm. Obviously, it is required automatic gain control in practice. By increasing the ROP, the Q factors of the received data improve until the ROP reaches −23 dBm, then they barely change. At 0 dBm ROP, the Q value for the PPF, J-SPM, CPE and E-RFP phase noise compensation algorithms are 10.2 dB, 9.6 dB, 9.0 dB and 8.7 dB, respectively. The PPF gives 0.6 dB improvement in the system Q factor compared to the Joint-SPM. Whereas, the PPF improves the Q factor by 1.2 dB compared to the CPE scheme and about 1.5 dB compared to the E-RFP method. The PPF method shows a better sensitivity than the CPE scheme, J-SPM technique and E-RFP phase noise compensation.

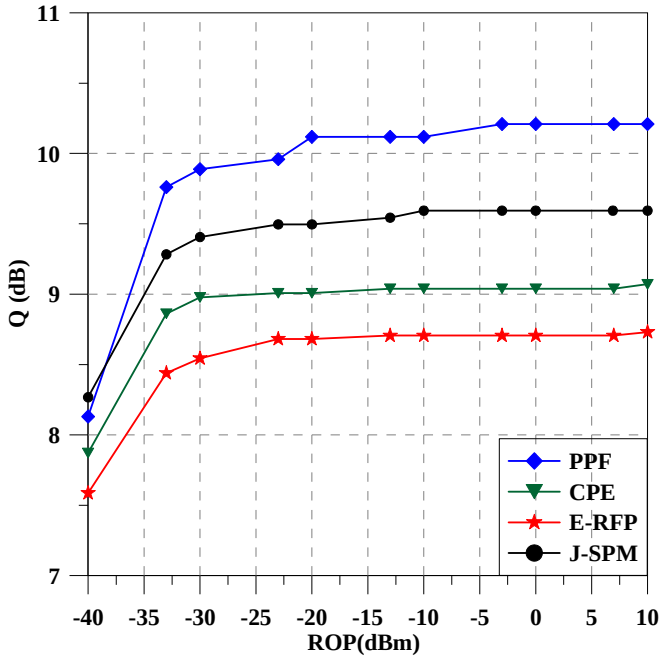

Fig. 4.34: System Q factor versus ROP of PPF, J-SPM, CPE and E-RFP for CO-OFDM systems over 1200-km transmission.

Figure 4.35(a) presents the system Q factor as a function of the launch power for 40 Gbps CO-OFDM transmission systems over 1200-km SSMF with 0 dBm of ROP and 11 dB of OSNR for the E-RFP, CPE, J-SPM and PPF models. The PPF scheme improved performance for all powers. The nonlinearity limitation is above −10 dBm. At −6 dBm launch power when total nonlinearity is high, the PPF gives 1.6 dB, 1.3 dB and 0.8 dB improvement in Q-factor compared to the E-RFP, CPE and J-SPM schemes, respectively. The proposed scheme mitigates the effect of fiber nonlinearity very much.

Figure 4.35(b) shows the system Q factor as a function of fiber length with 11 dB OSNR and −3 dBm ROP. The dash black line (FEC limit) indicates the required Q factor for BER = 10^{-3}. Over 1200 km, PPF gives nearly 1.5 dB and 1.2 dB improvement compared to the E-RFP and CPE schemes, respectively. Again, the results reveal that the PPF significantly reduces the SPM penalty of the fiber.

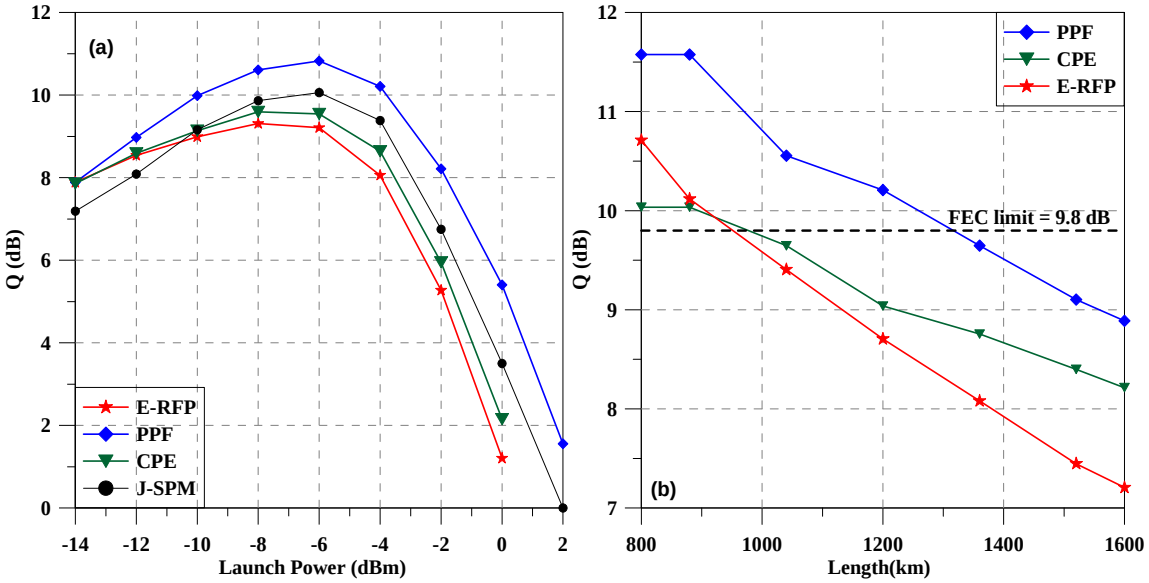

Fig. 4.35: System Q factor of PPF, CPE and E-RFP schemes for CO-OFDM systems versus (a) optical launch over 1200-km transmission; (b) fiber length.

Figure 36 shows the BER performance as a function of OSNR for single polarization and PDM CO-OFDM transmission systems. There are 4 training symbols every 50 OFDM data symbols for frame synchronization, frequency offset compensation and channel estimation as studied in Section 3.5. Hence, the net bit rate will be 61.4 Gbps. Subsequently, the spectral efficiency will be 2.7 bit/s/Hz. While in the single polarization transmission systems, the data rate will be 30.7 Gbps. Therefore, the spectral efficiency will be 1.36 bit/s/Hz. After frame synchronization, the frequency offset is mitigated and the laser phase noise is compensated in frequency domain using PPF scheme. The BER is simulated for each laser linewidths of 100 kHz and ROP of −3 dBm. The required OSNR for BER of 10^{-3} can be observed at 12.9 dB for 4-QAM single polarization. The OSNR requirement for PDM transmission system is increased about 3 dB which is theoretical penalty to reach 16 dB and 16.1 dB for *x* and *y* polarizations, respectively.

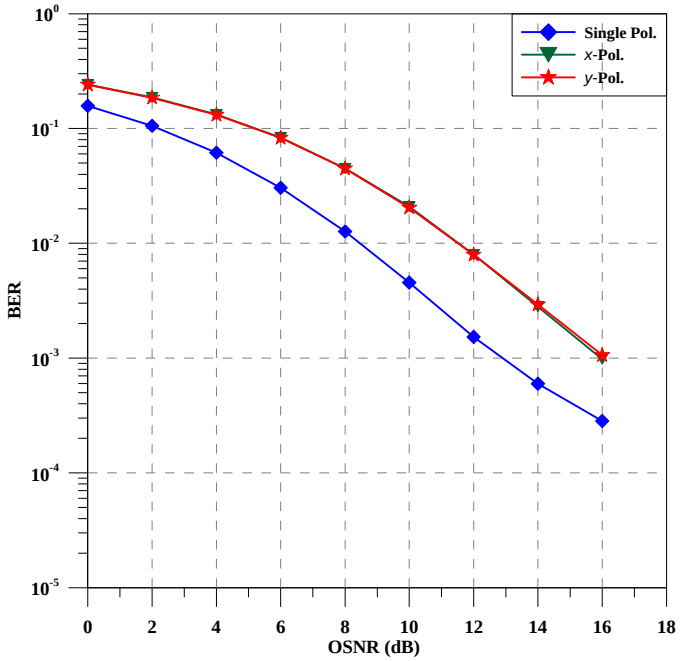

Fig. 4.36: BER versus OSNR for single and PMD CO-OFDM systems using PPF method.

4.5.3 Dual frequency compensators

A non-iterative method for phase noise mitigation in CO-OFDM transmission systems [105] is investigated. The authors used the linear interpolation method to mitigate the ICI effect in the time domain, to mitigate ICI by calculating the deterministic crosstalk from adjacent subcarriers from the variation of the CPE of following OFDM-symbols. The main drawbacks are the implementation complexity which is significantly higher for equalization and FFT processes. Moreover, it requires neglecting the first half of the first OFDM symbol and the second half of the last OFDM symbol which have no effect onto the interpolation process.

In the dual compensators (Dual-Comp), a few uniformly distributed pilots are transmitted with the OFDM data subcarriers. At the receiver, after the OFDM signal is demodulated by an FFT, the dual compensators work in the frequency domain. The first compensator is similar to the CPE compensator; it estimates the phase drift by computing the average of the difference between the received and transmitted pilots for each symbol. The second compensator estimates the phase noise of the remaining intermediate samples by linear interpolation using every two consecutive pilots [101].

4.5.3.1 Simulation setup of Dual frequency compensators

The generation and analysis of the OFDM signal and system performance are simulated using VPItransmissionMaker™ V9.0. Figure 4.37 shows the schematic of a CO-OFDM transmission system using the dual compensators. A 4-QAM OFDM signal with a nominal data rate of 40 Gbps is generated. The IFFT/FFT size is 512 with 26 zeros for oversampling to shift the alias which is generated by the sampling process away from the OFDM signal and 480 for the modulated data subcarriers. For phase noise compensation, $N_p = 6$ are reserved for pilots in the CPE, PPF schemes and in the Dual-Comp method. A CP of 12.5 % of the symbol length is set. The electrical signal is sampled at a sampling rate of 20 GS/s. A square root raised cosine filter with a roll-off factor of 0.2 removes the alias and filters the main OFDM signal. The bandwidth of OFDM will be 22.8 GHz and the data rate will be 33.3 Gbps. Therefore, the spectral efficiency will be 1.46 bit/s/Hz. A laser with 100 kHz linewidth is modeled to generate a continuous signal at 193.1 THz. It is modulated with the OFDM signal in a null-biased IQ-MZM with an extinction ratio of 30 dB. To evaluate the OSNR performance, ASE noise is added to control the received OSNR. Equal linewidths for transmitter and LO lasers are assumed. The LO power is assumed to be 0 dBm.

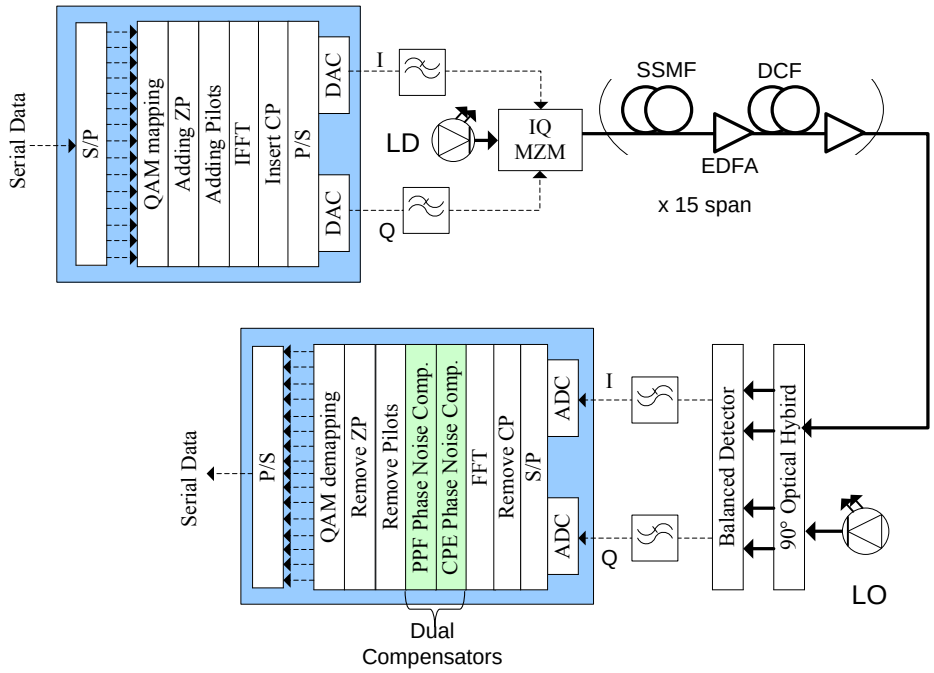

Fig. 4.37: Schematic for a CO-OFDM transmission system using dual compensators.

The optical transmission link consists of 15 fiber spans. Each of them comprises 80 km SSMF with an attenuation of 0.2 dB/km, a dispersion of 16 ps/nm/km, a dispersion slope of 0.08 ps/nm^2/km and a nonlinear coefficient (γ) of 1.3 W^{-1} km^{-1}. After each span, the fiber loss is compensated by a double-stage EDFA with a noise figure of 4 dB. Between each EDFA's stages, there is a 16 km of DCF with a dispersion of −80 ps/nm/km; thereby a fully periodic dispersion map is formed. The DCF launch power is 6 dB lower than the SSMF launch power to decrease the effect of DCF nonlinearity.

At the receiver, a homodyne detector is implemented. The OFDM signals from the balanced detectors are filtered by a LPF and then sampled with ADCs at a sampling rate of 20 GS/s.The serial digital signal is converted to complex parallel data blocks by an S/P converter. An FFT demodulates the OFDM signal. Phase noise is compensated by the dual compensators. After removal of the pilots, each QAM symbol is decoded by QAM de-mapping to produce parallel data. They can be converted to serial data by P/S conversion. Three schemes have been simulated: CO-OFDM with the Dual-Comp, CPE and PPF.

4.5.3.2 Simulation results of Dual frequency compensators

The performances of the laser phase noise mitigation schemes are simulated and compared for CO-OFDM back-to-back transmission systems. A BER is simulated for each laser having a linewidth of 100 kHz and a ROP of 0 dBm.

Figure 4.38 presents the BER performance as a function of OSNR. The required OSNR for BER of 10^{-3} is 9.65 dB, 10.34 dB and 9.81 dB for the Dual-Comp, CPE and PPF phase noise compensation algorithms, respectively. The Dual-Comp can improve OSNR at a BER of 10^{-3} by 0.16 dB compared to the PPF and about 0.69 dB compared the CPE method.

Figure 4.39 shows the system Q factor of the received data as a function of individual laser linewidth at 10 dB of OSNR and 0 dBm ROP. The system Q factor for a linewidth of 100 kHz is 10.06 dB, 9.41 dB and 9.93 dB for the Dual-Comp, CPE and PPF phase noise compensation algorithms, respectively. In all schemes, the Q factor decreases for laser linewidths beyond 100 kHz. The Dual-Comp scheme can improve the Q factor by 0.65 dB and 0.13 dB compared to the CPE and PPF schemes, respectively. By increasing the laser linewidth up to 1 MHz, the CPE performance gets closer to that of the Dual-Comp model while the PPF performance is increased.

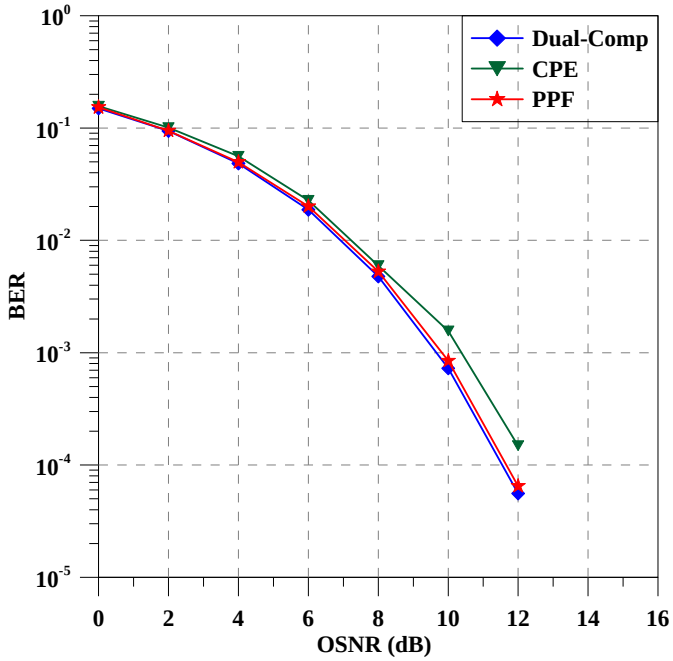

Fig. 4.38: BER versus OSNR of Dual-Comp, CPE and PPF schemes for CO-OFDM back-to-back systems.

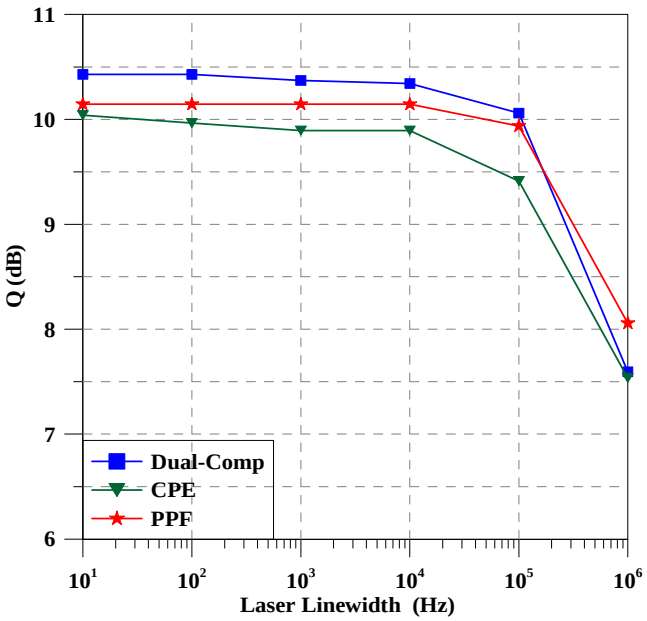

Fig. 4.39: System Q factor versus laser linewidth of Dual-Comp, CPE and PPF schemes for CO-OFDM back-to-back systems.

In Fig. 4.40, the influence of ROP on the system Q factor is shown for 40 Gbps CO-OFDM transmission systems with 10 dB of OSNR and 100 kHz laser linewidth for the PPF scheme, CPE method and Dual-Comp model. The ROP is varied from −40 dBm to +10 dBm. Obviously, it is required automatic gain control in practice. By increasing the ROP, the Q

factors of the received data improve until the ROP reaches −23 dBm; then they barely change. At 0 dBm ROP, the Q value for the Dual-Comp, CPE and PPF phase noise compensation algorithms are 10.06 dB, 9.41 dB and 9.93 dB, respectively. The Dual-Comp can improve the Q factor by 0.65 dB compared to the CPE scheme and about 0.13 dB compared to the Dual-Comp method. The Dual-Comp method shows smaller improvement than the CPE method and PPF phase noise compensation. But the system complexity is increased.

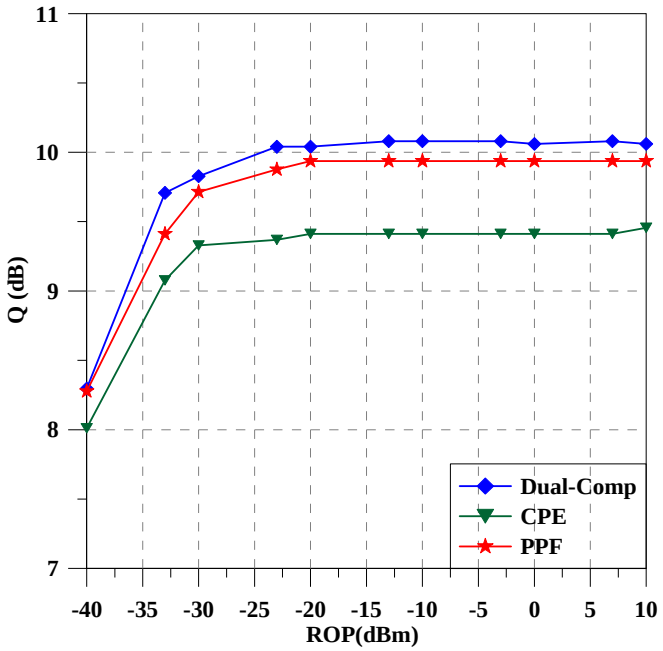

Fig. 4.40: System Q factor versus ROP of Dual-Comp, CPE and PPF schemes for CO-OFDM back-to-back systems.

The impact of SPM on a single channel configuration is investigated. The performances of the phase noise mitigation schemes are simulated and compared for CO-OFDM transmission systems due to fiber nonlinearity only. Ideal lasers without phase noise are assumed.

Figure 4.41 presents the BER performance as a function of OSNR for 40 Gbps CO-OFDM transmission systems over 1200-km SSMF with 0 dBm of ROP for the Dual-Comp, CPE and PPF models. The required OSNR for BER of 10^{-3} is 12 dB, 12.57 dB and 13.55 dB for the PPF, Dual-Comp and CPE phase noise compensation algorithms, respectively. The PPF improves the OSNR at a BER of 10^{-3} by 0.57 dB compared to the Dual-Comp and about 1.55 dB compared to the CPE method.

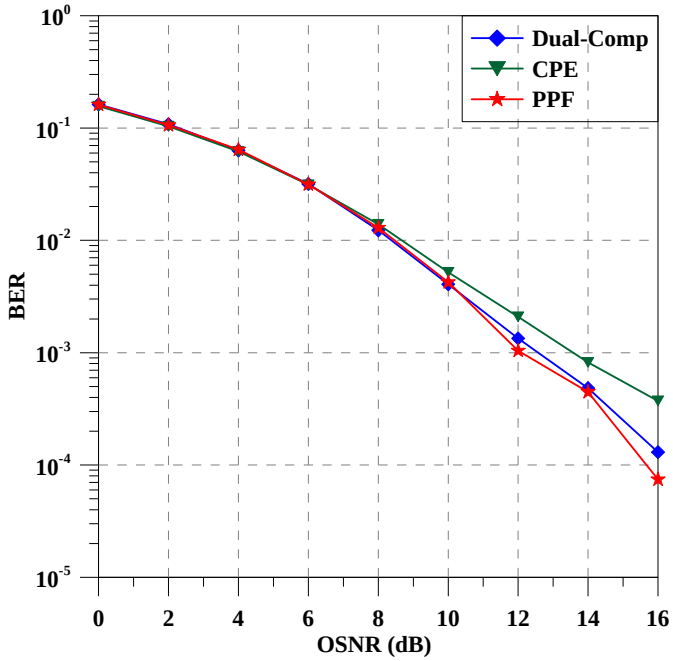

Fig. 4.41: BER versus OSNR of Dual-Comp, CPE and E-RFP schemes for CO-OFDM systems over 1200-km transmission.

Figure 4.42 shows the influence of ROP on the system Q factor for 40 Gbps CO-OFDM transmission systems with 12 dB OSNR, 0dBm ROP and −4 dBm launch power for the CPE scheme, Dual-Comp method and PPF model. The ROP is varied from −40 dBm to +10 dBm.

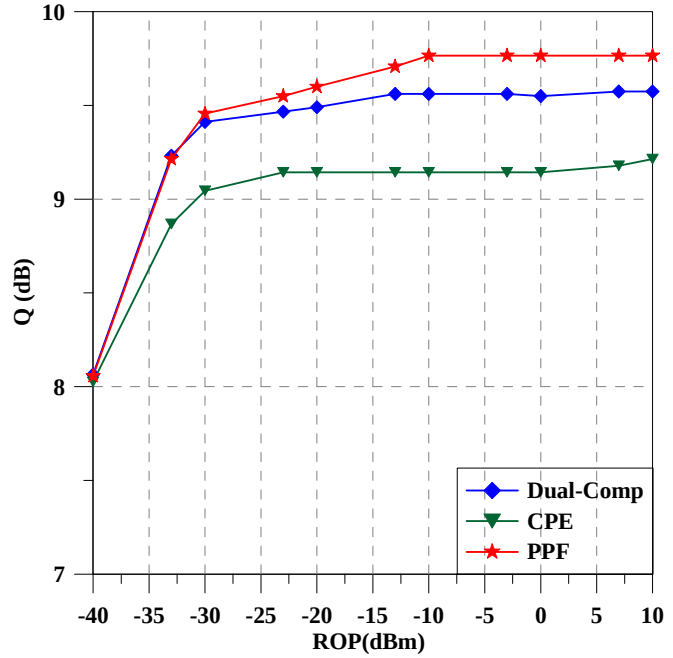

Fig. 4.42: System Q factor versus ROP of Dual-Comp, CPE and PPF for CO-OFDM systems over 1200-km transmission.

By increasing the ROP, the Q factors of the received data improve until the ROP reaches −13 dBm; then they barely change. At 0 dBm ROP, the Q value for the Dual-Comp, CPE and PPF phase noise compensation algorithms are 9.55 dB, 9.14 dB and 9.77 dB, respectively. Compared to the CPE, the Dual-Comp can improve the Q factor by 0.41 dB and the PPF method can improve the Q factor by 0.63 dB.

Figure 4.43 presents the system Q factor as a function of the launch power for 40 Gbps CO-OFDM transmission systems over 1200-km SSMF with 0 dBm of ROP and 12 dB of OSNR for the Dual-Comp, CPE and PPF models. For low launch powers, the CPE decreased the performance by about 0.4 dB while Dual-Comp and PPF schemes improved performance for all powers. The nonlinearity limitation is above −10 dBm. At −8 dBm launch power when total nonlinearity is high, the Dual-Comp and PPF give 0.5 dB improvement in Q-factor compared to the CPE scheme. Dual-Comp scheme mitigates the effect of fiber nonlinearity.

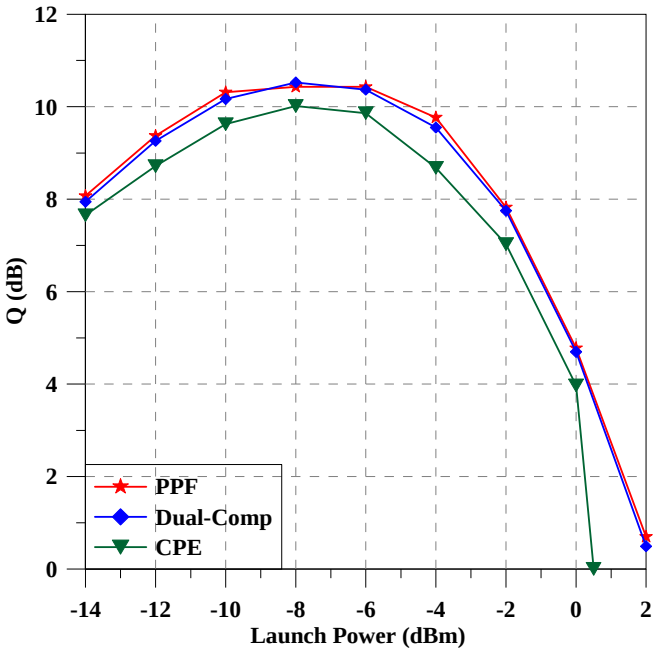

Fig. 4.43: System Q factor of Dual-Comp, CPE and PPF schemes for CO-OFDM systems versus optical launch over 1200-km transmission.

The simulation results reveal that there is a small gain in the performance in back-to-back configuration by combining two compensators but also the system complexity is increased. Hence, PPF phase noise compensation technique is more practical to use.

The comparison between PDM-CO-OFDM transmission system and single polarization is simulated. The same simulation parameters are used with 4 training symbols every 50

OFDM data symbols, these training symbols are inserted to the head of OFDM frame at the transmitter. The training symbols are used for frame synchronization, frequency offset compensation and channel estimation as explained in Section 3.5. Hence, the net bit rate will be 61.7 Gbps. Subsequently, the spectral efficiency will be 2.7 bit/s/Hz. While in the single polarization transmission systems, the data rate will be 30.8 Gbps. Therefore, the spectral efficiency will be 1.35 bit/s/Hz. After frame synchronization, the frequency offset is mitigated and the laser phase noise is compensated using Dual-Comp technique after FFT stage.

The influence of OSNR on the BER for using Dual-Comp phase noise technique is shown in Fig. 4.44. The BER is simulated for each laser linewidths of 100 kHz and ROP of 0 dBm. A BER of 10^{-3} can be observed at OSNR of 14.3 dB for single polarization. The OSNR requirement for PDM transmission system is increased about 3 dB compared with the single polarization, which is theoretical penalty. The OSNR requirement for *x* and *y* polarizations are 17.2 dB and 17.4 dB, respectively.

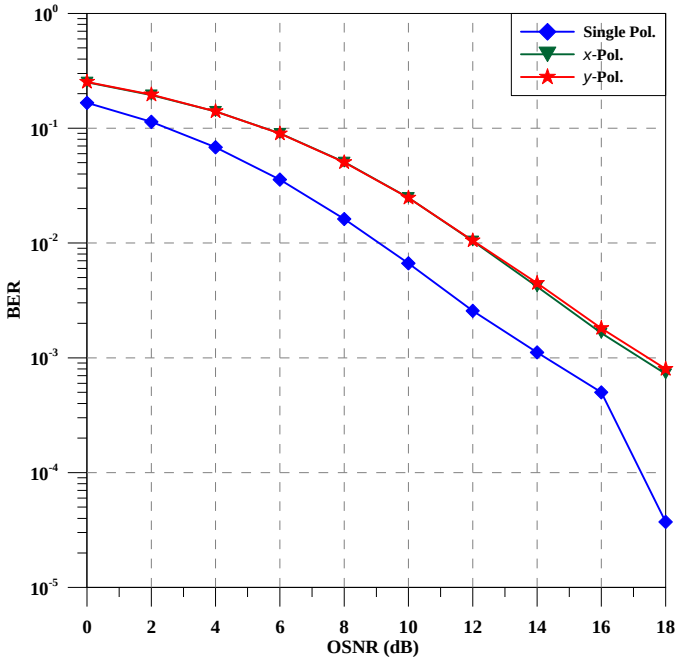

Fig. 4.44: BER versus OSNR for single and PMD CO-OFDM systems using Dual-Comp scheme.

Finally, Fig. 4.45 compares a BER performance versus OSNR of the RFP-CPE, PPF, Dual-Comp, CPE and E-RFP phase noise compensation schemes. The simulation is conducted in a conventional single polarization CO-OFDM system, based on direct up-

conversion and direct down-conversion. The nominal data at 40 Gb/s is first divided and mapped onto 480 subcarriers with 4-QAM modulation format, and transferred to the time-domain using an IFFT of size 512. In case of the PPF, CPE and Dual-Comp schemes 26 zeros for oversampling are inserted at the middle of the IFFT input sequence and $N_p = 6$ pilots are reserved. While in RFP-CPE scheme, 16 zeros for oversampling and 10 zeros for spectral gap are used. Also, $N_p = 6$ pilots are reserved. In case of the E-RFP scheme, 22 zeros for oversampling and 10 zeros for spectral gap are used. A cyclic prefix of 12.5% is used to accommodate dispersion. The electrical signal is sampled at a sampling rate of 20 GS/s. A square root raised cosine filter with a roll-off factor of 0.2 removes the alias and filters the main OFDM signal. Training symbols with 3 symbols are used for compensating the frequency offset, frame synchronization and channel estimation every 40 OFDM symbols. The electrical OFDM data signal is then converted using an I/Q-MZ to the optical domain. The optical transmission link consists of 15 SSMF spans and a double-stage EDFA with a noise figure of 4 dB after each span. Between each EDFA's stages, there is a 16 km of DCF to form a fully periodic dispersion map. The DCF launch power is 6 dB lower than the SSMF launch power to decrease the effect of DCF nonlinearity. The linewidths of the transmitter and receiver lasers are identical with 100 kHz.

Table 4.2 represents the OFDM bandwidth, net data rate and spectral efficiency for all phase noise compensation schemes.

	Bandwidth	Bit rate	Spectral efficiency
CPE	22.78 GHz	31 Gbps	1.36 bit/s/Hz
E-RFP	22.54 GHz	31 Gbps	1.37 bit/s/Hz
RFP-CPE	22.83 GHz	31 Gbps	1.35 bit/s/Hz
PPF	22.78 GHz	31 Gbps	1.36 bit/s/Hz
Dual-Comp	22.78 GHz	31 Gbps	1.36 bit/s/Hz

Table 4.2: Spectral efficiency for all compensation schemes.

A BER of less than 10^{-3} cannot be obtained with the E-RFP method. The required OSNR for BER of 10^{-3} is 12.7 dB, 12.8 dB, 13 dB and 14.8 for the RFP-CPE, PPF, Dual-Comp and CPE phase noise compensation algorithms, respectively. The investigated phase noise

compensation methods have better sensitivity than the E-RFP and CPE models for phase noise compensation and the CPE method.

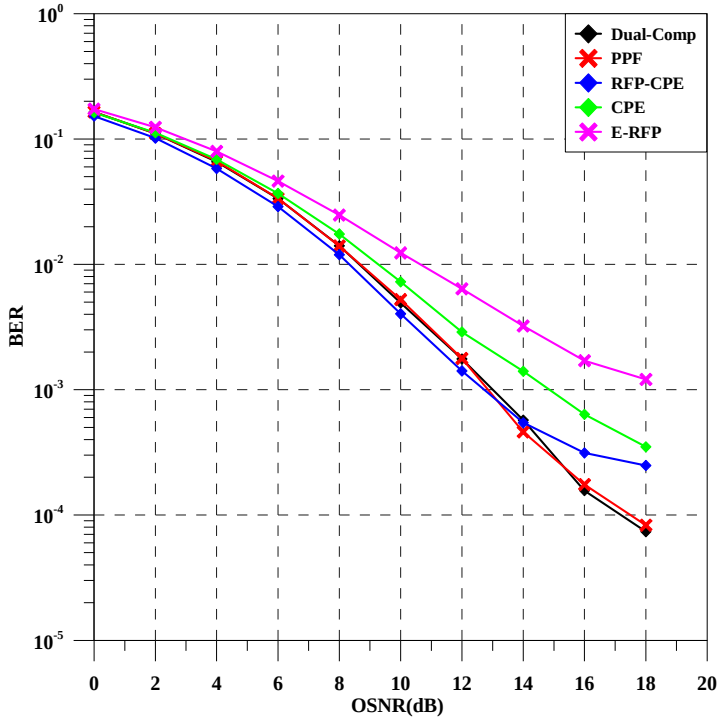

Fig. 4.45: BER versus OSNR for CO-OFDM systems using different phase noise compensation schemes.

The performance of RFP-CPE scheme depends on zeros for spectral gab as the more zeros padding, the more reduction in spectral efficiency and bit rate. Also, It is important to optimize the power ratio between RFP signal and OFDM signal and it requires a careful selection LPF bandwidth which is to separate the pilot tone at receiver. The Daul-Comp algorithm has the same performance as the PPF technique but also the system complexity is increased. Hence, The PPF phase noise compensation technique is more effective to use regardless the effect of different parameters.

Finally, the spectral efficiency of PDM-CO-OFDM transmission system using the presented phase noise compensation schemes and the spectral efficiency PDM-QPSK transmission systems are shown in Table 4.3.

	CPE	E-RFP	RFP-CPE	PPF	Dual-Comp	QPSK
Spectral efficiency	2.72 bit/s/Hz	2.74 bit/s/Hz	2.7 bit/s/Hz	2.72 bit/s/Hz	2.72 bit/s/Hz	2.24 bit/s/Hz

Table 4.3: Spectral efficiency for PDM-CO-OFDM and PDM-QPSK transmission systems.

Chapter 5: Discrete Fourier Transform Spread OFDM

5.1 Introduction

The CO-OFDM systems have been proven to be an appropriate modulation format for high-speed optical communication. One of the most important drawbacks of CO-OFDM is the high PAPR. A discrete Fourier transform spread OFDM (DFT-S-OFDM) is proposed to minimize the PAPR causing further enhancement in nonlinear tolerance. The SCO-OFDM system has been investigated to overcome LPN compensation stage at the receiver side, decrease the system complexity and increase the system performance. A new DFT-S-OFDM architecture is investigated by extracting the optical carrier from the optical OFDM signal at the receiver. Hence, it combines the benefits from both SCO-OFDM and DFT-S-OFDM systems. The effects of phase noise for various laser linewidths and of received optical power on system performance are evaluated. In addition, the tolerance of the investigated system for mitigation of fiber nonlinearities in long-haul systems is presented. The principles of DFT-S-OFDM were briefly explained in Section 5.2. Section 5.3 will introduce the new investigated system architecture which is called self coherent DFT-S-OFDM (SDFT-S-OFDM) optical system. The simulation setup and results between the new systems architecture and DFT-S-OFDM systems are investigated and compared in Section 5.4.

5.2 DFT-S-OFDM

A new technique known as DFT-S-OFDM has been investigated in wireless communication. It allows to implement a single carrier modulation and frequency domain equalizer which has recently been utilized in the uplink of the 3rd generation partnership project (3GPP) long term evolution (LTE) [106, 107]. It has turned out to be an effective scheme to mitigate PAPR due to its single carrier structure. Thus, it is called single carrier frequency division multiplexing (SC-FDM). The scheme utilizes additional DFT and IDFT at the transmitter and receiver to reduce the PAPR and effect of fiber nonlinearity. As a drawback, it increases computational complexity. In [108, 109], the authors used the DFT-S-OFDM in optical communication to overcome the fiber nonlinearity drawback related to the conventional CO-OFDM systems.

Figure 5.1 shows the schematic of a DFT-S-OFDM scheme in coherent optical transmission system. There are few different blocks compared to the conventional CO-

OFDM systems. At the transmitter side, the binary serial bits are converted to parallel data blocks. The data are mapped to multilevel modulation such as QPSK, 4-QAM and 16-QAM.

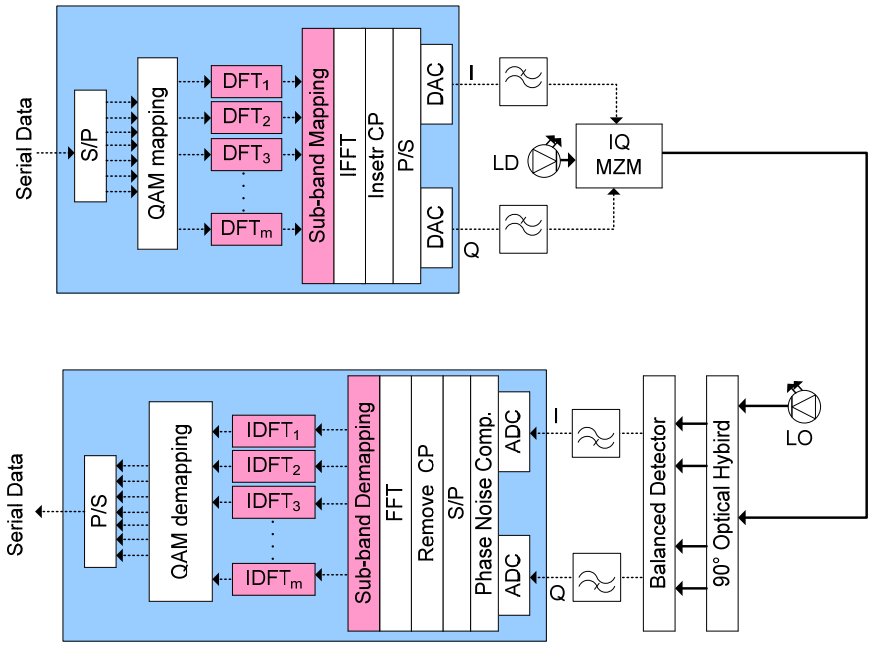

Fig. 5.1: Schematic diagram of DFT-S-OFDM system.

The modulated data x_{ik}^{m} are divided into m sub-bands with N subcarriers per sub-band in the i^{th} OFDM symbol. Therefore, the total subcarrier of all sub-bands $K = m \cdot N$. Each sub-band is converted to frequency domain by applying N-point of DFT. For simplicity, the DFT transformation and sub-band mapping for one sub-band is studied and the OFDM symbol index i is dropped. Figure 5.2 represents the generation diagram of DFT-S-OFDM transmit symbols. The DFT-Spread signal X_k of can be represented as

$$X_k = \frac{1}{N}\sum_{n=0}^{N-1} x_n e^{\frac{-j2\pi nk}{N}} \tag{5.1}$$

Then, sub-band mapping is achieved by adding zero subcarriers N_{zp}. The DFT spread signal is converted to the time domain using L-point IFFT. The IFFT generates DFT-S-OFDM signal where $L = N_{zp} + m \cdot N$. The time domain DFT-S-OFDM signal y_m is given by

$$y_m = \frac{1}{L}\sum_{l=0}^{L-1} \widetilde{X}_l \, e^{\frac{j2\pi ml}{L}} \tag{5.2}$$

where $\tilde{X}_l$ is the input subcarrier to L-point of IFFF including N-point of DFT modulated subcarriers and the zeros subcarriers N_{zp}. The DFT-S-OFDM signal has a low PAPR within each OFDM sub-band.

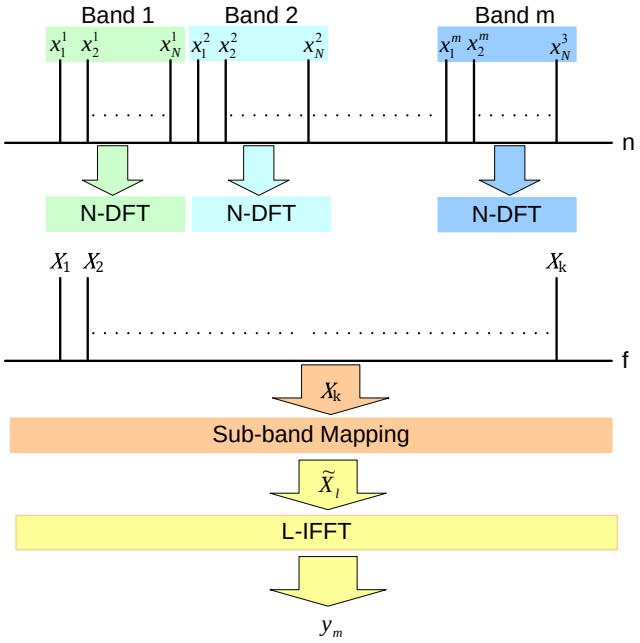

Fig. 5.2: Generation of DFT-S-OFDM symbols.

A CP is performed by copying the last samples of DFT-S-OFDM symbol to provide a guard time and prevent ISI. The information symbols are serialized and sampled with DACs. A LPF is utilized to remove the alias and filter the main DFT-S-OFDM signal. The signal is modulated and then launched to fiber optics. At the receiver, a homodyne detector is implemented. The receiver process is the reverse operation of the transmitter. The received signal is transformed into the frequency domain using the FFT. Then, it de-maps the output symbols. Finally, the recovered symbols use the IDFT to transform the frequency symbols to the time domain. By removing the pink blocks, the conventional CO-OFDM system is obtained.

Two approaches can be used to perform sub-band mapping of the DFT-spread subcarriers X_k which are distributed and localized mapping [107, 110]. The DFT outputs are inserted within zero subcarriers in case of distributed sub-band mapping DFT-S-OFDM (DDFT-S-OFDM). The zero subcarriers are without equidistance distribution. If the zero subcarriers are with equidistance distribution between the DFT outputs, a special case of the

DDFTS-OFDM is produced which is called interleaved sub-band mapping DFT-S-OFDM (IDFT-S-OFDM) [111].

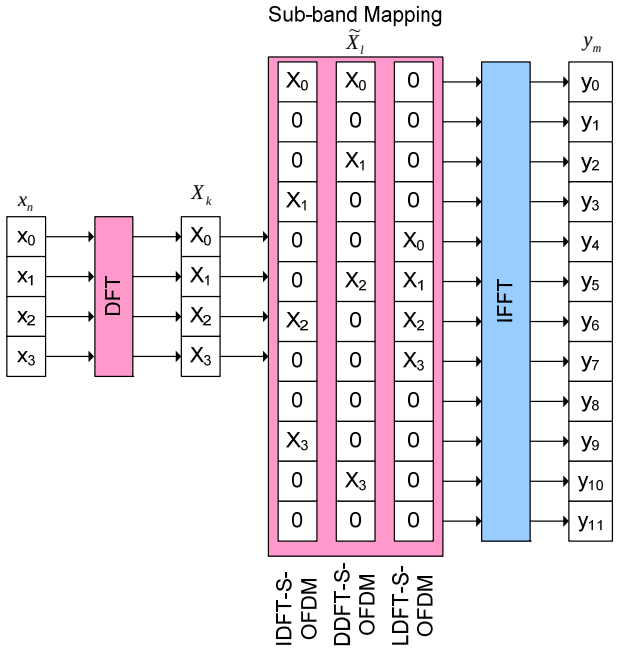

Fig. 5.3: Different sub-band mapping schemes.

In case of the localized sub-band mapping DFT-S-OFDM (LDFT-S-OFDM), the DFT outputs are inserted as consecutive subcarriers whereas the zeros are padded at both edges of IFFT input sequence [112]. The difference between the sub-band mapping approaches is shown in Fig. 5.3.

5.3 SDFT-S-OFDM

The DFT-S-OFDM is a single carrier technique which inherits all advantages of OFDM. The data subcarrier is divided into sub-bands with narrow bandwidth. Thereby, the PAPR will be reduced [107], but the computational complexity will be increased. Moreover, it will be more sensitive to phase noise due to the spreading noise over the whole sub-bands [113] and the interference between the sub-bands itself which produces more inter-carrier interference which is the main impact of the LPN. To decrease the complexity of the system and compensate for the LPN more efficiently, the concepts of SCO-OFDM and DFT-S-OFDM are combined. The optical carrier from the received optical OFDM signal is extracted with OBPF, so it looks like homodyne detection. Since the two interfering optical signals come

from the same laser source, their polarization and phase noise are identical. Therefore a phase noise compensation stage at the receiver side is not required. Subsequently, the complexity of DSP is decreased. Furthermore, no LO is required at the receiver. The quality of the extracted optical carrier is reduced by ASE, and the larger the optical filter bandwidth, the more noise passes with the optical carrier. Therefore a narrow bandwidth filter will improve the performance of SCO-OFDM [25, 55].

5.4 Simulation Setup and Results

The generation and analysis of the OFDM signal and system performance are simulated using VPItransmissionMaker™ V9.0. Figure 5.4 shows the schematic of SDFT-S-OFDM transmission system. An OFDM signal with a nominal data rate of 40 Gbps is generated. The bit stream is converted from serial to parallel and then mapped to 4-QAM. 768 modulated subcarriers are sub-divided into 6 sub-bands which represents the number of bands during the analysis. A 128-point DFT has been executed for each sub-band. Interleaved sub-band mapping with 256 zeros is used in the simulation. After adding the zeros to the DFT output, the 1024-IFFT is performed to transform the subcarriers to time domain signal. The CP of 6.25 % of the symbol length is set.

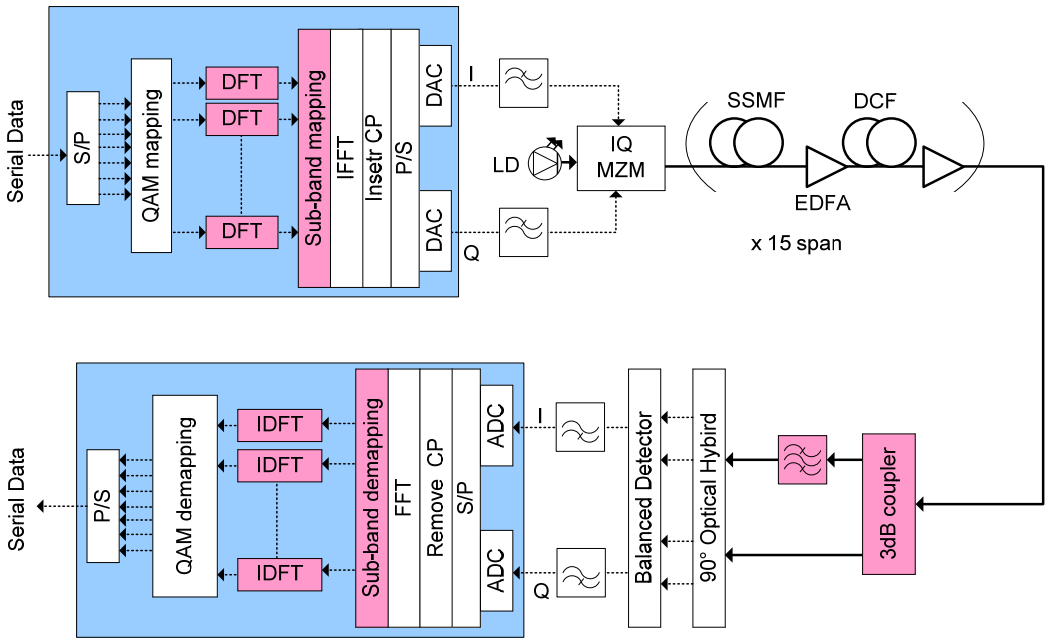

Fig. 5.4: Setup of SDFT-S-OFDM system.

The information symbols are serialized and the electrical signal is sampled at a rate of 20 GS/s. A square root raised cosine filter with a roll-off factor of 0.2 removes the alias and filters the main OFDM signal. Therefore, the bandwidth of OFDM will be 18 GHz and the data rate will be 28.2 Gbps. Hence, the spectral efficiency will be 1.6 bit/s/Hz A laser with a linewidth of 1 MHz is modeled to generate a continuous signal at 193.1 THz with 0 dBm power. The laser is modulated with the OFDM signal in a null-biased IQ-MZM with an extinction ratio of 30 dB. To evaluate the OSNR performance, ASE noise is added to control the received OSNR.

The optical transmission link consists of 15 fiber spans. Each of them comprises 80 km of SSMF with an attenuation of 0.2 dB/km, a dispersion of 16 ps/nm/km, a dispersion slope of 0.08 ps/nm^2/km and a nonlinear coefficient (γ) 1.3 W^{-1}km^{-1}. After each span, the fiber loss is compensated by a double-stage EDFA with a noise figure of 4 dB. Between each EDFA's stages, there is 16 km of DCF with a dispersion of –80 ps/nm/km; thereby forming a fully periodic dispersion map. The DCF launch power is 6 dB lower than the SSMF launch power to decrease the effect of DCF nonlinearity.

At the receiver, the optical carrier is extracted by the OBPF, and a homodyne detector is assumed. The OFDM signals from the balanced detectors are filtered LPF and then sampled with ADCs at a sampling rate of 20 GS/s. The serial digital signal is converted to complex parallel data blocks by an S/P converter. An FFT demodulates the OFDM signal. After the removal the zeros padding and de-mapping the sub-bands, the IDFT is performed on the signal stream. QAM symbols are decoded by QAM de-mapping to produce parallel data.

The performances of the proposed system are simulated and compared among SCO-OFDM, DFT-S-OFDM and CO-OFDM transmission systems. A BER is simulated for the laser having a linewidth of 1 MHz, a ROP of 0 dBm and a launch power of -4 dBm. The DFT-S-OFDM and CO-OFDM systems use RFP phase noise compensation scheme with the PSR value of 10.55 dB. A 4th order 100 MHz Butterworth LPF is used at the receiver side to extract a clear RFP signal. For CO-ODFM system, 64 zeros in the middle of IFFT input sequence for oversampling to separate the baseband signal from aliasing and 192 zeros as guard band at both edges of IFFT input sequence are inserted. For SDFT-S-OFDM and SCO-OFDM, the OBPF with 1 GHz band-width is used to extract the optical carrier at the receiver.

The system Q factor of different number of sub-bands is indicated in Fig. 5.5. The system Q factor obtains the optimal value while the number of sub-bands equals one and deteriorates with increasing number of sub-bands. Theoretically, the system Q factor with one sub-band will be similar to a single carrier which is special case of one sub-band DFT-S-OFDM. The PAPR is very low for single carrier. Increasing the number of sub-bands, the computational complexity is increased due to additional DFT/IDFT blocks in the transmitter and receiver. Also, the phase noise is spreading over the whole sub-bands and the interference between the sub-bands itself which produces more ICI or inter-block interference. Below 3 sub-bands, the system Q factor has been preserved less than 1 dB on average over all sub-bands. It can be seen that the best number of sub-bands is close to 3, but 6 has close performance. Therefore, the simulation is run for 6 sub-bands.

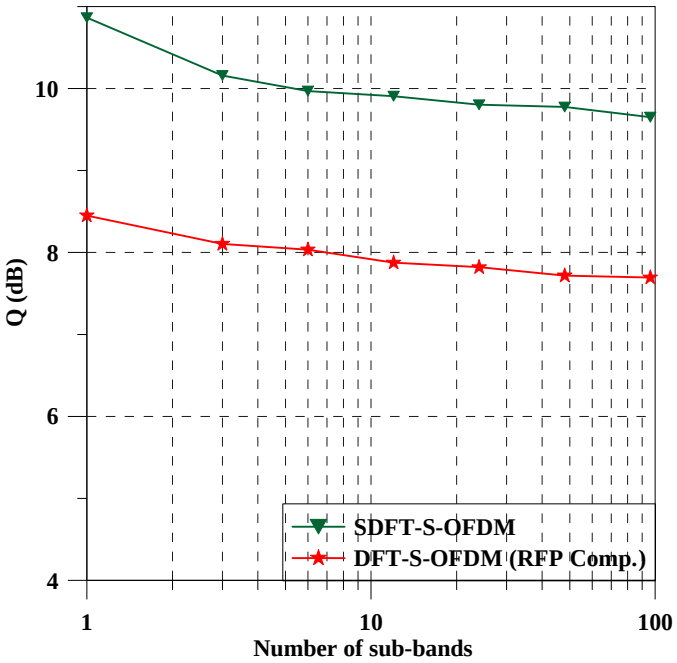

Fig. 5.5: System Q factor as a function of number of sub-bands.

Figure 5.6 presents the BER performance as a function of OSNR. DFT-S-OFDM system cannot achieve a BER of 10^{-3}. For each laser having a linewidth of 1 MHz, the required OSNRs for a BER of 10^{-3} is 11.3 dB, 11.5 and 24 dB for SDFT-S-OFDM, SCO-OFDM and CO-OFDM, respectively. The SDFT-S-OFDM system and SCO-OFDM system can improve OSNR at a BER of 10^{-3} by 12.5 dB and 12.7 dB compared to the CO-OFDM system, respectively. Compared with CO-OFDM system, the DFT-S-OFDM system is more sensitive

to laser phase noise [113]. Reducing linewidth for each laser having to 100 kHz, the required OSNRs for a BER of 10^{-3} is 11.4 dB and 16.3 for SDFT-S-OFDM and DFT-S-OFDM, respectively.

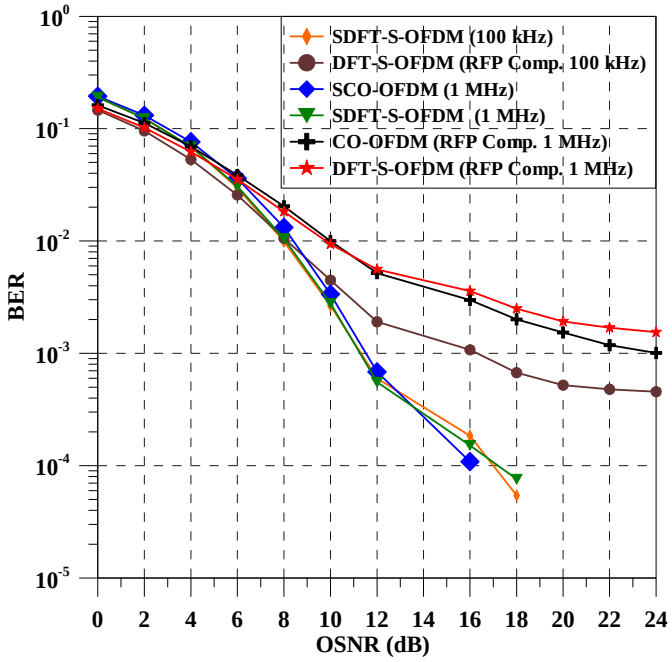

Fig. 5.6: BER performance as a function in OSNR for SDFT-S-OFDM system.

The following simulation results will be performed for SDFT-S-OFDM and DFT-S-OFDM systems only. Figure 5.7 shows the system Q factor of the received data as a function of individual laser linewidth at 12 dB of OSNR and 0 dBm ROP. The system Q factor for a linewidth of 1 MHz is 9.99 dB and 8.03 dB for the SDFT-S-OFDM and DFT-S-OFDM systems, respectively. The SDFT-S-OFDM system can improve the Q factor by 1.96 dB compared to the DFT-S-OFDM system. For a laser linewidth of even 10 MHz, SDFT-S-OFDM system has still better performance with a system Q factor of 9.8 dB. The SDFT-S-OFDM system performs better than DFT-S-OFDM system.

In Fig. 5.8, the influence of ROP on the system Q factor is shown for the SDFT-S-OFDM and DFT-S-OFDM transmission systems with 12 dB OSNR and 1 MHz laser linewidth. The ROP is varied from −40 dBm to +10 dBm. Obviously, it is required automatic gain control in practice. By increasing the ROP, the Q factors of the received data improve until the ROP reaches −23 dBm for SDFT-S-OFDM system and −33 dBm for DFT-S-OFDM system; then they barely change.

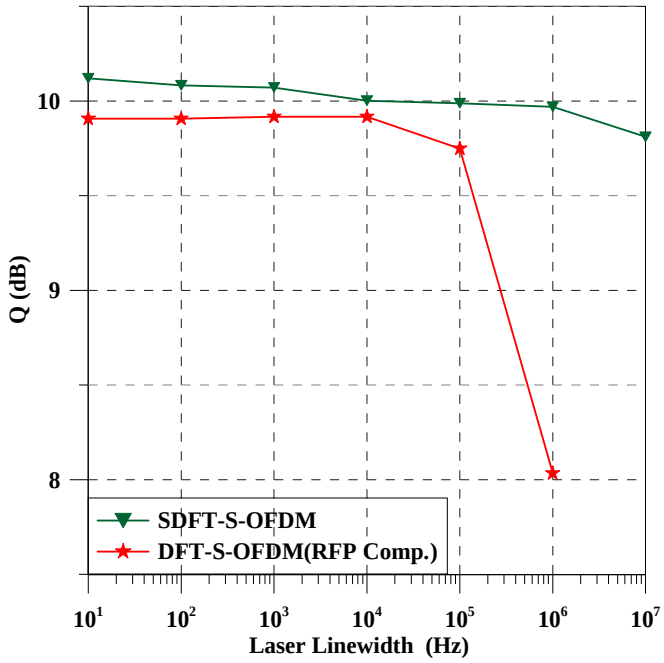

Fig. 5.7: System Q factor versus laser linewidth for SDFT-S-OFDM and DFT-S-OFDM systems.

At 0 dBm ROP, the Q value for SDFT-S-OFDM and DFT-S-OFDM systems are 9.99 dB and 8.03 dB, respectively. The SDFT-S-OFDM system can improve the Q factor by 1.96 dB compared to DFT-S-OFDM transmission system. The SDFT-S-OFDM systems show a better sensitivity than DFT-S-OFDM system.

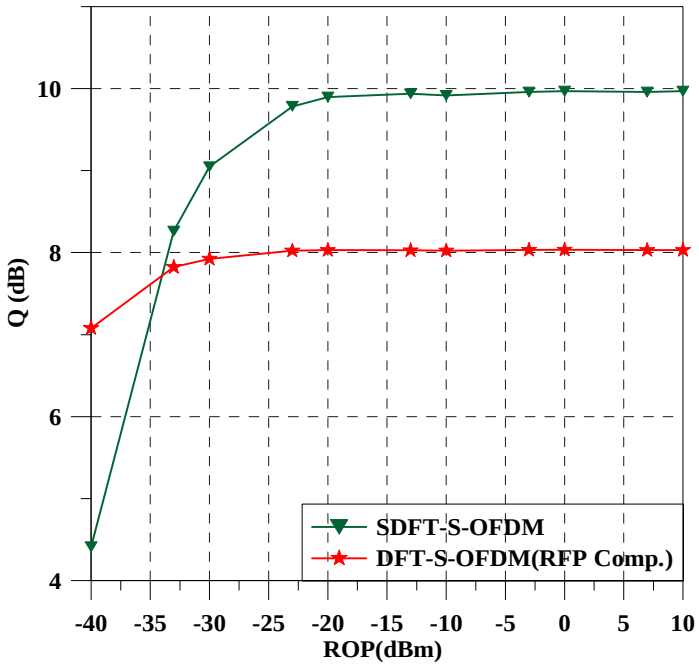

Fig. 5.8: System Q factor versus ROP for SDFT-S-OFDM and DFT-S-OFDM systems.

Figure 5.9 presents the system Q factor as a function of the launch power for SDFT-S-OFDM and DFT-S-OFDM systems over 1200 km SSMF fiber. For low launch powers, DFT-S-OFDM system decreased the performance by 1.8 dB while SDFT-S-OFDM system improved performance for all powers.

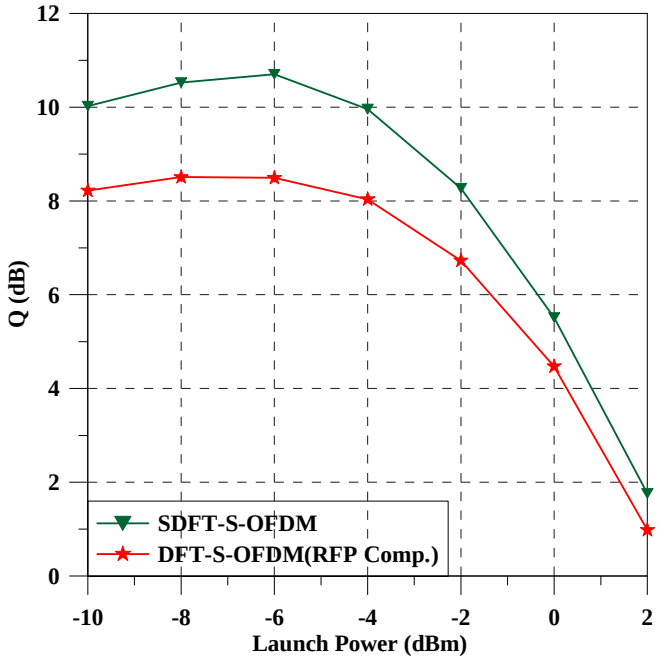

Fig. 5.9: System Q factor versus optical launch power for SDFT-S-OFDM and DFT-S-OFDM systems.

The nonlinearity limitation is above −8 dBm. At −6 dBm launch power when total nonlinearity is high, SDFT-S-OFDM system gives 2.2 dB improvement in Q-factor compared to DFT-S-OFDM system. The SDFT-S-OFDM mitigates the effect of fiber nonlinearity very much.

Chapter 6: Conclusions

The OFDM technology is used in many broadband wired and wireless communication systems to combat multipath fading. The CO-OFDM systems have been shown to be an appropriate modulation format for high speed optical communications.

In the present dissertation, the content of Chapter 2 presents the basic theoretical background regarding OFDM technology. The differences between single carrier systems and multicarrier systems are described highlighting the advantaged and disadvantages. The evolution of the multicarrier technology towards OFDM is discussed. The basic fundamentals of OFDM are introduced in details, emphasizing the importance of orthogonality between subcarriers. The mathematical description of OFDM signal, CP, FFT and training symbols are discussed. The CP insertion prevents ISI between successive OFDM symbols and preserves the orthogonality. Furthermore, the synchronization errors are presented, determining the required stages of synchronization in the receiver side before the transmitted symbol can be decided correctly. The required tap equalizer is presented to estimate and mitigate the effect of channel distortion. The concept of PAPR is presented. The advantages of OFDM and its limitation are reported. Moreover, the performance analyses of the single carrier systems and OFDM systems for different modulation levels are shown and compared.

The differences between optical OFDM systems and wireless OFDM systems are described in Chapter 3 including the advantaged and disadvantages of optical OFDM systems. The basic block diagrams of optical OFDM are introduced, describing the internal structure of the three existing systems. Furthermore, phase noise effects for various laser linewidths and the effect of ROP on the system performance for the three exiting optical OFDM systems are compared. The effect of a narrow OBPF in SCO-OFDM transmission systems is investigated. The simulation results show that SCO-OFDM has a good tolerance to laser linewidth. The 2×2 MIMO-CO-OFDM configuration system and signal processing algorithms for frame synchronization, frequency offset compensation and channel equalization are discussed. The use of SR-RC windowing rather than RC windowing substantially improves the performance of CO-OFDM systems. Non-rectangular window functions like SR-RC or RC windowing smoothen the spectra ends and suppress side-lobes

more strongly. Simulations reveal that using the SR-RC window, the system performance improves compared to the rectangular window.

Chapter 4 defines the different kinds of phase noise effects on the optical OFDM transmission systems. The impact of laser phase noise induced by the transmitter laser and LO is studied. Moreover, the impact of the nonlinear phase noise is explored. The mathematical expressions for the laser and nonlinear phase noise effects are presented. Different existing signal processing algorithms for laser and nonlinear phase noise estimation are reviewed. Different schemes of the RFP phase noise compensation algorithm are investigated. To separate the RF tone completely from the OFDM spectrum, zeros are inserted also at both edges of IFFT input sequence which generate a guard band between the RFP signal and OFDM sidebands. The guard band-RFP and E-RFP phase noise compensation schemes are provided to avoid the drawbacks of the original RFP scheme. The comparative analysis between the different RFP phase noise compensation schemes is elaborated.

Three approaches are investigated for laser and nonlinear phase noise compensation. First, the combination of CPE and RPF phase noise compensation schemes is investigated. It is proven that the combination of CPE and RPF phase noise compensation scheme is an effective method to compensate for laser phase noise in CO-OFDM transmission systems. Applied to a 40 Gbps CO-OFDM system with 4-QAM, simulation results reveal that using the RFP-CPE method, the OSNR can be improved compared to CPE and E-RFP phase noise compensation techniques. The simulation results show that the RFP-CPE technique is robust against laser phase noise for 4-QAM CO-OFDM transmission systems with 512-FFT. In addition, the RFP-CPE improves significantly the system performance when fiber nonlinearity is taken into account. At the highest launch power, The RFP-CPE gives 1 dB and 0.4 dB improvement in Q-factor compared to the CPE and RFP schemes, respectively. The proposed scheme mitigates the effect of fiber nonlinearity very much.

Second, the PPF phase noise compensation scheme using constant pilot frequencies based on linear interpolation is investigated. It is an effective method to compensate for laser phase noise in the CO-OFDM transmission systems. Compared with the nearest neighbor method, linear interpolation can improve the OSNR. Applied to a 40 Gbps CO-OFDM transmission system with 4-QAM, simulation results reveal that using the PPF method, the Q factor at an

individual laser linewidth of 100 kHz can be improved. Moreover, the investigation of PPF, CPE, RFP and Joint-SPM schemes tolerance due to SPM of a fully periodic dispersion-mapped system with nonlinear transmission fibers is discussed. The PPF improves significantly the system performance when fiber nonlinearity is taken into account. At the optimal launch power, the PPF scheme gives 1.6 dB and 1.3 dB improvement of Q-factor compared to the J-SPM and CPE and schemes, respectively. Such improvement shows that the PPF mitigates significantly the effect of SPM.

Third, dual frequency compensators are investigated to mitigate the laser and nonlinear phase noise in CO-OFDM transmission systems. The performance analysis of the proposed scheme is investigated via simulations. By comparing the Dual-Comp with the PPF and CPE, the Dual-Comp can perform as reliable as the PPF technique. However the computational complexity of the Dual-Comp scheme is increased. Therefore, the small gain in the performance and high computational complexity are the main drawbacks of the Dual-Comp approach.

The performance of RFP-CPE scheme depends on the effect of many parameters. While, the Daul-Comp algorithm has the same performance as the PPF technique but also the system complexity is increased. Hence, The PPF phase noise compensation technique is more effective to use regardless the effect of different parameters.

Chapter 5 presents the DFT-spread OFDM signal which is used to reduce the PAPR and compensate the fiber nonlinearity effect in the CO-OFDM transmission systems. It looks like the single carrier modulation. The most important drawback is that the system computational complexity is increased due to additional DFT and IDFT which is used at the transmitter and receiver. The basic principle of DFT-S-OFDM technique is introduced in details, describing the different sub-bands mapping schemes. The mathematical description of DFT-spread OFDM signal is discussed. Moreover, the SDFT-S-OFDM system is new system architecture by extracting the optical carrier from the optical OFDM signal at the receiver to compensate for laser phase noise. The concepts of SCO-OFDM and DFT-S-OFDM are combined to decrease the system complexity. The simulation results of SDFT-S-OFDM system are investigated. Applied to a 40 Gbps transmission system with 4-QAM, simulation results reveal that using SDFT-S-OFDM system, the OSNR can be improved by 10.3 dB compared to CO-OFDM system which uses RFP phase noise compensation technique. Furthermore,

SDFT-S-OFDM system improves the system Q factor significantly for individual laser linewidths up to 10 MHz. The simulation results show that SDFT-S-OFDM system is more robust against LPN than DFT-S-OFDM system. In addition, SDFT-S-OFDM system gives 2.2 dB improvement of Q-factor compared to DFT-S-OFDM. Such improvement shows that SCO-DFT-S-OFDM mitigates significantly the effect of SPM.

In summary, the contributions of the present work aim to improve the CO-OFDM transmission systems performance. Three key problems are addressed. Four contributions are provided to solve the addressed problems. The square root raised-cosine pulse shaping of OFDM symbols is proposed to enhance out-of-band power suppression of the OFDM spectral. Hence, the efficiency of CO-OFDM systems is improved. Three DSP techniques are developed to compensate the effect of the laser and nonlinear phase noise. A new SDFT-S-OFDM system architecture which combines the benefits from both SCO-OFDM and DFT-S-OFDM systems is investigated.

Appendix A

OFDM Orthogonality

OFDM signal is a special case of multicarrier system where the guard bands between adjacent subcarriers can be removed. The combined FDM signal $x(\mathrm{t})$can be written as [50]

$$x(t) = \sum_{i=-\infty}^{\infty} \sum_{k=1}^{N_{sc}} A_{ki}\, s_k(t - iT_s) \tag{A.1}$$

$$s_k(t) = U(t) e^{2\pi f_k t} \tag{A.2}$$

$$U(t) = \begin{cases} 1, & 0 < t \le T_s \\ 0, & t \le 0, t > T_s \end{cases} \tag{A.3}$$

where A_{ki} is the i^{th} data symbol at the k^{th} subcarrier, s_k is the waveform for the k^{th} subcarrier, N_{sc} is the number of subcarriers, f_k is the frequency of the k^{th} subcarrier, T_s is the symbol period and $U(t)$ is the pulse shaping function.

OFDM signal uses overlapping technique with orthogonal subcarrier. Two subcarriers are orthogonal if

$$\frac{1}{T_s} \int_0^{T_s} s_k(t) s_l^*(t) dt = 0 \tag{A.4}$$

The straightforward correlation between any two subcarriers provide the orthogonality condition which can be mathematically presented as

$$R_{kl}(t) = \frac{1}{T_s} \int_0^{T_s} s_k(t) s_l^*(t) dt = \frac{1}{T_s} \int_0^{T_s} e^{2\pi f_k t} e^{-2\pi f_l t} dt \tag{A.5}$$

$$R_{kl}(t) = \frac{1}{T_s} \left[\frac{e^{2\pi (f_k - f_l) t}}{2\pi (f_k - f_l)} \right]_0^{T_s} = e^{\pi (f_k - f_l) t} \frac{\sin\left(\pi (f_k - f_l) T_s\right)}{\left(\pi (f_k - f_l) T_s\right)} \tag{A.6}$$

$$R_{kl}(t) = e^{\pi (f_k - f_l) T_s} \cdot \operatorname{sinc}\left(\pi (f_k - f_l) T_s\right) \tag{A.7}$$

if the following condition is satisfied

$$f_k - f_l = \frac{n}{T_s} \tag{A.8}$$

where n is an integer number, therefore the two subcarriers are orthogonal to each other. In practice, n is set to obtain the highest spectral efficiency.

Bibliography

[1] S. Haykin, *Communication systems*. John Wiley & Sons, 4th ed., 2001.

[2] I. Glover and P. Grant, *Digital communications*. Pearson Education, 3rd ed., 2010.

[3] J. M. Senior, *Optical fiber communications: principles and practice*. Pearson Education, 3rd ed., 2009.

[4] G. P. Agrawal, *Fiber-optic communication systems*. John Wiley & Sons, 3rd ed., 2010.

[5] W. Shieh and I. Djordjevic, *OFDM for optical communications*. Elsevier, 1st ed., 2009.

[6] R. W. Chang, "Synthesis of band-limited orthogonal signals for multichannel data transmission," *Bell System Technical Journal*, vol. 45, pp. 1775–1796, 1966.

[7] A. Peled and A. Ruiz, "Frequency domain data transmission using reduced computational complexity algorithms," in *IEEE International Conference on Acoustics, Speech, and Signal Processing (ICASSP)*, vol. 5, pp. 964–967, 1980.

[8] L. Cimini Jr., "Analysis and simulation of a digital mobile channel using orthogonal frequency division multiplexing," *IEEE Transactions on Broadcasting Communication*, vol. 33, no. 7, pp. 665–675, 1985.

[9] S. Kumar, ed., *Impact of nonlinearities on fiber optic communications*, vol. 7. Springer, 2011.

[10] A. J. Lowery, L. Du, and J. Armstrong, "Orthogonal frequency division multiplexing for adaptive dispersion compensation in long haul WDM systems," in *Conference Optical Fiber Communication and National Fiber Optic Engineers (OFC/NFOEC)*, PDP39, 2006.

[11] W. Shieh and C. Athaudage, "Coherent optical orthogonal frequency division multiplexing," *Electronics Letters*, vol. 42, no. 10, pp. 587–589, 2006.

[12] W. Shieh, "PMD-supported coherent optical OFDM systems," *IEEE Photonics Technology Letters*, vol. 19, no. 3, pp. 134–136, 2007.

[13] L. Xu, J. Hu, D. Qian, and T. Wang, "Coherent optical OFDM systems using self optical carrier extraction," in *Conference Optical Fiber Communication and National Fiber Optic Engineers (OFC/NFOEC)*, OMU4, 2008.

[14] M. S. Roden, *Analog and digital communication systems*. Discovery Press, 3rd ed., 2003.

[15] R. v. Nee and R. Prasad, *OFDM for wireless multimedia communications*. Artech House, 1st ed., 2000.

[16] M. Doelz, E. Heald, and D. Martin, "Binary data transmission techniques for linear systems," *Proceedings of the IRE*, vol. 45, no. 5, pp. 656–661, 1957.

[17] B. Saltzberg, "Performance of an efficient parallel data transmission system," *IEEE Transactions on Communication Technology*, vol. 15, no. 6, pp. 805–811, 1967.

[18] J. A. Bingham, "Multicarrier modulation for data transmission: An idea whose time has come," *IEEE Communications Magazine*, vol. 28, no. 5, pp. 5–14, 1990.

[19] L. Litwin and M. Pugel, "The principles of OFDM," *RF Signal Processing*, vol. 2, pp. 30–48, 2001.

[20] J. Salz and S. Weinstein, "Fourier transform communication system," in *Proceedings of 1st ACM symposium on Problems in the optimization of data communications systems*, pp. 99–128, 1969.

[21] R. E. Blahut, *Fast algorithms for digital signal processing*. Addison-Wesley Longman Publishing Co., 1st ed., 1985.

[22] R. W. Ramirez, *The FFT Fundamentals and concepts*. Prentice Hall, 1st ed., 1985.

[23] S. L. Jansen, I. Morita, T. C. W. Schenk, N. Takeda, and H. Tanaka, "Coherent optical 25.8-Gb/s OFDM transmission over 4160-km SSMF," *IEEE Journal of Lightwave Technology*, vol. 26, no. 1, pp. 6–15, 2008.

[24] B. Schmidt, A. J. Lowery, and L. B. Du, "Low sample rate transmitter for direct-detection optical OFDM," in *Conference Optical Fiber Communication and National Fiber Optic Engineers (OFC/NFOEC)*, OWM4, 2009.

[25] S. Adhikari, S. L. Jansen, M. Alfiad, B. Inan, A. Lobato, V. A. J. M. Sleiffer, and W. Rosenkranz, "Experimental investigation of self coherent optical OFDM systems using Fabry-Perot filters for carrier extraction," in *36th European Conference and Exhibition on Optical Communication (ECOC)*, Tu.4.A.1, 2010.

[26] T.-D. Chiueh and P.-Y. Tsai, *OFDM baseband receiver design for wireless communications*. John Wiley & Sons, 1st ed., 2007.

[27] T. M. Schmidl and D. C. Cox, "Robust frequency and timing synchronization for OFDM," *IEEE Transactions on Communications*, vol. 45, no. 12, pp. 1613–1621, 1997.

[28] T. Keller and L. Hanzo, "Orthogonal frequency division multiplex synchronisation techniques for wireless local area networks," in *7th IEEE International Symposium on Personal, Indoor and Mobile Radio Communications (PIMRC)*, vol. 3, pp. 963–967, 1996.

[29] M. Sandell, J.-J. van de Beek, and P. O. Börjesson, "Timing and frequency synchronization in OFDM systems using the cyclic prefix," in *Proceedings of International Symposium on Synchronization*, pp. 16–19, 1995.

[30] P. R. Chevillat, D. Maiwald, and G. Ungerboeck, "Rapid training of a voice band data-modem receiver employing an equalizer with fractional-T spaced coefficients," *IEEE Transactions on Communications*, vol. 35, no. 9, pp. 869–876, 1987.

[31] X. Li and L. J. Cimini Jr, "Effects of clipping and filtering on the performance of OFDM," in *47th IEEE Vehicular Technology Conference (VTC)*, vol. 3, pp. 1634–1638, 1997.

[32] J. Armstrong, "Peak-to-average power reduction for OFDM by repeated clipping and frequency domain filtering," *Electronics letters*, vol. 38, no. 5, pp. 246–247, 2002.

[33] S. H. Muller and J. B. Huber, "A novel peak power reduction scheme for OFDM," in *8th IEEE International Symposium on Personal, Indoor and Mobile Radio Communications (PIMRC)*, vol. 3, pp. 1090–1094, 1997.

[34] J. Tellado and J. M. Cioffi, "PAR reduction in multicarrier transmission systems," ANSI document T1E1.4/79-367, Stanford University, 1998.

[35] A. J. Lowery, S. Wang, and M. Premaratne, "Calculation of power limit due to fiber nonlinearity in optical OFDM systems," *Optics Express*, vol. 15, no. 20, pp. 13282–13287, 2007.

[36] R. Dischler and F. Buchali, "Measurement of non linear thresholds in O-OFDM systems with respect to data pattern and peak power to average ratio," in *34th European Conference and Exhibition on Optical Communication (ECOC)*, Mo.3.E.5, 2008.

[37] D. Yoon, K. Cho, and J. Lee, "Bit error probability of M-ary quadrature amplitude modulation," in *52nd IEEE Vehicular Technology Conference (VTC)*, vol. 5, pp. 2422–2427, 2000.

[38] J. G. Proakis and M. Salehi, *Digital communications*. McGraw-Hill, 5th ed., 2007.

[39] J. van Wyk and L. Linde, "Bit error probability for a M-ary QAM OFDM-based system," in *IEEE AFRICON Conference*, pp. 1–5, 2007.

[40] J. Armstrong, "OFDM for optical communications," *IEEE Journal of Lightwave Technology*, vol. 27, no. 3, pp. 189–204, 2009.

[41] C. Fludger, T. Duthel, D. Van den Borne, C. Schulien, E. D. Schmidt, T. Wuth, J. Geyer, E. De Man, G.-D. Khoe, and H. de Waardt, "Coherent equalization and POLMUX-RZ-DQPSK for robust 100-GE transmission," *IEEE Journal of Lightwave Technology*, vol. 26, no. 1, pp. 64–72, 2008.

[42] E. Ip and J. M. Kahn, "Digital equalization of chromatic dispersion and polarization mode dispersion," *IEEE Journal of Lightwave Technology*, vol. 25, no. 8, pp. 2033–2043, 2007.

[43] S. Jansen, D. Van den Borne, and S. Adhikari, "Past, present and future of optical OFDM," in *Communications and Photonics Conference and Exhibition (ACP)*, pp. 1–2, 2009.

[44] W. Shieh, X. Yi, and Y. Tang, "Transmission experiment of multi-gigabit coherent optical OFDM systems over 1000km SSMF fibre," *Electronics Letters*, vol. 43, no. 3, pp. 183–184, 2007.

[45] H. Louchet and A. Richter, "Novel scheme for high-bit-rate coherent-OFDM transmission without PLL," in *33rd European Conference and Exhibition on Optical Communication (ECOC)*, P087, 2007.

[46] W. Shieh, Q. Yang, and Y. Ma, "107 Gb/s coherent optical OFDM transmission over 1000-km SSMF fiber using orthogonal band multiplexing," *Optics Express*, vol. 16, no. 9, pp. 6378–6386, 2008.

[47] S. L. Jansen, I. Morita, T. C. Schenk, and H. Tanaka, "121.9-Gb/s PDM-OFDM transmission with 2-b/s/Hz spectral efficiency over 1000 km of SSMF," *IEEE Journal of Lightwave Technology*, vol. 27, no. 3, pp. 177–188, 2009.

[48] Y. Ma, Q. Yang, Y. Tang, S. Chen, and W. Shieh, "1-Tb/s single-channel coherent optical OFDM transmission over 600-km SSMF fiber with subwavelength bandwidth access," *Optics Express*, vol. 17, no. 11, pp. 9421–9427, 2009.

[49] R. Dischler and F. Buchali, "Transmission of 1.2 Tb/s continuous waveband PDM-OFDM-FDM signal with spectral efficiency of 3.3 bit/s/Hz over 400 km of SSMF," in *Conference Optical Fiber Communication and National Fiber Optic Engineers (OFC/NFOEC)*, PDPC2, 2009.

[50] W. Shieh, H. Bao, and Y. Tang, "Coherent optical OFDM: theory and design," *Optics Express*, vol. 16, no. 2, pp. 841–859, 2008.

[51] Y. Tang, W. Shieh, X. Yi, and R. Evans, "Optimum design for RF-to-optical up-converter in coherent optical OFDM systems," *IEEE Photonics Technology Letters*, vol. 19, no. 7, pp. 483–485, 2007.

[52] D.-S. Ly-Gagnon, S. Tsukamoto, K. Katoh, and K. Kikuchi, "Coherent detection of optical quadrature phase-shift keying signals with carrier phase estimation," *IEEE Journal of Lightwave Technology*, vol. 24, no. 1, pp. 12–21, 2006.

[53] M. E. Mousa Pasandi, D. V. Plant, *et al.*, "Improvement of phase noise compensation for coherent optical OFDM via data-aided phase equalizer," in *Conference Optical Fiber Communication and National Fiber Optic Engineers (OFC/NFOEC)*, JThA10, 2010.

[54] R. Noé, *Essentials of modern optical fiber communication*. Springer, 1st ed., 2009.

[55] S. Hussin, K. Puntsri, and R. Noé, "Performance analysis of optical OFDM systems," in *3rd IEEE International Congress on Ultra Modern Telecommunications and Control Systems (ICUMT)*, pp. 1–5, 2011.

[56] A. Molisch, "MIMO systems with antenna selection - an overview," in *Radio and Wireless Conference (RAWCON)*, pp. 167–170, 2003.

[57] A. Paulraj, D. Gore, R. Nabar, and H. Bolcskei, "An overview of MIMO communications - a key to gigabit wireless," *Proceedings of the IEEE*, vol. 92, no. 2, pp. 198–218, 2004.

[58] K.-W. Park, E. S. Choi, K. H. Chang, and Y.-S. Cho, "A MIMO-OFDM technique for high-speed mobile channels," in *57th IEEE Vehicular Technology Conference (VTC)*, vol. 2, pp. 980–983, 2003.

[59] A. J. Lowery and L. Du, "Optical orthogonal division multiplexing for long haul optical communications: A review of the first five years," *Optical Fiber Technology*, vol. 17, pp. 421–438, 2011.

[60] C. Xie, "PMD insensitive direct-detection optical OFDM systems using self-polarization diversity," in *Conference Optical Fiber Communication and National Fiber Optic Engineers (OFC/NFOEC)*, OMM2, pp. 1–3, 2008.

[61] B. Schmidt, A. Lowery, and J. Armstrong, "Impact of PMD in single-receiver and polarization-diverse direct-detection optical OFDM," *IEEE Journal of Lightwave Technology*, vol. 27, no. 14, pp. 2792–2799, 2009.

[62] D. Qian, N. Cvijetic, J. Hu, and T. Wang, "108 Gb/s OFDMA-PON with polarization multiplexing and direct detection," *IEEE Journal of Lightwave Technology*, vol. 28, no. 4, pp. 484–493, 2010.

[63] R. Luis, B. Puttnam, J.-M. Mendinueta, S. Shinada, and N. Wada, "Self-homodyne CO-OFDM packet transmitter with polarization-multiplexed pilot tone," in *OptoElectronics and Communications Conference (OECC)*, TuT3-2, pp. 1–2, 2013.

[64] R. Luis, B. Puttnam, J.-M. Mendinueta, J. Sakaguchi, S. Shinada, M. Nakamura, Y. Kamio, and N. Wada, "Self-homodyne detection of polarization-multiplexed pilot

tone signals using a polarization diversity coherent receiver," in *39th European Conference and Exhibition on Optical Communication (ECOC)*, pp. 1–3, 2013.

[65] W. Shieh, X. Yi, Y. Ma, and Y. Tang, "Theoretical and experimental study on PMD supported transmission using polarization diversity in coherent optical OFDM systems," *Optics Express*, vol. 15, no. 16, pp. 9936–9947, 2007.

[66] S. L. Jansen, I. Morita, T. C. Schenk, and H. Tanaka, "Long-haul transmission of 16×52.5 gbits/s polarization-division-multiplexed OFDM enabled by MIMO processing," *Journal of Optical Networking*, vol. 7, no. 2, pp. 173–182, 2008.

[67] S. Chen, Q. Yang, Y. Ma, and W. Shieh, "Real-time multi-gigabit receiver for coherent optical MIMO-OFDM signals," *IEEE Journal of Lightwave Technology*, vol. 27, no. 16, pp. 3699–3704, 2009.

[68] K. Puntsri, S. Hoffmann, S. Hussin, A. Al-Bermani, and R. Noé, "A low complexity and high accuracy frame synchronization for optical OFDM systems," in *Opto-Electronics and Communication Conference (OECC)*, pp. 579–580, 2011.

[69] K. Puntsri, D. Sandel, S. Hussin, O. Jan, A. Al-Bermani, M. F. Panhwar, and R. Noé, "A low complexity and high accuracy frame synchronization for optical OFDM and PolMux-optical OFDM," in *IEEE Photonics Conference (IPC)*, pp. 181–182, 2012.

[70] K. Puntsri, O. Jan, A. Al-Bermani, C. Wrdehoff, D. Sandel, S. Hussin, M. F. Panhwar, R. Noé, and U. Rückert, "An ultralow complexity algorithm for frame synchronization and IQ alignment in co-OFDM systems," in *Conference Optical Fiber Communication and National Fiber Optic Engineers (OFC/NFOEC)*, JTh2A.43, pp. 1–3, 2013.

[71] S. Weinstein and P. Ebert, "Data transmission by frequency-division multiplexing using the discrete Fourier transform," *IEEE Transactions on Communication Technology*, vol. 19, no. 5, pp. 628–634, 1971.

[72] M. Gudmundson and P.-O. Anderson, "Adjacent channel interference in an OFDM system," in *46th IEEE Vehicular Technology Conference (VTC)*, vol. 2, pp. 918–922, 1996.

[73] C. Muschallik, “Improving an OFDM reception using an adaptive nyquist windowing,” *IEEE Transactions on Consumer Electronics*, vol. 42, no. 3, pp. 259–269, 1996.

[74] J. Armstrong, “Analysis of new and existing methods of reducing inter-carrier interference due to carrier frequency offset in OFDM,” *IEEE Transactions on Communications*, vol. 47, no. 3, pp. 365–369, 1999.

[75] P. Tan and N. C. Beaulieu, “Reduced ICI in OFDM systems using the "better than" raised-cosine pulse,” *IEEE Communications Letters*, vol. 8, no. 3, pp. 135–137, 2004.

[76] R. M. Schmogrow, B. Baeuerle, D. Hillerkuss, B. Nebendahl, C. Koos, W. Freude, and J. Leuthold, “Raised-cosine OFDM for enhanced out-of-band suppression at low subcarrier counts,” in *Signal Processing in Photonic Communications (SPPCOM)*, SpTu2A, 2012.

[77] S. Hussin, K. Puntsri, D. Sandel, M. F. Panhwar, and R. Noé, “Efficiency enhancement of CO-OFDM systems using different pulse shapes,” in *Opto-Electronics and Communication Conference (OECC)*, TuR4-4, 2013.

[78] S. L. Jansen, I. Morita, N. Takeda, and H. Tanaka, “20-Gb/s OFDM transmission over 4,160-km SSMF enabled by RF-pilot tone phase noise compensation,” in *Conference Optical Fiber Communication and National Fiber Optic Engineers (OFC/NFOEC)*, PDP15, 2007.

[79] X. Yi, W. Shieh, and Y. Ma, “Phase noise effects on high spectral efficiency coherent optical OFDM transmission,” *IEEE Journal of Lightwave Technology*, vol. 26, no. 10, pp. 1309–1316, 2008.

[80] X. Zhu and S. Kumar, “Nonlinear phase noise in coherent optical OFDM transmission systems,” *Optics Express*, vol. 18, no. 7, pp. 7347–7360, 2010.

[81] S. Wu and Y. Bar-Ness, “OFDM systems in the presence of phase noise: consequences and solutions,” *IEEE Transactions on Communications*, vol. 52, no. 11, pp. 1988–1996, 2004.

[82] A. G. Armada and M. Calvo, "Phase noise and sub-carrier spacing effects on the performance of an OFDM communication system," *IEEE Communications Letters*, vol. 2, no. 1, pp. 11–13, 1998.

[83] G. P. Agrawal, *Nonlinear fiber optics*. Academic Press, Elsevier, 3rd ed., 2001.

[84] X. Yi, W. Shieh, and Y. Tang, "Phase estimation for coherent optical OFDM," *IEEE Photonics Technology Letters*, vol. 19, no. 12, pp. 919–921, 2007.

[85] X. Liu and R. W. Tkach, "Joint SPM compensation for inline-dispersion-compensated 112-Gb/s PDM-OFDM transmission," in *Conference Optical Fiber Communication and National Fiber Optic Engineers (OFC/NFOEC)*, OTuO1, 2009.

[86] S. Randel, S. Adhikari, and S. L. Jansen, "Analysis of RF-pilot-based phase noise compensation for coherent optical OFDM systems," *IEEE Photonics Technology Letters*, vol. 22, no. 17, pp. 1288–1290, 2010.

[87] S. Hussin, K. Puntsri, and R. Noé, "Performance analysis of RF-pilot phase noise compensation techniques in coherent optical OFDM systems," in *17th IEEE European Conference Networks and Optical Communications (NOC)*, pp. 1–5, 2012.

[88] X. Yi, W. Shieh, and Y. Ma, "Phase noise on coherent optical OFDM systems with 16-QAM and 64-QAM beyond 10 Gb/s," in *33rd European Conference and Exhibition on Optical Communication (ECOC)*, Tu.5.2.3, 2007.

[89] K. Kikuchi, M. Fukase, and S.-Y. Kim, "Electronic post-compensation for nonlinear phase noise in a 1000-km 20-Gbit/s optical QPSK transmission system using the homodyne receiver with digital signal processing," in *Conference Optical Fiber Communication and National Fiber Optic Engineers (OFC/NFOEC)*, OTuA2, 2007.

[90] A. J. Lowery, "Fiber nonlinearity pre- and post-compensation for long-haul optical links using OFDM," *Optics Letters*, vol. 15, no. 20, pp. 12965–12970, 2007.

[91] A. Lobato, B. Inan, S. Adhikari, and S. L. Jansen, "On the efficiency of RF-pilot-based nonlinearity compensation for CO-OFDM," in *Conference Optical Fiber Communication and National Fiber Optic Engineers (OFC/NFOEC)*, OThF2, 2011.

[92] S. Hussin, K. Puntsri, and R. Noé, "Efficiency enhancement of RF-pilot-based phase noise compensation for coherent optical OFDM systems," in *17th IEEE International OFDM Workshop (InOWo)*, pp. 1–5, 2012.

[93] B. Inan, S. Randel, S. L. Jansen, A. Lobato, S. Adhikari, and N. Hanik, "Pilot-tone-based nonlinearity compensation for optical OFDM systems," in *36th European Conference and Exhibition on Optical Communication (ECOC)*, Tu.4.A.6, 2010.

[94] L. B. Du and A. J. Lowery, "Pilot-based cross-phase modulation compensation for coherent optical orthogonal frequency division multiplexing long-haul optical communications systems," *Optics Letters*, vol. 36, no. 9, pp. 1647–1649, 2011.

[95] L. B. Du and A. J. Lowery, "Pilot-based XPM nonlinearity compensator for CO-OFDM systems," *Optics Express*, vol. 19, no. 26, pp. B862–B867, 2011.

[96] S. Hussin, R. Noé, and M. F. Panhwar, "Improvement of RF-pilot phase noise compensation for coherent optical OFDM systems via CPE equalizer," in *Opto-Electronics and Communication Conference (OECC)*, WEPS2-53, 2014.

[97] S. Hussin, K. Puntsri, M. F. Panhwar, and R. Noé, "Partial pilot filling for phase noise compensation in coherent optical OFDM systems," in *Opto-Electronics and Communication Conference (OECC)*, TuPR-17, 2013.

[98] S. Hussin, K. Puntsri, and R. Noé, "Analysis of partial pilot filling phase noise compensation for CO-OFDM systems," *IEEE Photonics Technology Letters*, vol. 25, no. 12, pp. 1099–1102, 2013.

[99] S. Hussin, R. Noé, and M. F. Panhwar, "Fiber nonlinearity tolerance of partial pilot filling in CO-OFDM in transmission systems," in *Opto-Electronics and Communication Conference (OECC)*, WEPS2-52, 2014.

[100] K. Puntsri, O. Jan, A. Al-Bermani, D. Sandel, C. Wrdehoff, S. Hussin, M. F. Panhwar, U. Rückert, and R. Noé, "Pilot-aided CD and PN compensation simultaneously in co-OFDM systems," in *Opto-Electronics and Communication Conference (OECC)*, TuR4-7, 2013.

[101] S. Hussin and R. Noé, "Fiber nonlinearity mitigation in CO-OFDM systems using dual compensators," in *IEEE Photonics Conference (IPC)*, MG2.2, 2014.

[102] J. Rinne and M. Renfors, “Pilot spacing in orthogonal frequency division multiplexing systems on practical channels,” *IEEE Transactions on Consumer Electronics*, vol. 42, no. 4, pp. 959–962, 1996.

[103] P. Rabiei, W. Namgoong, and N. Al-Dhahir, “A non-iterative technique for phase noise ICI mitigation in packet-based OFDM systems,” *IEEE Transactions on Single Processing*, vol. 58, no. 11, pp. 5945–5950, 2010.

[104] H. Bao and W. Shieh, “Transmission simulation of coherent optical OFDM signals in WDM systems,” *Optics Express*, vol. 15, no. 8, pp. 4410 – 4418, 2007.

[105] M. E. Mousa-Pasandi and D. V. Plant, “Noniterative interpolation-based partial phase noise ICI mitigation for CO-OFDM transport systems,” *IEEE Photonics Technology Letters*, vol. 23, no. 21, pp. 1594–1596, 2011.

[106] DoCoMo, NTT, NEC, and SHARP, “R1-050702: DFT-spread OFDM with pulse shaping filter in frequency domain in evolved UTRA uplink,” 2005.

[107] H. G. Myung, J. Lim, and D. J. Goodman, “Peak-to-average power ratio of single carrier FDMA signals with pulse shaping,” in *17th IEEE International Symposium on Personal, Indoor and Mobile Radio Communications (PIMRC)*, pp. 1–5, 2006.

[108] W. Shieh and Y. Tang, “Ultrahigh-speed signal transmission over nonlinear and dispersive fiber optic channel: The multicarrier advantage,” *IEEE Photonics Journal*, vol. 2, no. 3, pp. 276–283, 2010.

[109] Y. Tang, W. Shieh, and B. S. Krongold, “DFT-spread OFDM for fiber nonlinearity mitigation,” *IEEE Photonics Technology Letters*, vol. 22, no. 16, pp. 1250–1252, 2010.

[110] H. G. Myung, J. Lim, and D. J. Goodman, “Single carrier FDMA for uplink wireless transmission,” *IEEE Vehicular Technology Magazine*, vol. 1, no. 3, pp. 30–38, 2006.

[111] U. Sorger, I. De Broeck, and M. Schnell, “Interleaved FDMA-a new spread-spectrum multiple-access scheme,” in *IEEE International Conference on Communications (ICC)*, vol. 2, pp. 1013–1017, 1998.

[112] Q. Yang, Z. He, Z. Yang, S. Yu, X. Yi, and W. Shieh, "Coherent optical dft-spread ofdm transmission using orthogonal band multiplexing," *Optics Express*, vol. 20, pp. 2379–2385, January 2012.

[113] L. Tao, J. Yu, Y. Fang, J. Zhang, Y. Shao, and N. Chi, "Analysis of noise spread in optical DFT-S OFDM systems," *IEEE Journal of Lightwave Technology*, vol. 30, no. 20, pp. 3219–3225, 2012.

Publications

1. **S. Hussin**, and R. Noé, "Fiber nonlinearity Mitigation in CO-OFDM Systems using Dual Compensators," in *Proc. 27th IEEE PHOTONICS CONFERENCE (IPC)*, 12-16 OCT. 2014, San Diego, California, USA,
2. **S. Hussin** and R. Noé, M.F. Panhwar, "Fiber Nonlinearity Tolerance of Partial Pilot Filling in CO-OFDM in Transmission Systems," in *IEEE 19th Opto-Electronics and Communications Conference (OECC)*, 6-10 July 2014, Melbourne, Australia.
3. **S. Hussin** and R. Noé, M.F. Panhwar, "Improvement of RF-Pilot Phase Noise Compensation for CO-OFDM Transmission Systems via Common Phase Error Equalizer," *in IEEE 19th Opto-Electronics and Communications Conference (OECC)*, 6-10 July 2014, Melbourne, Australia.
4. M.F. Panhwar, D. Sandel, C. Wördehoff, K. Puntsri, S. Hussin and R, Noé," PU-CMA-QAM based MIMO Equalization in DSP-enabled PMD-16-QAM Receivers, ," *in IEEE 19th Opto-Electronics and Communications Conference (OECC)*, 6-10 July 2014, Melbourne, Australia.
5. M. F. Panhwar, D. Sandel, C. Wördehoff, S. Hussin and R. Noé," PU-CMA-QAM based MIMO Equalization for Digital PMD Compensation in PDM-16-QAM Receivers," *in 15th ITG-symposium "Photonics Networks"*, 5-6 May 2014, Leipzig, Germany.
6. **S. Hussin**, K. Puntsri, M.F. Panhwar and R, Noé, "Partial Pilot Filling for Phase Noise Compensation in Coherent Optical OFDM Systems", *in IEEE 18th Opto-Electronics and Communications Conference (OECC)*, 30 Jun-4 July 2013, Kyoto, Japan.
7. K. Puntsri, O. Jan, A. Al-Bermani, D. Sandel, C. Wördehoff, **S. Hussin**, M. F. Panhwar, U. Rückert and R. Noé, "Pilot-aided CD and PN Compensation Simultaneously in CO-OFDM Systems", *in IEEE 18th Opto-Electronics and Communications Conference (OECC)*, 30 Jun-4 July 2013, Kyoto, Japan.
8. **S. Hussin**, K. Puntsri, M.F. Panhwar, D. Sandel and R, Noé, "Efficiency Enhancement of CO-OFDM Systems Using Different Pulse Shapes", *in IEEE 18th*

Opto-Electronics and Communications Conference (OECC), 30 Jun-4 July 2013, Kyoto, Japan.

9. M.F. Panhwar, C. Wördehoff, K. Puntsri, S. Hussin, U. Rückert and R, Noé, "Reduced Oversampling Rate for Adaptive Search Based Blind FD CD Estimation", *in IEEE 18th opto-Electronics and Communications Conference (OECC)*, 30 Jun-4 July 2013, Kyoto, Japan.
10. B. Koch, R, Noé, V. Mirvoda, K. Puntsri, O. Jan and S. Hussin, "40-krad/s-Fast Polarization Demultiplexing in a 430-km, 20-Gb/s-PDM-RZ-DPSK Transmission", *in IEEE 18th opto-Electronics and Communications Conference (OECC),* 30 Jun-4 July 2013, Kyoto, Japan.
11. **S. Hussin**, K. Puntsri and R. Noé, "Analysis of partial pilot filling phase noise compensation for CO-OFDM systems," *IEEE Photonics Technology Letters*, vol. 25, no. 12, pp. 1099–1102, 2013.
12. K. Puntsri,O. Jan, Omar, A. Al-Bermani, C. Wördehoff, D. Sandel, David, M. F. Panhwar, **S. Hussin**, U. Rückert and R. Noé ," ISI Tolerance of Cyclic Prefix Free Coherent Optical OFDM Communication systems", *in 14th ITG- symposium* "*Photonische Netze",* 6-7 May 2013, Leipzig, Germany.
13. K. Puntsri, O. Jan, A. Al-Bermani, C. Wördehoff, D. Sandel, **S. Hussin**, M. F. Panhwar, R. Noé and U. Rückert, "An Ultralow Complexity Algorithm for Frame Synchronization and IQ Alignment in CO-OFDM Systems," *in Optical Fiber Communication and National Fiber Optic Engineers Conference (OFC/NFOEC),* JTh2A.4.3, 19-21 March. 2013, Anaheim, California, USA.
14. K. Puntsri, D. Sandel, **S. Hussin**, O. Jan, A. Al-Bermani, M. F. Panhwar and R. Noé ," A Low Complexity and High Accuracy Frame Synchronization for Optical OFDM and PolMux-Optical OFDM, " *in 25th IEEE Photonics Conference (IPC)*, 23-27 Sept. 2012, San Francisco, California , USA.
15. **S. Hussin**, K. Puntsri and R. Noé, "Efficiency Enhancement of RF-Pilot-Based Phase Noise Compensation for Coherent Optical OFDM,*" in IEEE 17th International OFDM Workshop (InOWo'12)*, 29-30 Aug. 2012, Essen, Germany.
16. K. Puntsri, V. Mirvoda, **S. Hussin**, Omar H.A. Jan, A. Al-Bermani, M. F. Panhwar and R. Noé, " A Low Complexity and High Accuracy Frame Synchronization for

PolMux-Optical OFDM," *in ITG-Workshop section 5.3.1 Modeling of photonic components and systems*, 5-6 July 2012, Nurnberg, Germany.

17. K. Puntsri, D. Sandel, **S. Hussin**, O. Jan, A. Al-Bermani and R. Noé, " A Novel Method for IQ Imbalance Compensation in CO- OFDM systems," *in IEEE 17th Opto-Electronics and Communications Conference (OECC)*, 2-6 July 2012, Busan, Korea.
18. **S. Hussin**, K. Puntsri and R. Noé, "Performance Analysis of RF-Pilot Phase Noise Compensation Techniques in Coherent Optical OFDM Systems," *in IEEE 17th European Conference on Network and Optical Communications (NOC)*, 20-22 June 2012, Barcelona, Spain.
19. **S. Hussin**,K. Puntsri and R. Noé, "Performance Analysis of Optical OFDM systems," *in IEEE 3rd International Congress on Ultra Modern Telecommunications and Control Systems (ICUMT)*, 5-7 Oct. 2011, Budapest, Hungary.
20. K. Puntsri, S. Hoffmann, **S. Hussin**, A. Al-Bermani and R. Noé, "A Low Complexity and High Accuracy Frame Synchronization for Optical OFDM Systems," *in IEEE 16th Opto-Electronics and Communications Conference (OECC)*, 4-8 July 2011, Kaohsiung, Taiwan.